

POLITECNICO DI TORINO

Collegio di Ingegneria Meccanica e Aerospaziale

**Corso di Laurea Magistrale
in Ingegneria Meccanica**

Tesi di Laurea Magistrale

**Design of an energy harvesting system
for a sailboat**



Relatore

Prof.ssa Giuliana Mattiazzo

Candidato

Giacomo Dell'Atti

Anno accademico 2017/18

Contents

1	Introduction.....	1
2	Wave Energy.....	3
2.1	Advantages and Disadvantages of Wave Energy	4
2.2	Worldwide wave energy	5
2.3	Wave characteristics	6
2.4	Wave Energy Converters (WEC)	8
2.4.1	WEC classification	9
3	Mathematical model of the behavior of a boat on a regular wave	14
3.1	Notations and conventions.....	14
3.2	Regular wave	15
3.3	Buoyancy force	15
3.4	Hydrostatic Force.....	16
3.5	Excitation force: sum of Froude – Krylov and diffraction forces.....	18
3.6	Radiation force.....	20
3.7	Drag force	20
3.8	Boundary element method (BEM).....	21
3.8.1	General formula in zero forward speed	21
3.8.2	Boundary conditions.....	24
3.8.3	Solutions and equation of motion.....	26
3.9	Definition of RAO	28
3.10	Corrections for small forward speed.....	29
4.	Hydrodynamic analysis of the hull	31
4.1	Characteristics of the hull	31
4.1.1	Fineness Coefficient of the transversal section	32
4.1.2	Fineness Coefficient of the floating section	33
4.1.3	Fineness Coefficient of longitudinal section	33
4.1.4	Approximate calculation of moments of inertia	34

4.1.5	Stabilization diagram	34
4.2	Characteristics of the incident wave	36
4.3	Longitudinal incident wave: results	37
4.3.1	Considerations	42
4.3.2	Calculation of the wave length and resonance frequency of the system	43
5	Gyroscope system	47
5.1	The ISWEC working principles	47
5.2	The gyroscope mathematical model (Newtonian Approach)	48
5.3	Gyroscope equations in hull reference frame	50
5.4	Simplifications	51
6.	Design of a 1:7 scale of a gyroscopic model	52
6.1	Dimensions of the system	52
6.2	External structure	53
6.3	Internal structure	54
6.4	Functioning	56
6.5	Bearing study	57
6.5	Gyroscope bearing adopted	58
6.5.1	SKF spherical roller bearing 21310 EK	62
6.5.2	SKF four - point contact ball bearing QJ 306 MA	64
6.5.3	SKF spherical roller bearing 21307 CC	65
6.5.4	Adapter sleeve H 307 E for 21307 CC bearing	66
6.5.5	Adapter sleeve H 310 for 21310 EK bearing	67
6.5.6	Description of bearing mounting	68
6.6	Hexagonal head bolt with nut	70
7.	Power losses on a gyroscopic system	73
7.1	Hypotheses	73
7.2	Flywheel shaft power losses	73
7.2.1	Fluid – dynamic power losses	74
7.2.2	Bearing power losses	76
7.2.3	Seal power losses	77

7.3	Power losses scaling law.....	78
7.3.1	Froude scaling law.....	80
7.3.2	Trends of scaled power losses	81
8.	Conclusions.....	83
	References	85

List of figures

Figure 1: Wave power density World map (values in kW/m)[4]	1
Figure 2: Wave power density Europe map (values in kW/m)	2
Figure 3: World energy map.....	5
Figure 4: Wave characteristic	6
Figure 5: water particles trajectories for deep water (right) and shallow water (left)	8
Figure 6: Six types of WEC.....	10
Figure 7: Bulge wave.....	11
Figure 8: rotating mass	12
Figure 9: The 5 stages of development of a WEC proposed by Equimar	13
Figure 10: Definition of axis system	14
Figure 11: Buoyancy force [18].....	16
Figure 12: hydrostatic force after a small displacement [18]	17
Figure 13: Froude - Krylov force [18].....	18
Figure 14: Diffraction forces [18]	19
Figure 15: Excitation force [18]	19
Figure 16: Radiated wave [18]	20
Figure 17: Generation of vortices [18]	20
Figure 18: Decomposition of the hydrodynamic problem in sea keeping.....	22
Figure 19: Surfaces described by the boundary conditions [18].....	25
Figure 20: Linearized wave [18]	26
Figure 21: Small displacements of a body [18].....	27
Figure 22: Definition of RAO	29
Figure 23: Hull's shape. Type A: displacement hull.....	31
Figure 24: Hull of the sailboat.....	32
Figure 25: Transversal section of the hull	33
Figure 26: Floating section of the hull	33
Figure 27: Longitudinal section of the hull	34
Figure 28: Stable, neutral, unstable equilibrium.....	35
Figure 29: Relation between B, G, M.....	35
Figure 30: Stabilization curve	36
Figure 31: Added mass in pitching degree	37
Figure 32: Damping in pitching degree	38
Figure 33: Froude - Krylov and Diffraction forces in pitching degree	39
Figure 34: RAO in pitching motion.....	40
Figure 35: RAO in roll motion	41
Figure 36: Water plane area [18].....	45
Figure 37: Floating plane of the hull	45

Figure 38: Gyroscope system reference frame.....	48
Figure 39: General dimensions of the system	52
Figure 40: External chamber view.....	53
Figure 41: Aerodynamic drag acting on the ISWEC flywheel as a function of the chamber pressure.....	54
Figure 42: Internal chamber view.....	55
Figure 43: Flywheel with the two half shafts	55
Figure 44: flywheel dimensions with the two half shaft	56
Figure 45: Annual productivity for ISWEC system	57
Figure 46: Bearings of the gyroscopic system.....	59
Figure 47: Spherical roller bearing.....	60
Figure 48: self - alignment property of the bearing.....	60
Figure 49: self - adjusting property of the rollers	61
Figure 50: load distribution over the roller length.....	61
Figure 51: optimal roller guidance	61
Figure 52: four contact point ball bearing	62
Figure 53: dimensions of 21310 EK bearing [26]	63
Figure 54: dimensions of QJ 306 MA bearing [26]	64
Figure 55: dimensions of 21307 CC bearing [26]	65
Figure 56: dimensions of H 307 E adapter sleeve [26]	67
Figure 57: dimensions of H 310 adapter sleeve [26].....	68
Figure 58: mounting of spherical roller bearing above the flywheel	69
Figure 59: mounting of bearings down the flywheel.....	69
Figure 60: mounting of spherical roller bearing outside the vacuum chamber	70
Figure 61: bolt ISO 4016.....	71
Figure 62: particular of bolt ISO 4016	71
Figure 63: nut ISO 4161	72
Figure 64: particular of nut ISO 4161	72
Figure 65: Flywheel and vacuum chamber scheme.....	74
Figure 66: Simplified flywheel shaft scheme.....	76
Figure 67: Friction force on seal surface in function of pressure difference on it	78
Figure 68: Flywheel power losses on ISWEC[25].....	82

List of tables

Table 1: Geometrical dimensions of 21310 EK bearing [26].....	63
Table 2: Calculation data of 21310 EK bearing [26].....	63
Table 3: Geometrical dimensions of QJ 306 MA bearing[26]	64
Table 4: Calculation data of QJ 306 MA bearing [26]	65
Table 5: geometrical dimensions of 21307 CC bearing [26]	65
Table 6: Calculation data of 21307 CC [26].....	66
Table 7: geometrical dimensions of H 307 E adapter sleeve [26].....	67
Table 8: Geometrical dimensions of H 310 adapter sleeve [26]	68
Table 9: Geometrical dimensions of bolt ISO 4016	71
Table 10: Geometrical dimensions of nut ISO 4161	72
Table 11: Values of torque coefficient in relation to Reynolds number in lateral meatus..	75
Table 12: Values of torque coefficient in relation to Reynolds number in the top and bottom meatus	75
Table 13: Scale factors for geometric characteristics	79
Table 14: Scale factors for kinematic characteristics	79
Table 15: Scale factors for dynamic characteristics	79
Table 16: Scale factors for fluid - dynamic power losses.....	80
Table 17: Scale factors for bearing power losses	80
Table 18: Scale factors for seal power losses	80
Table 19: Kinematic parameters of the system	81
Table 20: Geometric parameters of the system	81
Table 21: Fluid properties	81

1 Introduction

Day and night, all over the world, the power of the sea can be seen and heard, crashing on beaches and rocky shores. The infinite cycle of waves, tides and currents is driven by the wind, by the gravitational effects of the moon and, ultimately, by the power of the sun.

After decades of research, the ability to tap into this source of energy is growing strongly. What promises is very precious: an unlimited and reliable supply of clean energy that helps reduce our dependence on fossil fuels and therefore our footprint on planet earth [1].

Tapping into the power of waves and tides to generate electricity also promises to create a new energy sector, offering jobs (up to 420000 by 2050) and economic growth, especially for areas affected by the decline of traditional fishing industries like shipbuilding and fishing.

Estimates suggest that wave and tidal energy could meet 15% of European electricity demand; by 2050 it could help Europe to avoid 136 MT / MWh of CO₂ emissions [2] [3].

The wave power density is very variable around the world and its highest values are detected in the Oceans between the latitudes of 30° and 60° on both hemispheres (see figures 1 and 2). In Europe the West coasts of the U.K. and Ireland along with Norway and Portugal receive the highest power densities [4].

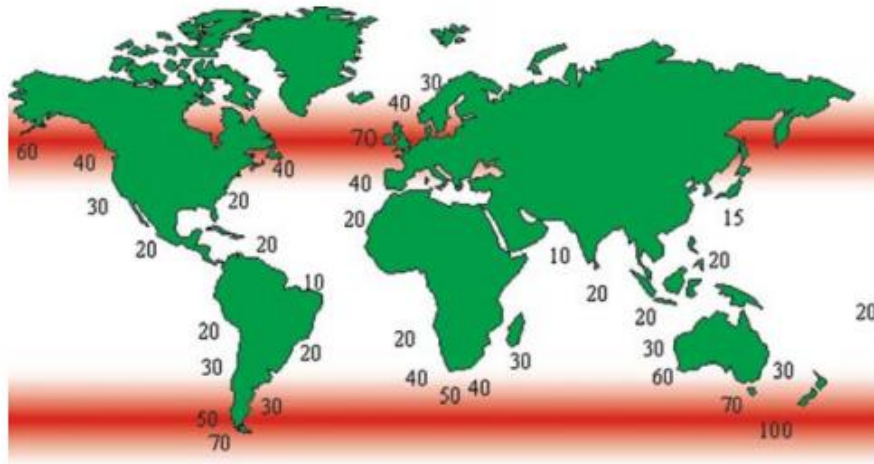


Figure 1: Wave power density World map (values in kW/m)[4]

2 Wave Energy

Wave energy, also known as *oceanic energy* or *marine wave energy*, is energy that is exploited by ocean or sea waves [5]. The vertical movement of surface ocean waves is made up of a lot of kinetic energy that is accumulated by wave energy technologies to perform useful tasks, for example, electricity generation, desalination of water and pumping of water in tanks. The wave energy or the waves power is the power absorbed by the waves. When the wind blows on the surface of the sea, it transfers energy to the waves. The energy emitted is measured by the velocity of the wave, the height of the wave, the wavelength and the density of the water. If the waves are stronger they will produce more energy. The captured energy can then be used to generate electricity, feed plants or pump water. When we look at a seaside and see the waves crashing against the beach, we are witnessing the power of the waves. It is not exploited or used for the benefit of anyone in that state, but it is producing energy.

But how are these waves formed? When the wind blows hard enough on the surface of the water it creates waves. This occurs more often and more forcefully on the ocean due to the lack of land surrounding that resists the force of the wind. The types of waves that are formed depend on where they are affected. Long and constant waves that run endlessly against the beach are probably formed by extreme storms and extreme weather conditions. When we see high waves and moves that rise and fall very quickly, we are likely to see waves created by a nearby meteorological system. These waves are usually newly formed occurrences. The power of these waves can then be exploited by a wave energy converter (WEC).

Wave energy is, essentially, a condensed form of solar power produced by the wind action blowing across ocean water surface, which can then be utilized as an energy source [6]. When the intense sun rays hit the atmosphere, they get it warmed up. The intensity of sun rays hitting the earth's atmosphere varies considerably in different parts of the world. This disparity of atmospheric temperature around the world causes the atmospheric air to travel from hotter to cooler regions, giving rise to winds. As the wind glides over the ocean surface, a fraction of the kinetic energy from the wind is shifted to the water beneath, resulting in waves. As a matter of fact, the ocean could be seen as a gigantic energy storehouse collector conveyed by the sun rays to the oceans, with the waves transporting the conveyed kinetic energy across the ocean surface. With that in mind, we can safely conclude that waves are a form of energy and it's the same energy, not water that glides over the surface of the ocean.

These waves are able to travel throughout the expansive oceans without losing a lot of energy. However, when they reach the shoreline, where the depth of water is considerable shallow, their speed reduces, while their size significantly increase. Ultimately, the waves strike the shoreline, discharging huge quantities of kinetic energy.

2.1 Advantages and Disadvantages of Wave Energy

Advantages are:

- Wave formation and characteristics are parameters that vary constantly but are highly predictable. Waves crash against the beach day and night and host more energy than other renewable sources such as wind and solar. Wind energy and solar energy, on the other hand, are highly unpredictable. Wind speeds fall unexpectedly, which affects the generation of electricity. Solar energy depends on sun exposure, which means that cloud cover and night time significantly reduce this exposure, leading to lower efficiency.
- Wave energy is a completely clean energy source, which means it does not emit dangerous greenhouse gases into the atmosphere. For example, fossil fuels, oil, coal and natural gas contribute significantly to environmental pollution by releasing harmful greenhouse gases into the atmosphere, including carbon dioxide, nitrous oxide, methane and ozone
- The exploited wave energy can be channeled to remote locations, and this means giving rise to industries and businesses. These remote areas will show strong economic growth going forward.
- The creation of a strongwave energy infrastructure can greatly help a country overcome the excess of dependence on fossil fuels. The fossil fuel market is largely volatile and could damage a country's economy in the event of a shortage. Wave energy is the foolproof way to fill this gap of volatility because it is cheap, reliable and efficient.

Disadvantages are:

- The construction of wave energy plants requires huge capital. Maintenance of energy plants, connection to the electricity grid, wave resources, reduction of the expected energy costs once the infrastructure is operational and in progress and the duration of the technology are just some of the variables that drive the cost of wave energy.
- The wave magnitude is so unpredictable in the seas. Sometimes it comes with a vengeance and could cause heavy wear and tear to the wave energy generation turbines. Damage to these equipment can be costly in terms of repair.
- Offshore wave energy projects are a lot more sophisticated than onshore ones. The projects include platforms, cables, turbines, interconnections, dredging and much more. From ecological standpoint, shallow waters are fertile breeding and resting grounds for most marine life. So, activities from construction and operation of the wave energy plant greatly affect marine ecosystem.

2.2 Worldwide wave energy

In order to evaluate the application of wave energy for electricity production it is essential to estimate how much is large the potential for utilization. When considering wave states (characterized by statistical wave parameters covering e.g. periods of 1000 waves) these are steadier than the wind field which generates the waves. The wave energy flux may exhibit significant variation in time and space, ranging from a few W/m up to some MW/m in extreme conditions (stormy). The wave level is also characterised by a significant seasonal variation[7].

Early estimates of the global available wave power indicated a total potential of 2,7 TW [8]. In “Assessing the global wave energy potential”[9], an updated study of the world wide wave energy potential is presented, broken down into regions of the world. Here, the global gross theoretical resource is estimated at about 3,7 TW, where 3,5 TW is the computed resource excluding areas with a benign wave climate (areas with less than 5kW/m), and the net resource (where also areas with potential ice cover is excluded) is about 3 TW; the total reduction from gross to net resource is the about 20%. In Europe there is a decrease of 25% from gross to net resource, mostly a result of ice coverage, the gross and net values being 381 and 286 GW, respectively. Thus, the total wave energy resource exceeds the global consumption of electricity[10].

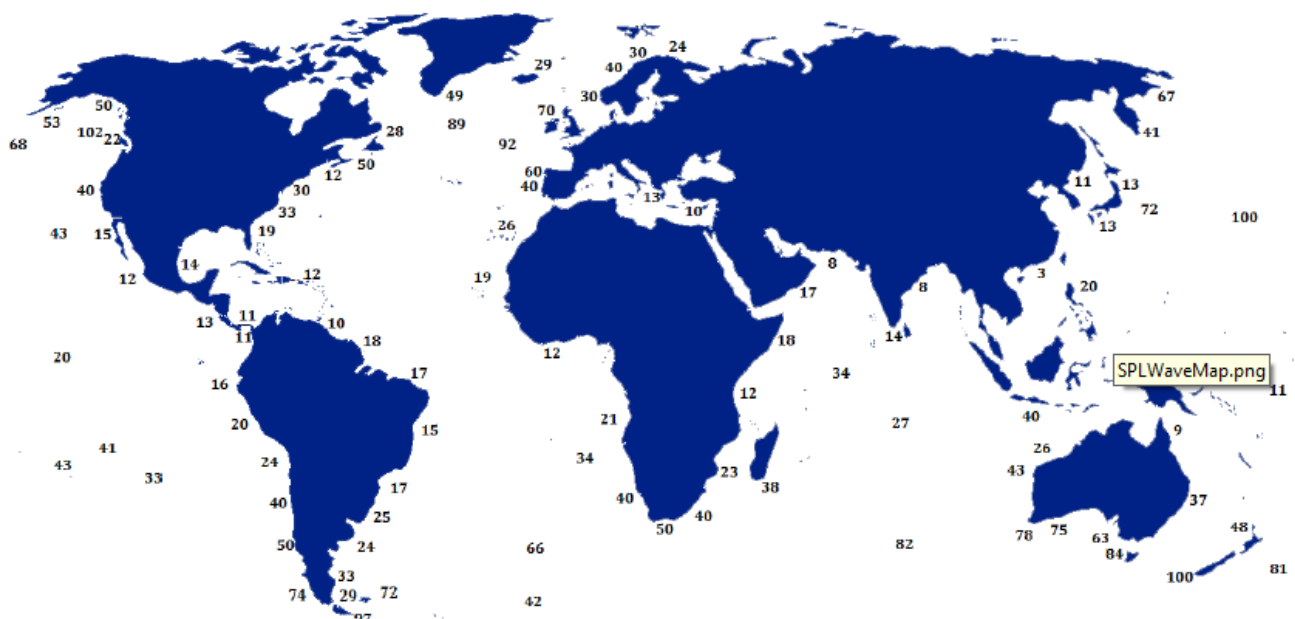


Figure 3: World energy map

In many regions of the world more local studies of the wave energy resource have been performed[11]. Here, not only the gross theoretical resource is estimated for the US, but also the total recoverable resource (under specific assumptions) is estimated to be 44% of the gross theoretical resource. So, if it is assumed that the numbers for the US can be applied worldwide it is reasonable to expect that the total recoverable global wave energy resource is approximately 2/3's of the global electricity consumption.

The interest in wave energy as a source of renewable energy is growing worldwide. This growing interest has led, over the past ten years, to investments in analysis of the sea state on the world's coastlines. An example of that is given in the quantification of the availability of energy from wave motion on a European scale that has been assessed in WERATLAS[12]. As a part of this project offshore wave energy statistics have been developed. The main data sources are the forecasts made with the mathematical model WAM and satellite altimetry data from ECMWF. A similar project named ONDATLAS was developed [13]. It consists in an atlas of energy for the Portuguese coast with a 20 meters depth focus. Today, the attention of the scientific community, is also focused on the development of protocols for the evaluation of the efficiency of the WECS and the potential of coastal sites. In the project EUROWAVES [14] some methods for the calibration of satellite data have been developed. Recently MEDATLAS, an atlas of the wind and waves for the Mediterranean sea, has been published by WEAO. It is also worth mentioning the project PRIST 2007 (Research Project of Relevant Interest Science and technology) in which a useful assessment of wave energy along the Italian coast was carried out. The main objectives of the project were to provide an accurate estimate of the potential energy around the Italian coast through the definition of a wave resource atlas and to increase the knowledge on this issue in Italy.

2.3 Wave characteristics

The assumptions that are made in order to linearized the wave equation are:

- The fluid is ideal;
- Surface tension effect are negligible;
- Waves are small.

The wave motion can be represented by a sinusoidal progressive wave and its characteristic are represented in the figure below[14].

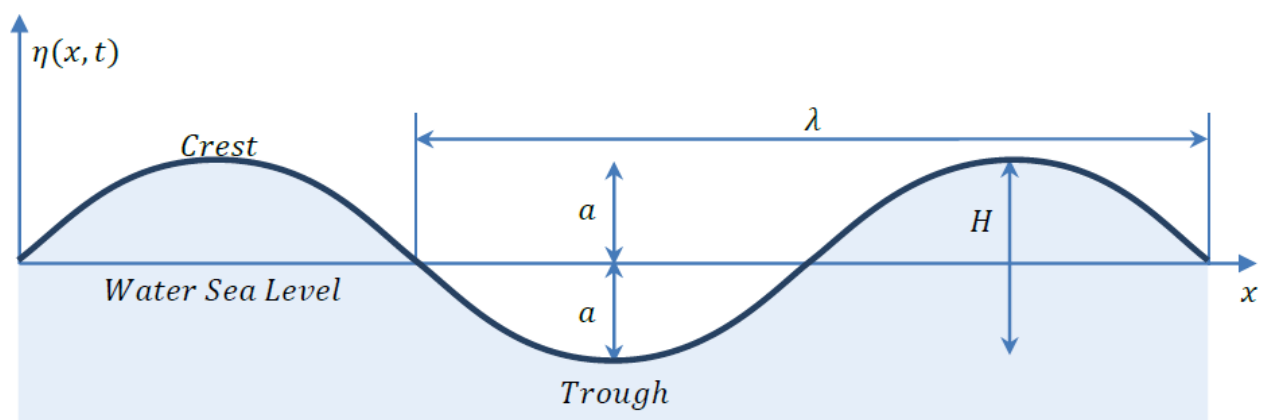


Figure 4: Wave characteristic

- Wave elevation $\eta(x, t)$ [m]: is the water surface profile and depends on the time and the position;

- Amplitude a [m]: is the magnitude of the maximum displacement from mean sea level;
- Height H [m]: is the difference in surface elevation between the wave crest and the previous one. For a simple sinusoidal wave is $H = 2a$;
- Wavelength λ [m]: is the horizontal distance between two crests;
- Period T [s]: is the time interval between two crests;
- Phase speed c [m/s]: is the speed at which the wave profile travels. For a simple sinusoidal wave is $c = \lambda/T$.

So the equation of a wave can be expressed as:

$$\eta(x, t) = \frac{H}{2} \sin(\omega t - kx)$$

Where k is the wave number and ω the wave natural frequency:

$$k = \frac{2\pi}{\lambda} \text{ [rad/m]}$$

$$\omega = \frac{2\pi}{T} \text{ [rad/s]}$$

The wave moves with speed c that is the ratio of the wave length by the wave period. Moreover it is related to the wave angular frequency and the wave number as follows:

$$c = \frac{\lambda}{T} = \frac{\omega}{k}$$

The main wave parameters are influenced from the water depth h . Indeed both the sea surface and deeper water particles are in motion when the wave propagates. The water particle describes orbital trajectories with highest diameter at the surface and reducing exponentially with depth. In deep water waves the particle paths are circular and the orbits are closed. As depth decreases, the sea floor begins to influence the waves and the motion becomes elliptical until it will be disrupted. The wave steepness is defined as H/λ . If such parameter is greater than 7 the wave becomes unstable and its crest breaks. As well as the if the velocity of the wave period is reduced the wave steepness increase. If such value overcome 7 the wave breaking occurs and this is what happens when the sea waves reach the beach. Below a depth corresponding to $\lambda/2$, the influence of the water particles at the bottom can be considered negligible and the wave is considered travelling in deep water.

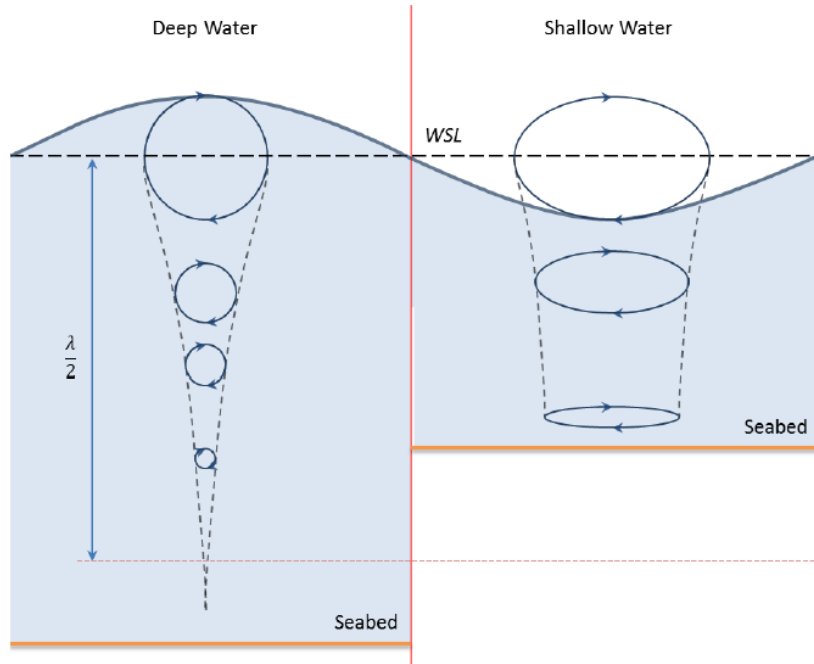


Figure 5: water particles trajectories for deep water (right) and shallow water (left)

According to the linear theory of gravity waves the phase velocity depend on both wavelength and water depth:

$$c = \sqrt{gh} \quad \text{for shallow water}$$

$$c = \frac{g}{2\pi} T \quad \text{for deep water}$$

Thus the wavelength could be related to the wave period in deep water as:

$$\lambda = cT = \frac{g}{2\pi} T^2 \approx 1,56 T^2$$

2.4 Wave Energy Converters (WEC)

The development of the wave energy converter dates back to a long time ago: the first attempts were made at the end of 1800[14].

In the modern era it was not considered until the energy crisis after which, in fact, in the '70s, the industry received a lot of interest, greatly enhanced by a Salter article in a scientific journal in 1974[15]. However, despite significant research efforts mainly in the UK, activities were reduced again until the 1980s and early 90's. At the end of the last millennium, activities have resumed new speed all over the world, although most of the efforts have been made in coastal European countries. In the last ten years the United Kingdom has again invested enormous resources in the development of marine renewable energy, including wave energy, and must now be considered the world leader in the sector.

2.4.1 WEC classification

There are several wave energy converters that can be grouped in different ways. Often the most used categorization is that based on [2]:

- *Terminators* are devices with large horizontal extensions parallel to the direction of wave propagation;
- *Attenuators* have large horizontal extensions orthogonal to the direction of wave propagation;
- *Point absorbers* are characterized by reduced horizontal dimensions compared to the predominant wavelength of the prevailing waves.

Wave energy converters can also be categorized by their location:

- Onshore, or shore mounted devices are nature terminators and are rigidly connected to land. Typical examples are oscillating waver columns and overtopping devices;
- Near – shore. It is located with ocean depth of 10 – 30 meters and typically has a distance of 0,5 – 2 km from coastline.
- Offshore: will generally be floating and have access to the waves unaltered by the presence of the seabed.

Classification of wave energy converters is also seen by their main working principles. The European Marine Energy Center at the Orkney Island is using six main types as shown in the next figure.

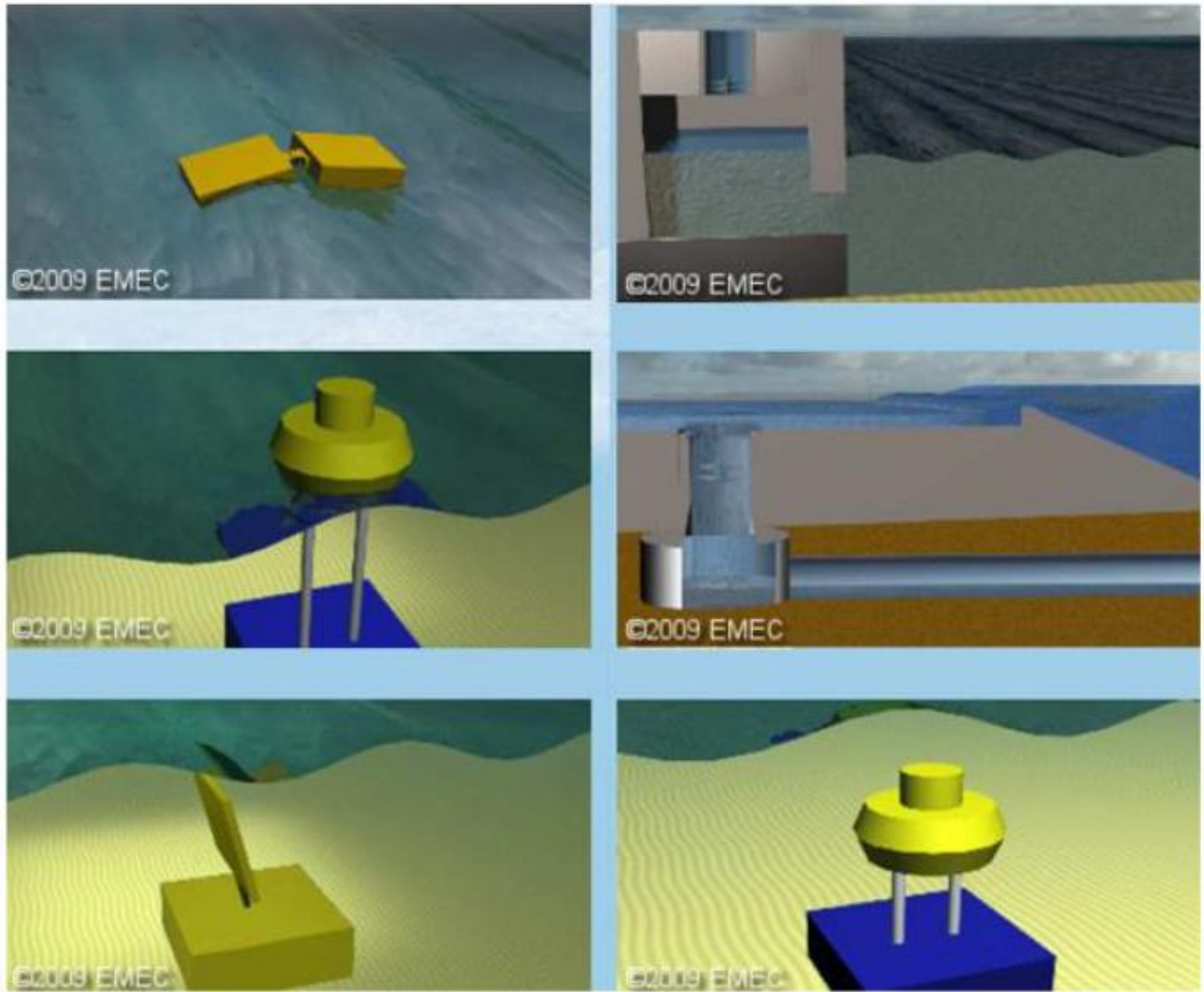


Figure 6: Six types of WEC

The indicated categories are [16], referring to figure 4:

- *Attenuator* (top left) it is a device positioned on the sea surface, placed in a parallel direction to the wave. it consists of two mechanical arms that move together with the wave and energy is accumulated from the relative movement of these two
- *Point absorber* (middle left) it consists of two parts: a float one on the sea surface and a fixed one on the seabed connected to each other by a mechanical arm. The relative movement of the floating part with respect to the fixed part is converted into energy. It is a device that absorbs energy from all directions (not only along the direction of the wave).
- *Oscillating wave surge converter* (bottom left) is completely immersed in water. It consists of a fixed part that stay on the seabed and an arm that oscillates like a pendulum towards the wave. The relative movement between the two parts generates energy.

- *Oscillating water column* (top right) is a structure partially immersed in water. The movement of the sea waves causes the ascent and descent of the water inside the column below. This movement generates a compression and expansion of the air above that goes into a narrower column passing through a turbine and making it rotate. Energy is obtained from the rotary movement.
- *Overtopping/ terminator device* (middle right) the water is captured inside a cistern where passing through a turbine will then be returned to the sea. The rotary motion of the turbine generates energy.
- *Submerged pressure differential device* (bottom right) is completely immersed in the sea. The movement of the waves makes the device rise and fall. This relative movement is transformed into energy through the presence of pressure pumps.
- *Bulge wave* (figure 6) consists of a rubber tube, placed in the direction of the wave, inside which the water enters. The wave entering in the tube generates pressure variations that create “bulges” which grow travelling inside the tube. Energy is collected to drive a standard low-head turbine located at the bow, where the water then returns to the sea.

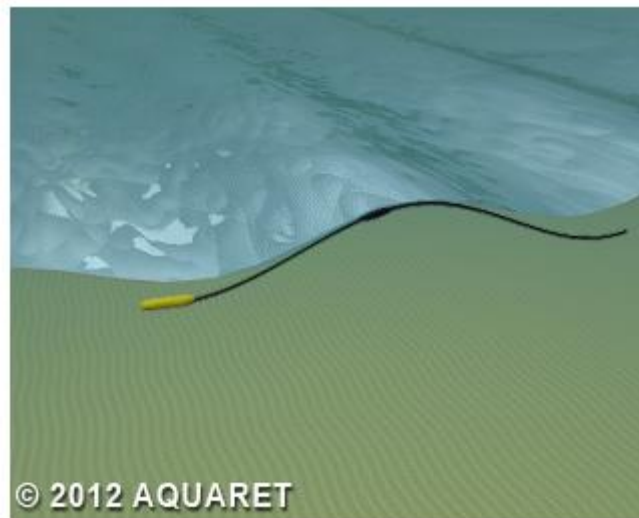


Figure 7: Bulge wave

- *Rotating mass* (figure 7) consists of a hull that moves along with the waves. This movement causes the precession movement of an eccentric mass or a gyroscope placed inside it. There is also an electric generator that stores energy.

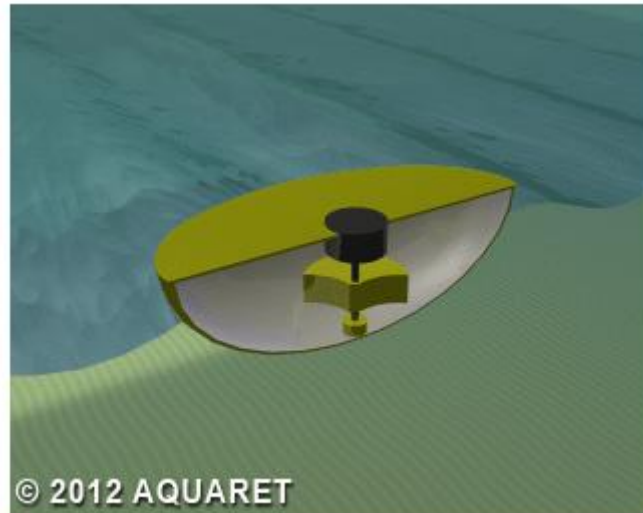


Figure 8: rotating mass

In order to obtain a more in-depth categorization of the WEC, additional guidelines were provided through the Equimar project which divides the WEC into further subsystems[17]. WECs are divided into the following subsystems:

- Primary energy extraction;
- Power take off / control system ;
- Reaction system;

For the development of WEC, Equimar has also drawn up an approach consisting of 5 basic steps through which it is possible to classify and study WECs. Every single step should provide necessary informations to the designer and the investors about the reliability of the project, technical analysis, component analysis, analysis of operations and finally a careful economic analysis[2].



Figure 9: The 5 stages of development of a WEC proposed by Equimar

3 Mathematical model of the behavior of a boat on a regular wave

ANSYS AQWA software was used to make a hydrodynamic study on the boat. Aqwa provides a toolset for investigating the effects of environmental loads on floating and fixed offshore and marine structure. Aqwa can simulate linearized hydrodynamic fluid wave loading on floating or fixed rigid bodies. The real –time motion of a floating body while operating in regular or irregular waves can be simulated, in which non linear Froude - Krylov and hydrostatic forces are estimated under instantaneous incident wave surface.

In the next paragraphs there is a description of the mathematical model adopted by ANSYS AQWA.

3.1 Notations and conventions

In hydrodynamic problems that include a fluid free – surface boundary, it is common practice to define a system of axes with the origin in the mean free surface of the fluid, as shown in figure 9.

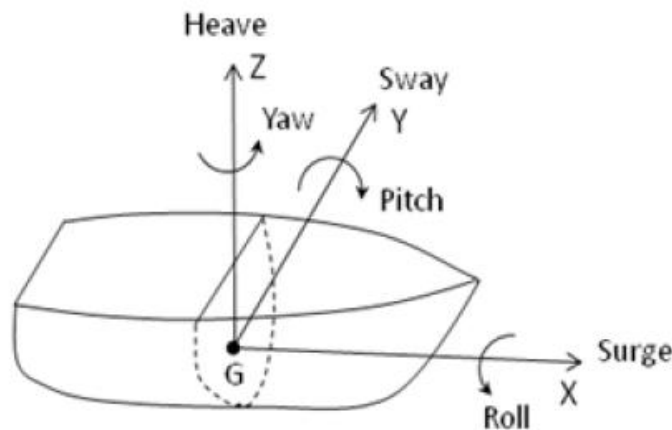


Figure 10: Definition of axis system

The six degree of freedom of a floating object in the open ocean are:

$$X = \begin{pmatrix} u_1 \\ u_2 \\ u_3 \\ \theta_1 \\ \theta_2 \\ \theta_3 \end{pmatrix} \begin{matrix} \text{surge (along } X) \\ \text{sway (along } Y) \\ \text{heave (along } Z) \\ \text{roll (about } X) \\ \text{pitch (about } Y) \\ \text{yaw (about } Z) \end{matrix}$$

3.2 Regular wave

Linear wave is considered and it is based on the assumption of:

- Homogeneous fluid;
- Incompressible fluid;
- Inviscid fluid;
- Irrotational flow;

In addition, the linear free surface condition is used hence the wave amplitude is assumed to be small compared to the wave length and water depth.

In the fixed reference axes (FRA), the water surface elevation at position X and Y can be expressed in complex value form as

$$\zeta = a_w e^{i[-\omega t + k(X \cos \chi + Y \sin \chi) + \alpha]} \quad (3.1)$$

Where:

- a_w is the wave amplitude;
- ω is the wave frequency in [rad/s];
- $k = 2\pi/\lambda$ is the wave number;
- χ is the wave propagation direction;
- α is the wave phase;

Since fluid is ideal and irrotational, the flow can be represented by a velocity potential satisfying the Laplace equation in the whole fluid domain. In finite depth water the velocity potential at the location $\vec{X} = (X, Y, Z)$ is

$$\phi_I(\vec{X}, t) = \varphi_I(\vec{X}) e^{-i\omega t} = -\frac{ig a_w \cosh [k(Z + d)]}{\omega \cosh (kd)} e^{i[-\omega t + k(X \cos \chi + Y \sin \chi) + \alpha]} \quad (3.2)$$

Where d is water depth and g is gravitational acceleration.

3.3 Buoyancy force

Buoyant forces are the result of summing up all the hydrostatic stresses acting on a submerged (or partially submerged) body [18].

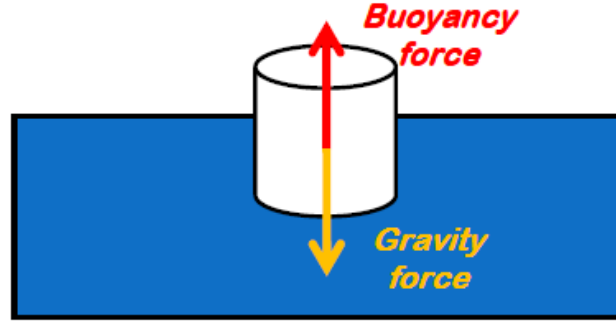


Figure 11: Buoyancy force [18]

Remembering the Archimedes' principle: "any object, wholly or partially immersed in a fluid, is buoyed up by a force equal to the weight of the fluid displaced by the object", the volume of displacement water can be determined by integrating over its submerged surface:

$$\nabla = \int_{S_0} Z n_3 dS \quad (3.3.1)$$

Where:

- S_0 is the wetted surface of the body in still water;
- $\vec{n} = (n_1, n_2, n_3)$ is the unit normal vector of the body surface pointing outwards;
- Z is the vertical coordinate of a wetted surface point in FRA

The buoyancy of a submerged body is the vertical up – thrust due to displacement of water:

$$F_B = \rho g \nabla \quad (3.3.2)$$

Where ρ is the water density and g is the gravitational acceleration.

And the center of buoyancy $\vec{X}_B = (X_B, Y_B, Z_B)$ can be calculated by

$$\vec{X}_B = \frac{1}{m} \int_V \rho(\vec{X}) \cdot \vec{X} dV = \frac{1}{m} \rho \int_{S_0} \vec{X} Z n_3 dS = \frac{\rho g \int_{S_0} \vec{X} Z n_3 dS}{F_B} \quad (3.3.3)$$

Where $\vec{X} = (X, Y, Z)$ is the location of a point on the submerged body surface in the FRA.

3.4 Hydrostatic Force

More generally, the hydrostatic force is referred to as the fluid loads acting on a body when placed in still water. The hydrostatic force can be calculated by integrating the hydrostatic pressure over the wetted surface of the body, up to the still water level. The expression of hydrostatic force is:

$$\overline{F}_{hys} = - \int_{S_0} p_s \vec{n} dS \quad (3.4.1)$$

Where $p_s = -\rho g Z$ is the hydrostatic pressure.

If we consider a *small displacement* \vec{X} hydrostatic force is the sum [18]:

$$F_{hys}(\vec{X}) = F_B(\vec{X}) + F_{gravity} \quad (3.4.2)$$

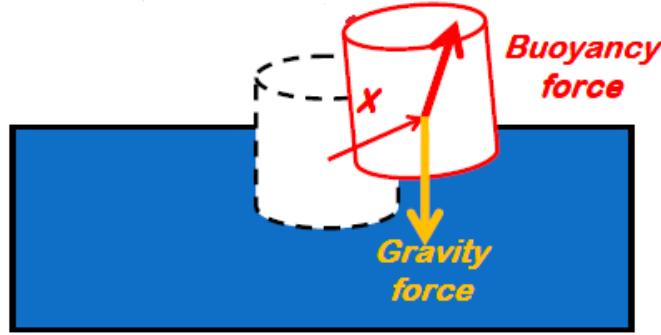


Figure 12: hydrostatic force after a small displacement [18]

And it can be modeled as a restoring force:

$$F_{hys}(\vec{X}) = -K_H X \quad (3.4.3)$$

Where K_H is the hydrostatic stiffness matrix:

$$K_H = \begin{pmatrix} 0 & 0 & 0 & 0 & 0 & 0 \\ 0 & 0 & 0 & 0 & 0 & 0 \\ 0 & 0 & K_{33} & K_{34} & K_{35} & 0 \\ 0 & 0 & K_{34} & K_{44} & K_{45} & 0 \\ 0 & 0 & K_{35} & K_{45} & K_{55} & 0 \\ 0 & 0 & 0 & 0 & 0 & 0 \end{pmatrix} \quad (3.4.4)$$

Where the various terms in the stiffness matrix are:

$$K_{33} = \rho g A_w$$

$$K_{44} = \rho g \int_{A_w} (y - y_B)^2 dS$$

$$K_{34} = \rho g \int_{A_w} (y - y_B) dS$$

$$K_{45} = -\rho g \int_{A_w} (x - x_B)(y - y_B) dS$$

$$K_{35} = -\rho g \int_{A_w} (x - x_B) dS$$

$$K_{55} = \rho g \int_{A_w} (x - x_B)^2 dS$$

The hydrostatic stiffness matrix specifies how the net weight and buoyancy load on the vessel varies with

$$X = \begin{pmatrix} u_1 \\ u_2 \\ u_3 \\ \theta_1 \\ \theta_2 \\ \theta_3 \end{pmatrix} \begin{matrix} \text{surge (along } X) \\ \text{sway (along } Y) \\ \text{heave (along } Z) \\ \text{roll (about } X) \\ \text{pitch (about } Y) \\ \text{yaw (about } Z) \end{matrix}$$

relative to the vessel in its datum configuration. Only surge, sway, heave, roll, pitch and yaw are specified, all the other components are zero.

The hydrostatic stiffness matrix, K_H , encodes how the weight and buoyancy loads on the vessel change due to small changes in the vessel's position and orientation. Two effects contribute to K_H : the change in load due to the change in the submerged volume of the vessel when it moves, and the change in moment caused by movement of the vessel's centre of gravity and centre of buoyancy when it moves. As stated, the hydrostatic stiffness matrix is only applicable for small changes in the vessel's position and orientation.

3.5 Excitation force: sum of Froude – Krylov and diffraction forces

Considering a regular wave propagating at the free surface as in the equation (4.1) and an unsteady pressure associated with a regular wave at the free surface (in deep water),

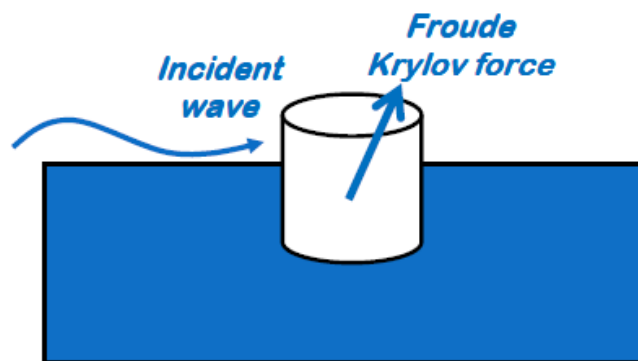


Figure 13: Froude - Krylov force [18]

We can define the Froude – Krilov force as the force on the body introduced by the unsteady pressure field generated by the undisturbed wave field [18]:

$$F_{FK}(t) = - \iint_{S_B} p \vec{n} dS \quad (3.5.1)$$

Where :

- S_B is the wetted surface on the surface body;
- p is the pressure in the undisturbed waves;
- \vec{n} the body's normal vector pointing into the water

When an incident wave encounters a body, there will be a generation of diffracted waves that can be seen on the free surface.

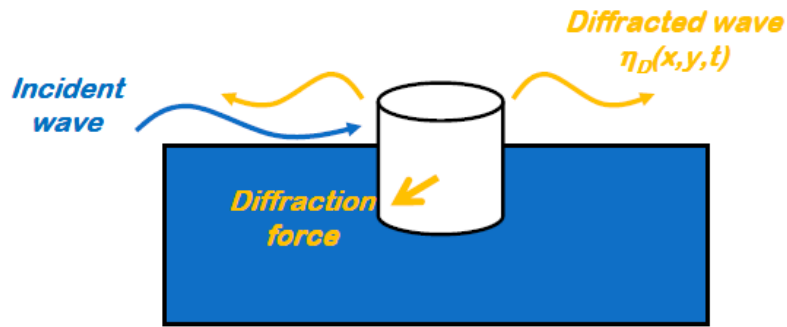


Figure 14: Diffraction forces [18]

In the fluid unsteady pressure field $p_D(x, y, z)$ associated with the diffracted wave field the diffraction force is defined as:

$$F_D(t) = - \iint_{S_B} p_D \vec{n} dS \quad (3.5.2)$$

Excitation force is the sum of the Froude – Krylov force and the diffraction force

$$F_{ex}(t) = F_{FK}(t) + F_D(t) \quad (3.5.3)$$

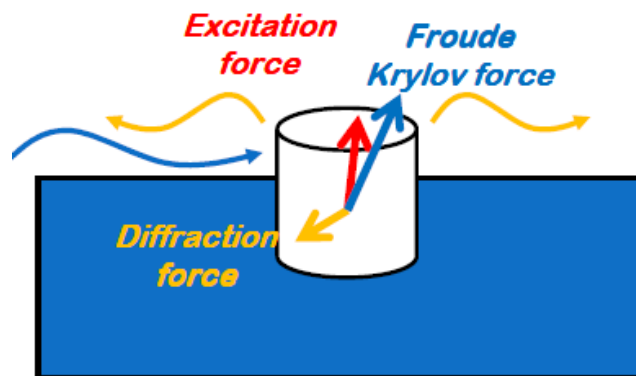


Figure 15: Excitation force [18]

3.6 Radiation force

Unsteady motion of the buoy generates radiated waves. Let V be the velocity vector of the buoy and $\eta_R(x, y, t)$ the radiated waves [18].

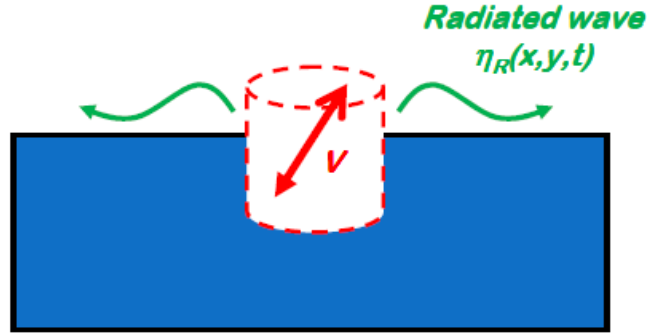


Figure 16: Radiated wave [18]

The fluid is characterized by unsteady pressure field $p_R(x, y, z, t)$ associated with the radiated wave field and the radiation force is defined as:

$$F_R(t) = - \iint_{S_B} p_R \vec{n} dS \quad (3.6.1)$$

Radiation force is split in two parts: the first one has a part proportional to the acceleration of the buoy, where the coefficient $[A]$ is the *added mass matrix* and it can be seen as the added mass of water which is carried out by the body in its motion. The *damping part* corresponds to the energy that is sent in the far field (radiated) [18].

3.7 Drag force

If the flow gets detached from the body, vortices are generated in the flow.

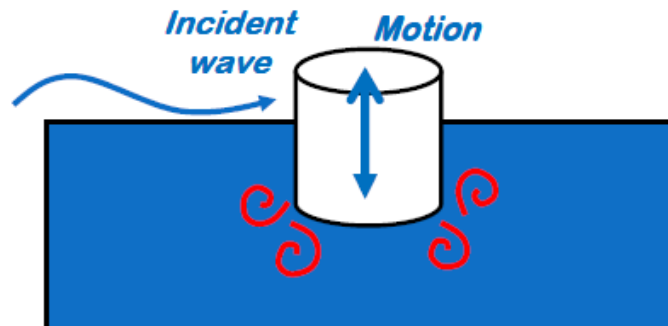


Figure 17: Generation of vortices [18]

It will happen, especially when the buoy (or in general the vessel) has sharp corners. It can happen even with rounded corners, if the buoy is small in comparison with the fluid motion.

Energy is transferred from the motion to the vortices and the drag force is described by this equation:

$$F_V = -\frac{1}{2}\rho[C_D]A|V|V \quad (3.7.1)$$

Where:

- ρ is the density of water;
- V is the relative velocity;
- A is the reference area, is typically the projection of the body on a plane perpendicular to the direction of motion;
- C_D is the drag coefficient is a function of the number of Reynolds and the number of Keulegan – Carpenter (it is referred to the geometry of the body immersed).

3.8 Boundary element method (BEM)

The main theoretical assumptions and limitations of linear potential theory employed in ANSYS AQWA are listed below:

- The body or bodies have zero or very small forward speed;
- The fluid is inviscid and incompressible, and the fluid flow is irrotational;
- The incident regular wave train is of small amplitude compared to its length;
- The motions are to the first order and hence must be of small amplitude. All body motions are harmonic[19].

3.8.1 General formula in zero forward speed

The fluid flow field surrounding a floating body by a velocity potential is defined by:

$$\phi(\vec{X}, t) = a_w \varphi(\vec{X}) e^{-i\omega t} \quad (3.8.1)$$

Where a_w is the incident wave amplitude and ω is the wave frequency[19].

In equation (4.8.1), the dependent term $\varphi(\vec{X})$ can be separated into contributions from the radiation waves due to six basic modes of body motion, the *incident wave* and the *diffracted wave*. The potential functions are complex but the resultant physical quantities such as fluid pressure and body motions in time domain analysis will be obtained by considering the real part only.

The potential function due to *incident*, *diffraction* and *radiation waves* may therefore be written as:

$$\varphi(\vec{X})e^{-i\omega t} = \left[(\varphi_I + \varphi_d) + \sum_6^{j=1} \varphi_{rj}x_j \right] e^{-i\omega t} \quad (3.8.2)$$

Where:

- φ_I is the first order incident wave potential with unit wave amplitude;
- φ_d is the corresponding diffraction wave potential;
- φ_{rj} is the radiation wave potential due to the j-th motion with unit motion amplitude[19].

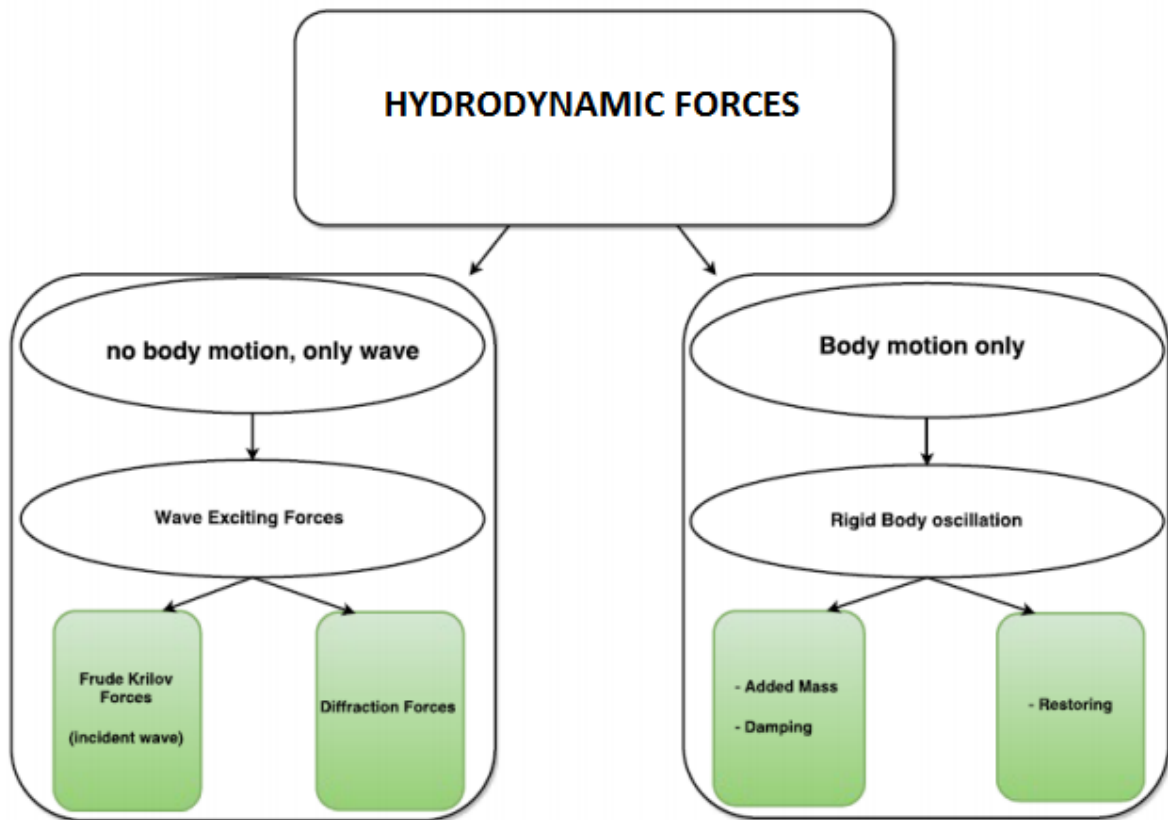


Figure 18: Decomposition of the hydrodynamic problem in sea keeping

When the wave velocity potentials are known, the first order hydrodynamic pressure distribution may be calculated by using the linearized Bernoulli's equation,

$$p^{(1)} = -\rho \frac{\partial \varphi(\vec{X}, t)}{\partial t} = i\omega \rho \varphi(\vec{X}) e^{-i\omega t} \quad (3.8.3)$$

From the pressure distribution, the various fluid forces may be calculated by integrating the pressure over the wetted surface of the body. To have a general form for the forces and moments acting on the body, we extend the notation of unit normal vector of hull surface into six components corresponding to the six basic rigid body motions. Employing this notations,

the first order hydrodynamic force and moment components can be expressed in a generalized form[19]:

$$F_j e^{-i\omega t} = - \int_{S_0} p^{(1)} n_j dS = [-i\omega\rho \int_{S_0} \varphi(\vec{X}) n_j dS] e^{-i\omega t} \quad (3.8.4)$$

Where S_0 is the mean wetted surface of the body.

From equation (4.8.2), the total first order hydrodynamic force can be written as

$$F_j = [(F_{Ij} + F_{dj}) + \sum_{k=1}^6 F_{rjk} x_k] \quad (3.8.5)$$

Where $j=1,6$ and the j -th Froude – Krylov force due to incident wave is

$$F_{Ij} = -i\omega\rho \int_{S_0} \varphi_I(\vec{X}) n_j dS \quad (3.8.6)$$

The j -th diffracting force due to diffraction wave is

$$F_{dj} = -i\omega\rho \int_{S_0} \varphi_d(\vec{X}) n_j dS \quad (3.8.7)$$

The j -th radiation force due to the radiation wave induced by the k -th unit amplitude body rigid motion is

$$F_{rjk} = -i\omega\rho \int_{S_0} \varphi_{rk}(\vec{X}) n_j dS \quad (3.8.8)$$

Fluid forces can be further described in terms of reactive and active components. The active force, or the wave exciting force, is made up of the Froude – Krilov force and the diffraction force. The reactive force is the radiation force due to the radiation waves induced by body motions[19].

The radiation wave potential, φ_{rk} , may be expressed in real and imaginary parts and substituted into equation (4.8.8) to produce the added mass and wave damping coefficients

$$\begin{aligned} F_{rjk} &= -i\omega\rho \int_{S_0} \{Re[\varphi_{rk}(\vec{X})] + i Im[\varphi_{rk}(\vec{X})]\} n_j dS \quad (3.8.9) \\ &= \omega\rho \int_{S_0} Im[\varphi_{rk}(\vec{X})] n_j dS - i\omega\rho \int_{S_0} Re[\varphi_{rk}(\vec{X})] n_j dS \\ &= \omega^2 A_{jk} + i\omega B_{jk} \end{aligned}$$

Where the added mass and damping are:

$$A_{jk} = \frac{\rho}{\omega} \int_{S_0} \text{Im}[\varphi_{rk}(\vec{X})] n_j dS \quad (3.8.10)$$

$$B_{jk} = -\rho \int_{S_0} \text{Re}[\varphi_{rk}(\vec{X})] n_j dS \quad (3.8.11)$$

3.8.2 Boundary conditions

Let's write the boundary condition of the potential velocity as follow[20]:

Where the flow velocity V derives from a potential function ϕ (irrotational flow)

$$V = \nabla\phi$$

1. Fluid is incompressible, Laplace equation:

$$(\nabla\phi)^2 = 0$$

2. Kinematic condition of the linearized free surface (S_{FS}):

$$\frac{\partial z}{\partial t} = \frac{\partial\phi}{\partial z}$$

3. Kinematic condition on the seabed, horizontal seabed (S_{bottom}):

$$\frac{\partial\phi}{\partial z} = 0 \text{ per } z = -h$$

4. Dynamic condition on the surface (S_{FS}), tells us that the pressure on the surface must be equal to the atmospheric pressure:

$$\rho \frac{\partial\phi}{\partial t} + \rho g z = 0$$

5. Limit condition on the body (S_B):

$$\frac{\partial\phi}{\partial n} = \vec{V} \vec{n}$$

Then deriving condition 4 with respect to the time:

$$\frac{\partial^2\phi}{\partial t^2} + g \frac{\partial z}{\partial t} = 0$$

And putting condition 3 in the last equation, we obtain:

$$\frac{\partial^2\phi}{\partial t^2} + g \frac{\partial\phi}{\partial z} = 0$$

That is considered as the only one condition on the free surface.

So summing up the boundary condition, we get:

$(\nabla\phi)^2 = 0$	Laplace
----------------------	---------

$\frac{\partial z}{\partial t} = \frac{\partial \phi}{\partial z}$	Kinematic condition on S_{bottom}
$\frac{\partial \phi}{\partial z} = 0$	Per $z=-h$, kinematic condition on S_{bottom}
$\frac{\partial^2 \phi}{\partial t^2} + g \frac{\partial \phi}{\partial z} = 0$	Dynamic condition on the surface S_{FS}
$\frac{\partial \phi}{\partial n} = \vec{V} \vec{n}$	Surface body S_B

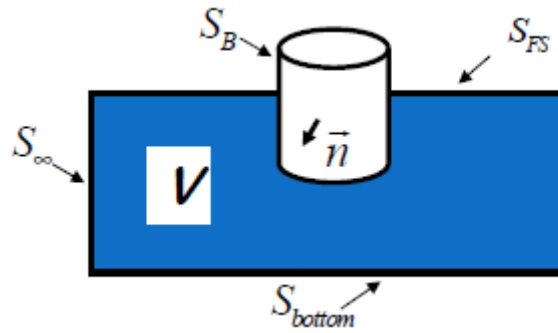


Figure 19: Superficies described by the boundary conditions [18]

Dividing the total potential in wave incident potential and perturb potential:

$$\phi = \phi_i + \phi_p \quad (3.8.2.1)$$

Where the perturb potential is defined as:

$$\phi_p = \phi_D + \sum_{i=1}^N \phi_R \quad (3.8.2.2)$$

It is possible to extend the boundary conditions also to diffracted potential and body motion potential:

- Incident potential ϕ_i

$\frac{\partial \phi_i}{\partial z} = 0$	Per $z=-h$, kinematic condition on S_{bottom}
$\frac{\partial^2 \phi_i}{\partial t^2} + g \frac{\partial \phi_i}{\partial z} = 0$	Dynamic condition on the surface S_{FS}

- Diffracted potential ϕ_D

$\Delta\phi_d = 0$	In the domain D
$\frac{\partial\phi_d}{\partial n} = -\frac{\partial\phi_i}{\partial n}$	$i=1,\dots,n$ on the body
$\frac{\partial\phi_d}{\partial z} = 0$	Per $z=-h$, kinematic condition on S_{bottom}
$\frac{\partial^2\phi_d}{\partial t^2} + g\frac{\partial\phi_d}{\partial z} = 0$	Dynamic condition on the surface S_{FS}
$\phi_d \rightarrow 0$	To infinite

- body motion potential

$\Delta\phi_r = 0$	In the domain D
$\frac{\partial\phi_r}{\partial n} = \vec{V} \cdot \vec{n}$	$i=1,\dots,n$ on the body
$\frac{\partial\phi_r}{\partial z} = 0$	Per $z=-h$, kinematic condition on S_{bottom}
$\frac{\partial^2\phi_r}{\partial t^2} + g\frac{\partial\phi_r}{\partial z} = 0$	Dynamic condition on the surface S_{FS}
$\phi_r \rightarrow 0$	To infinite

Now it is possible to define the Green's function and apply the solution of the problem of body motion; the whole treatment is reported in [19] and [20].

3.8.3 Solutions and equation of motion

Because of linearization:

- wave steepness is supposed to be small respect to its wave length $H/\lambda \ll 1$

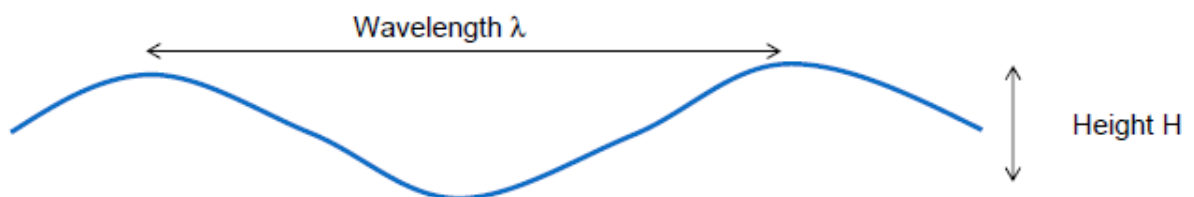


Figure 20: Linearized wave [18]

- body motions around its mean position are small $\frac{x}{D} \ll 1$

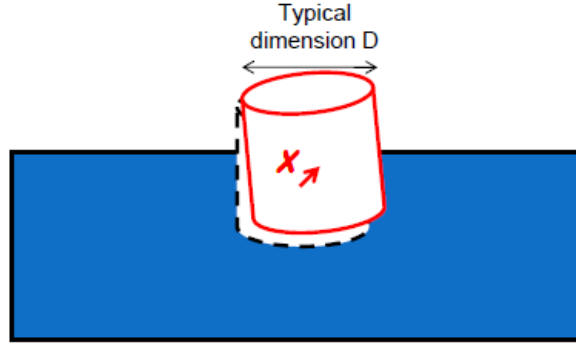


Figure 21: Small displacements of a body [18]

the potential of a moving body in the waves is the sum of the potential calculated separately.

$$\phi_{total} = \phi_{incident} + \phi_{diffraction} + \phi_{radiation} \quad (3.8.3.1)$$

Solution is usually calculated in the frequency domain.

So mathematical expression of radiation and diffraction forces in linear potential theory in frequency domain are:

- For a *regular wave*

$$\eta(t) = A\Re(e^{-i\omega t}) \quad (3.8.3.2)$$

The excitation force is given by:

$$F_{ex}(t) = A\Re(\widehat{F}_{ex}(\omega)e^{-i\omega t}) \quad (3.8.3.3)$$

Where \widehat{F}_{ex} is the force transfer function. It is a six rows vector (three translations and three rotations).

$$\widehat{F}_{ex}(\omega) = \begin{pmatrix} \widehat{F}_{ex,1} \\ \widehat{F}_{ex,2} \\ \widehat{F}_{ex,3} \\ \widehat{F}_{ex,4} \\ \widehat{F}_{ex,5} \\ \widehat{F}_{ex,6} \end{pmatrix}$$

- For a *regular motion* the radiation force is given by

$$F_{radiation}(t) = -A(\omega)\ddot{X}(t) - B(\omega)\dot{X}(t) \quad (3.8.3.4)$$

- For an *arbitrary motion*, the radiation force is given by

$$F_{radiation}(t) = -\mu_{\infty}\ddot{X}(t) - \int_0^t K_{rad}(t-\tau)\dot{X}(\tau)d\tau \quad (3.8.3.5)$$

So, finally, the equation of motion is:

- In time domain

$$(M + \mu_{\infty})\ddot{X} + \int_0^t K_{rad}(t-\tau)\dot{X}(\tau)d\tau + K_H X = F_{ex}(t) \quad (3.8.3.6)$$

- In frequency domain

$$(M + A(\omega))\dot{X}(\omega) + B(\omega)\dot{X}(\omega) + K_H X(\omega) = \widehat{F}_{ex}(\omega) \quad (3.8.3.7)$$

3.9 Definition of RAO

The above forces (hydrodynamic, inertial, damping, Froude – Krylov, diffraction forces) can be assembled in the equation 4.8.3.7, where $\widehat{F}_{ex}(\omega)$ is the harmonic excitation force proportional to the incident wave [21]

$$\zeta = \zeta_0 e^{i\omega t} \quad (3.9.1)$$

Here ζ_0 is the wave amplitude.

If we assume

$$X = X_0 e^{i\omega t} \quad (3.9.2)$$

Is possible to derive

$$-(M + A(\omega))\omega^2 X_0 e^{i\omega t} + i\omega B(\omega)X_0 e^{i\omega t} + K_H X_0 e^{i\omega t} = F_0 e^{i\omega t} \quad (3.9.3)$$

And we obtain

$$RAO(\omega) = \frac{F_0}{K_H - (M + A(\omega))\omega^2 + i\omega B(\omega)} \quad (3.9.4)$$

The amplitude of the RAO represents the motion amplitude per unit wave amplitude

$$RAO = \frac{X_0}{\zeta_0} \quad (3.9.5)$$

So RAO is a transfer function that is only defined when the ship motions can be assumed to be linear. From the below figure we have an example where RAO is the amplitude of response per unit of *input* of a linear system for a given period/frequency:

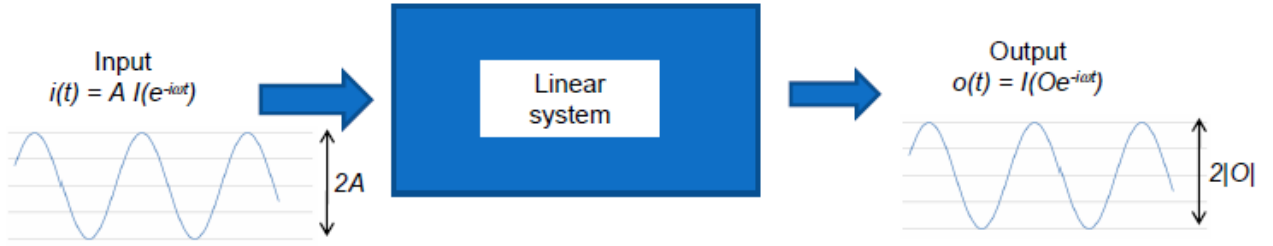


Figure 22: Definition of RAO

Where:

$$RAO = \frac{|O|}{A} \quad (3.9.6)$$

3.10 Corrections for small forward speed

Using a reference frame moving with the forward speed of a structure, the coordinate of a point in this reference frame satisfies [19]

$$\vec{X} = \vec{U}t + \vec{x} \quad (3.10.1)$$

Where:

- $\vec{U} = (U_1, U_2, 0)$ is the forward speed of the structure with respect to the fixed reference axes (FRA),
- \vec{X} is the coordinate of the point with respect to the FRA,
- \vec{x} is the coordinate of the point with respect to the moving reference frame.

The total unsteady fluid potential varies with the encounter frequency:

$$\phi(\vec{X}, t) = a_w \phi(\vec{x}) e^{-i\omega_e t} \quad (3.10.2)$$

Where the *encounter frequency* can be given as

$$\omega_e = \omega - \frac{\omega^2 U}{g} \cos\beta \quad (3.10.3)$$

Where

- $U=|\vec{U}|$
- β is the heading angle between the vessel forward speed and wave propagation direction.

In this moving reference frame the linear free surface equation is satisfied like:

$$(-i\omega_e + \vec{U} \cdot \nabla)^2 \varphi + g \frac{\partial \varphi}{\partial z} = 0 \quad (3.10.4)$$

Where $z=0$.

Similar to equation 4.8.5 through equation 4.8.9, we have the j-th Froude – Krylov force due to incident wave

$$F_{Ij} = -\rho \int_{S_0} \{(i\omega_e + \vec{U} \cdot \nabla)\varphi_I(\vec{x})\}n_j dS \quad (3.10.5)$$

The j-th diffracting force due to diffraction wave

$$F_{dj} = -\rho \int_{S_0} \{(i\omega_e + \vec{U} \cdot \nabla)\varphi_d(\vec{x})\}n_j dS \quad (3.10.6)$$

And the j-th radiation force due to the radiation wave induced by the k-th unit amplitude body rigid motion

$$\begin{aligned} F_{rjk} &= \omega_e^2 A_{jk} + i\omega_e B_{jk} = -\rho \int_{S_0} \{(i\omega_e + \vec{U} \cdot \nabla)\varphi_{rk}(\vec{x})\}n_j dS \quad (3.10.7) \\ &= -i\rho\omega_e \int_{S_0} \left\{ \left(n_j + \frac{i}{\omega_e} \vec{U} \cdot \nabla n_j \right) \varphi_{rk}(\vec{x}) \right\} dS \end{aligned}$$

For a more complete discussion refer to the ANSYS AQWA manual [19].

4. Hydrodynamic analysis of the hull

Two tests were carried out with ANSYS AQWA, one with an incident wave in the longitudinal direction with respect to the hull and another in a transversal direction. The individual tests were carried out with different forward speed values.

4.1 Characteristics of the hull

The hull is very similar to that of a *displacement hull* (figure 24, type A), where the pre-exuberance below the vessel consists of the *keel* (figure 25), a long slim plank that provides an underwater balancing force that keeps the boat from tipping over.

The *displacement hulls* are mainly used for large boats that travel for a long period at low forward speed. This type of hull offers a great resistance to water, being structurally a type of hulls more robust and heavy, greater balance and greater solidity. Obviously, these types of hulls are not practical for any type of boats that are born to run at a relatively high speed, given their high resistance to the wave, and consequently a great friction. Their main characteristic is the resistance to the motion of the boats themselves, so this is indicated for greater maneuverability and sea – keeping [22].

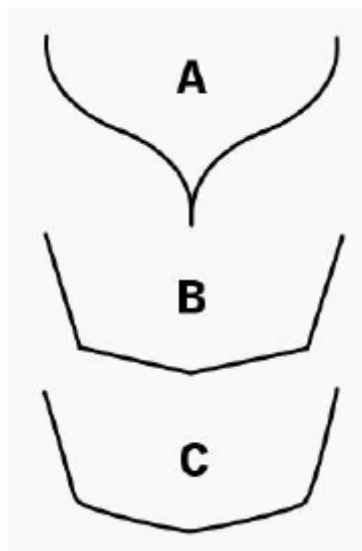


Figure 23: Hull's shape. Type A: displacement hull

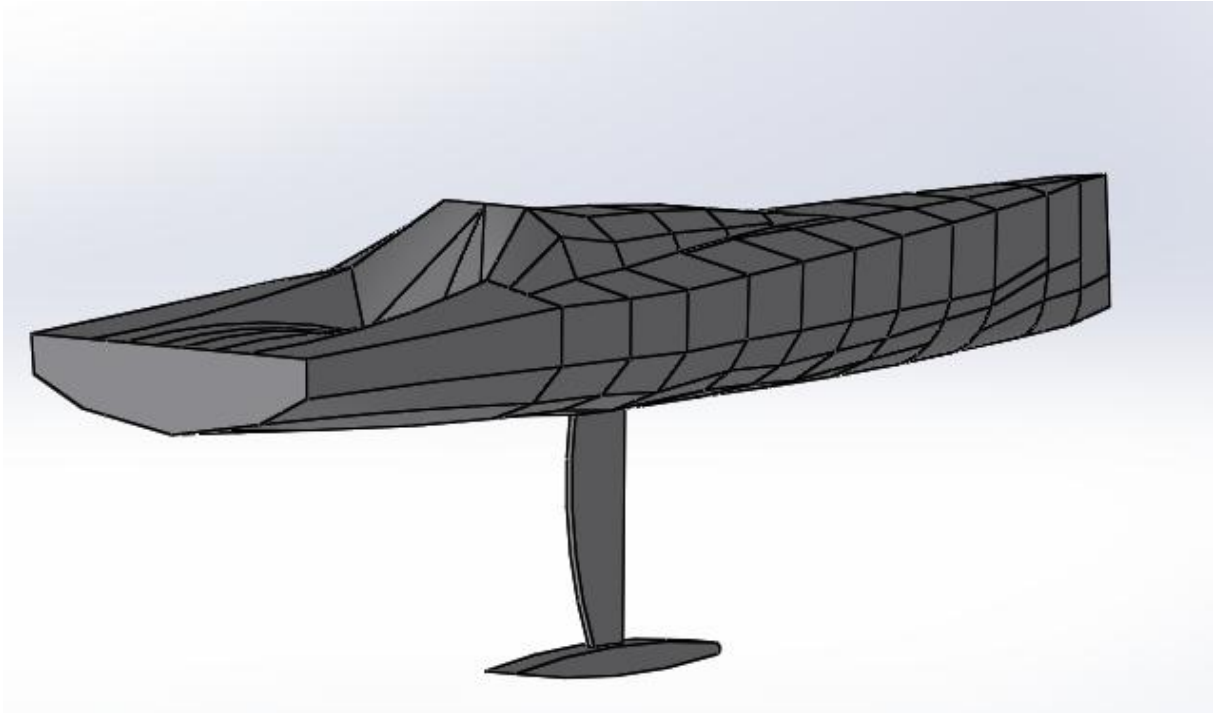


Figure 24: Hull of the sailboat

The main characteristics are:

Mass	4500 kg
Length	12 m
Width	3,2 m

In order to better understand the geometry of the sailing ship it is good to define the fineness coefficients that can be used in the design phase. In the next paragraphs the fineness coefficients have been calculated.

4.1.1 Fineness Coefficient of the transversal section

It is obtained by the value of transversal section divided by the area of the rectangle circumscribed:

$$C_M = \frac{A_M}{B_M T_M} = 0,1$$

Where:

- $A_M = 0.82 \text{ m}^2$;
- $B_M = T_M = 3 \text{ m}$;

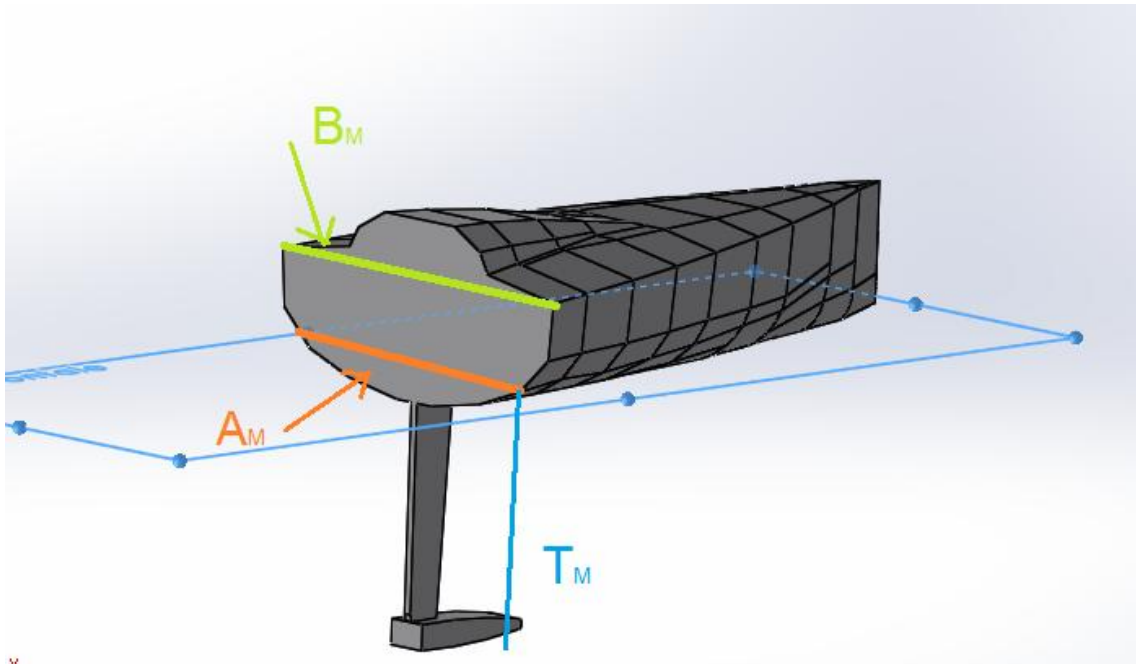


Figure 25: Transversal section of the hull

4.1.2 Fineness Coefficient of the floating section

It is the relationship between the area of the floating figure and the rectangle circumscribed in it:

$$C_{wl} = \frac{A_w}{B_{wl}L_{wl}} = 0.67$$

Where:

- $A_w = 25,5 \text{ m}^2$
- $B_{wl} = 3,19 \text{ m}$
- $L_{wl} = 12 \text{ m}$

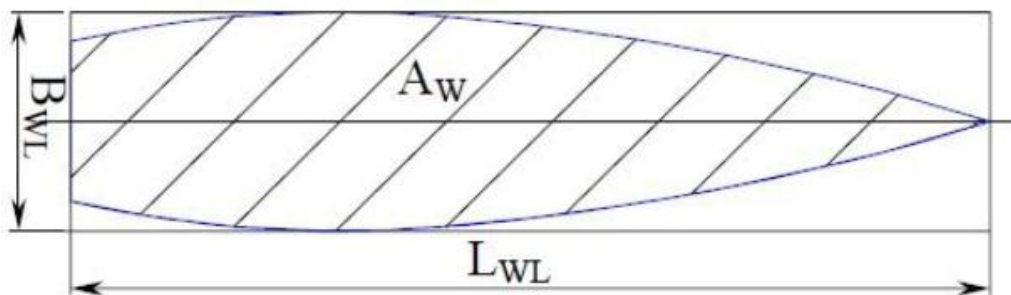


Figure 26: Floating section of the hull

4.1.3 Fineness Coefficient of longitudinal section

It is the ratio between the area of the longitudinal figure and the rectangle in it circumscribed:

$$C_{lp} = \frac{A_{lp}}{T L_{wl}} = 0,13$$

Where:

- $A_{lp} = 4,72 \text{ m}^2$

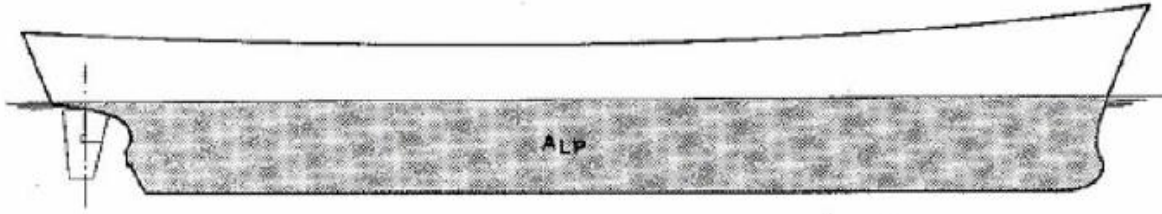


Figure 27: Longitudinal section of the hull

4.1.4 Approximate calculation of moments of inertia

When the longitudinal mass distribution is not known, an approximate method based on Pavlenko's formula has been used to calculate the longitudinal moment of inertia:

$$I_{yy} = 0,065 C_{wl} M L^2 = 28220 \text{ Kg m}^2$$

Where:

- M is the mass of the hull;
- L is the length of the hull;
- C_{wl} is the fineness coefficient of the floating section;

While for the calculation of I_{xx} we have used the empiric formula:

$$I_{xx} = k_{xx}^2 M = 7326 \text{ kg m}^2$$

Where:

- $k_{xx} = 0,4 B$, approximation of the radius of the inertia;

The moment of inertia along z axis I_{zz} is assumed equal to I_{yy} .

4.1.5 Stabilization diagram

From the static of rigid bodies we know that a necessary and sufficient condition for a body to be in equilibrium is that: the sum of the forces acting on the body is zero, the sum of the moments of these forces with respect to a point is zero.

On a totally or partially immersed body two forces act: the weight force and the vertically directed hydrostatic thrust (Archimedes thrust) upwards which counterbalances the gravity force.

The stability of a body depend on two main aspects:

- The position of the center of gravity
- The shape of the body.

If the body starts to rotate, due to an external force, the center of buoyancy (point B) changes its position. The shift of point B depends on the shape of the hull and the relative position between the center of gravity G and B determines the type of equilibrium: stable (figure,a), neutral (figure, b), unstable equilibrium (figure, c).

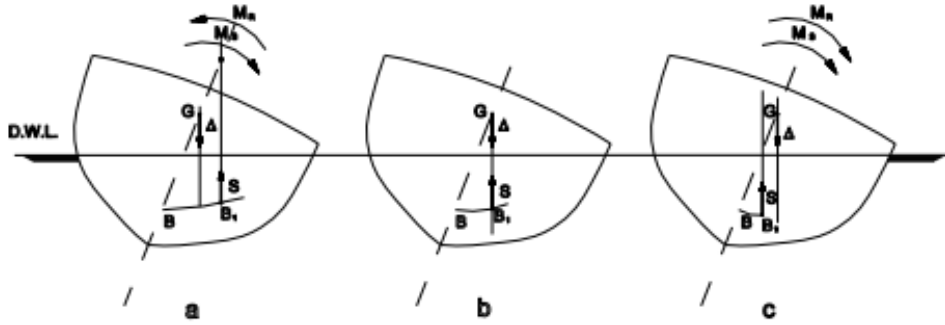


Figure 28: Stable, neutral, unstable equilibrium

If the equilibrium is stable the moment is *righting* but if the equilibrium is unstable the moment is *heeling*.

When the body rotates, for small degrees, is possible to approximate the curve from B to B₁ as a circumference with the center of curvature in M. In order to have the stable equilibrium M must stay over G and higher is the distance between them (r) higher is the righting momentum. So it is possible to write:

$$M_R = \Delta \cdot b = \Delta \cdot \overline{GH} = \Delta \cdot \overline{GM} \text{sen} \alpha = \Delta \cdot (r - a) \text{sen} \alpha$$

$$M_R = \Delta \cdot (r - a) \text{sen} \alpha$$

Where $\Delta = V\rho g$ (V is the portion of the hull under the water plane and $\rho = 1025 \text{ kg/m}^3$). Therefore higher is the value (r-a) higher will be the righting momentum.

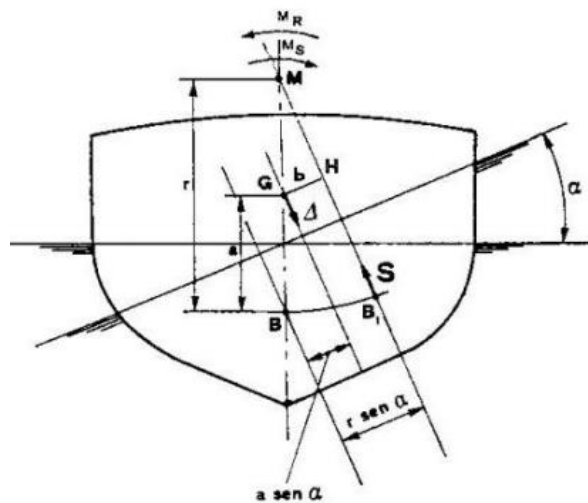


Figure 29: Relation between B, G, M

The stabilization diagram represents the momentum in function of the rotation angle α computed by the previous equation. There are two equilibrium position, at $\alpha = 0$ and at $\alpha = \alpha_c$ in which there is the *statical overturning*. Instead for $\alpha > \alpha_c$ the momentum becomes negative.

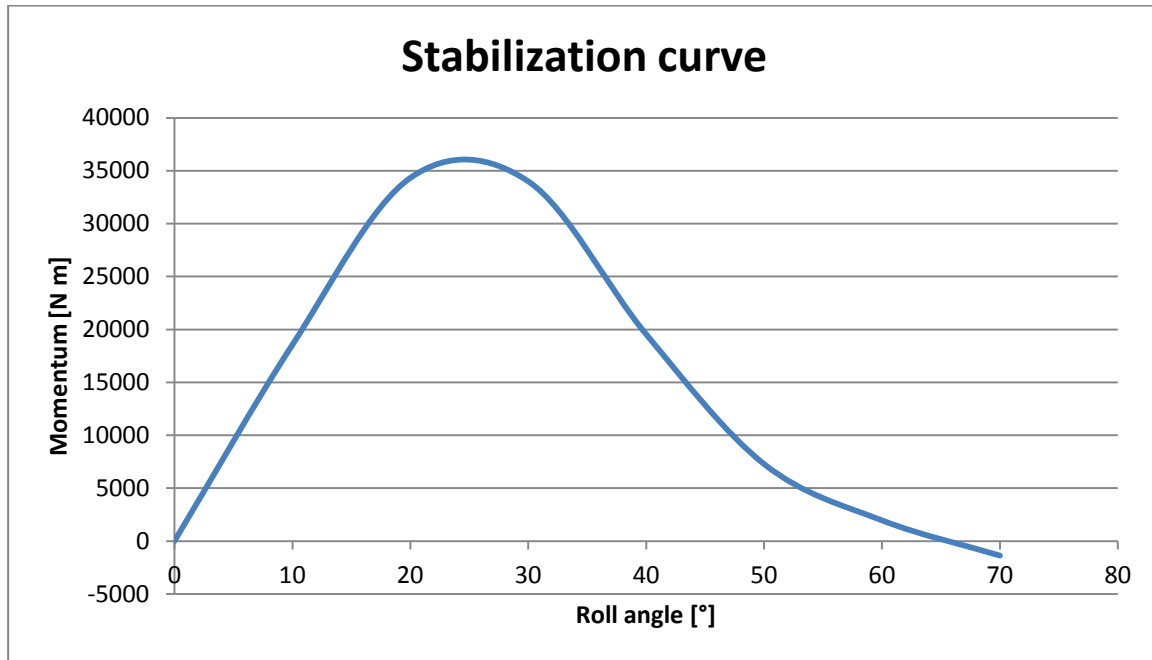


Figure 30: Stabilization curve

From the graph we can see that after $\alpha = 23^\circ$ the momentum is negative, we must avoid this condition.

4.2 Characteristics of the incident wave

We adopt a *regular wave* as described in 4.2 paragraph. Its characteristic are an amplitude of 1m and we analyze the intervals period from 2s to 12s.

4.3 Longitudinal incident wave: results

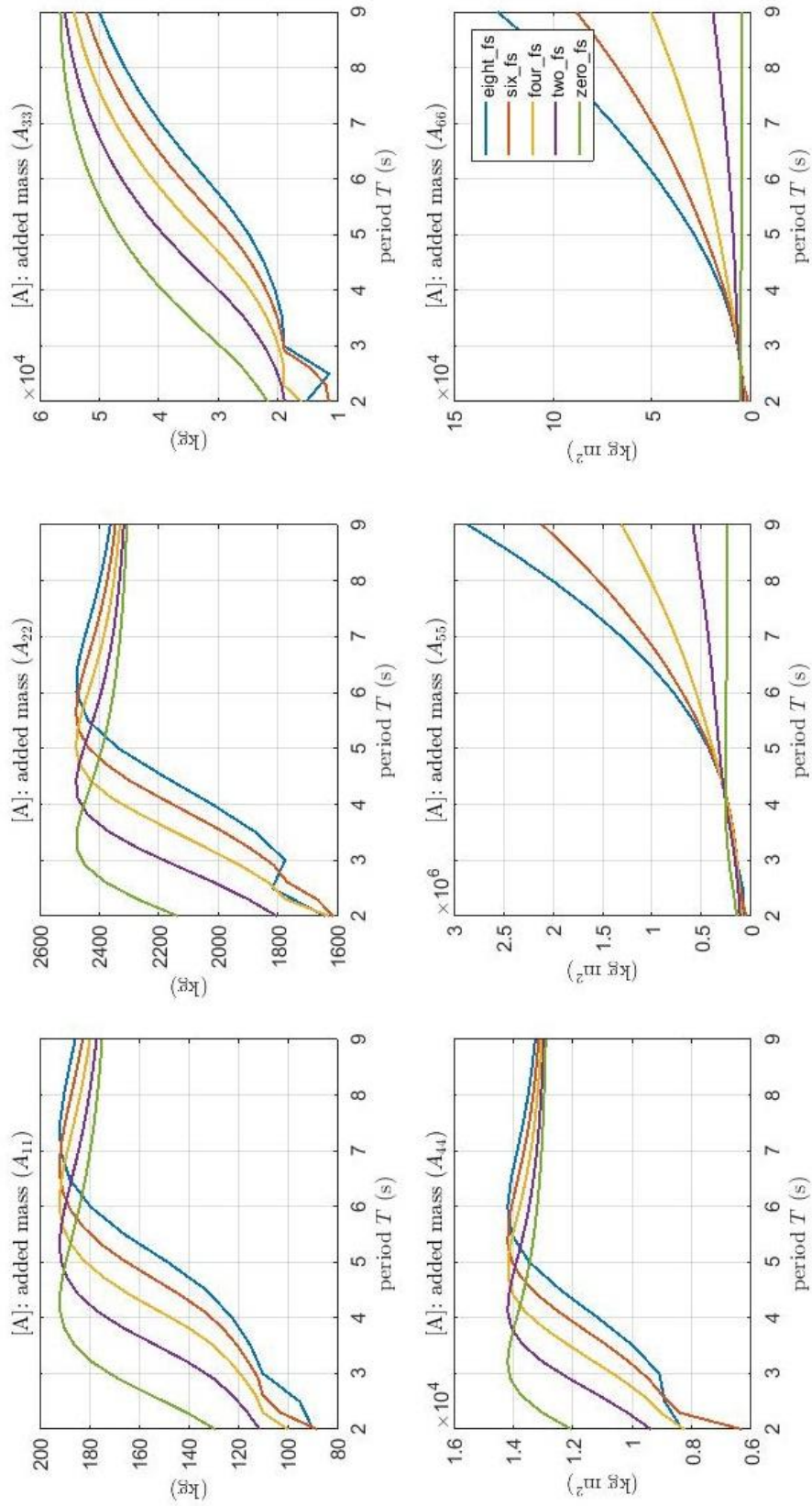


Figure 31: Added mass in pitching degree

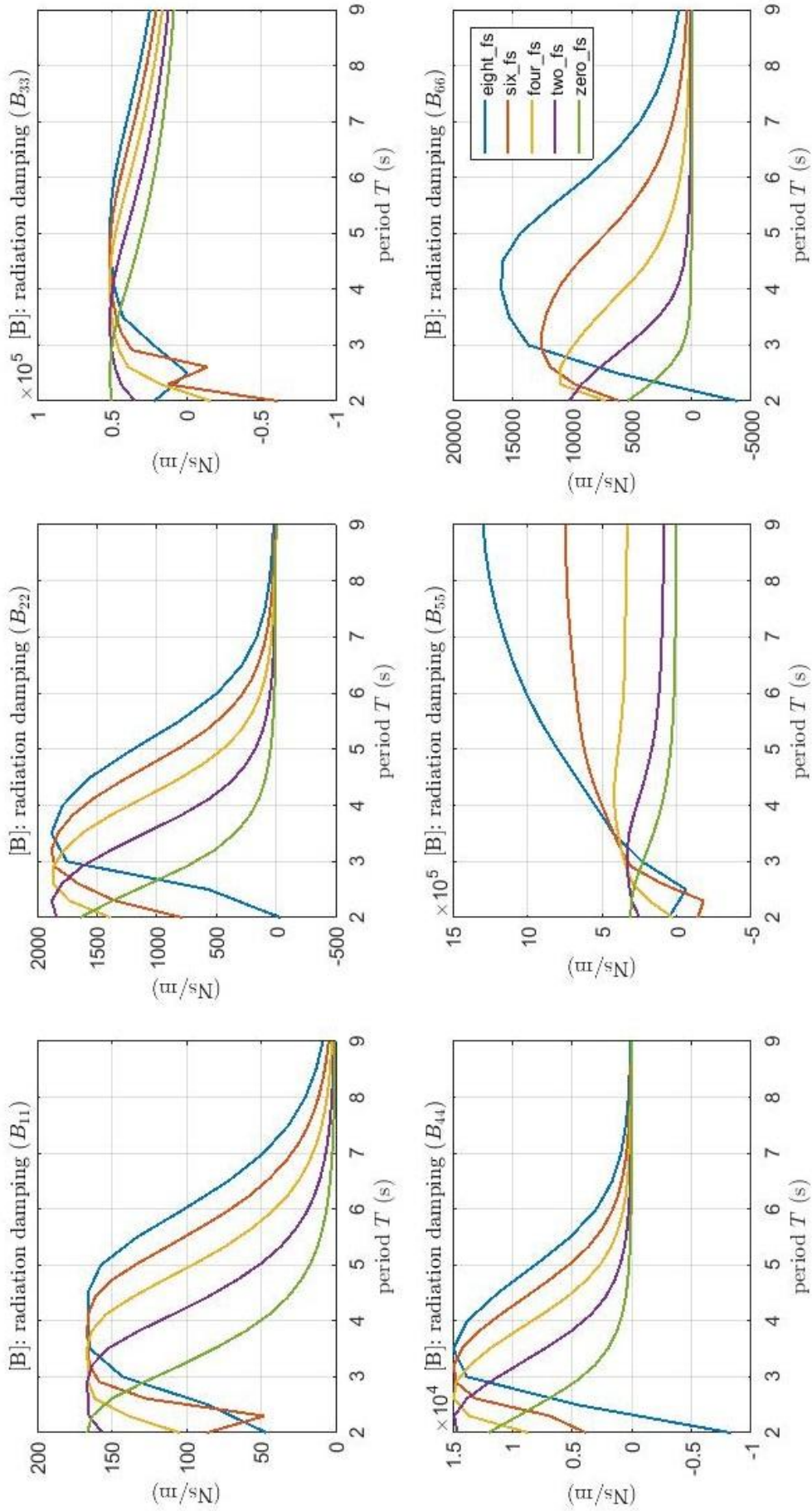


Figure 32: Damping in pitching degree

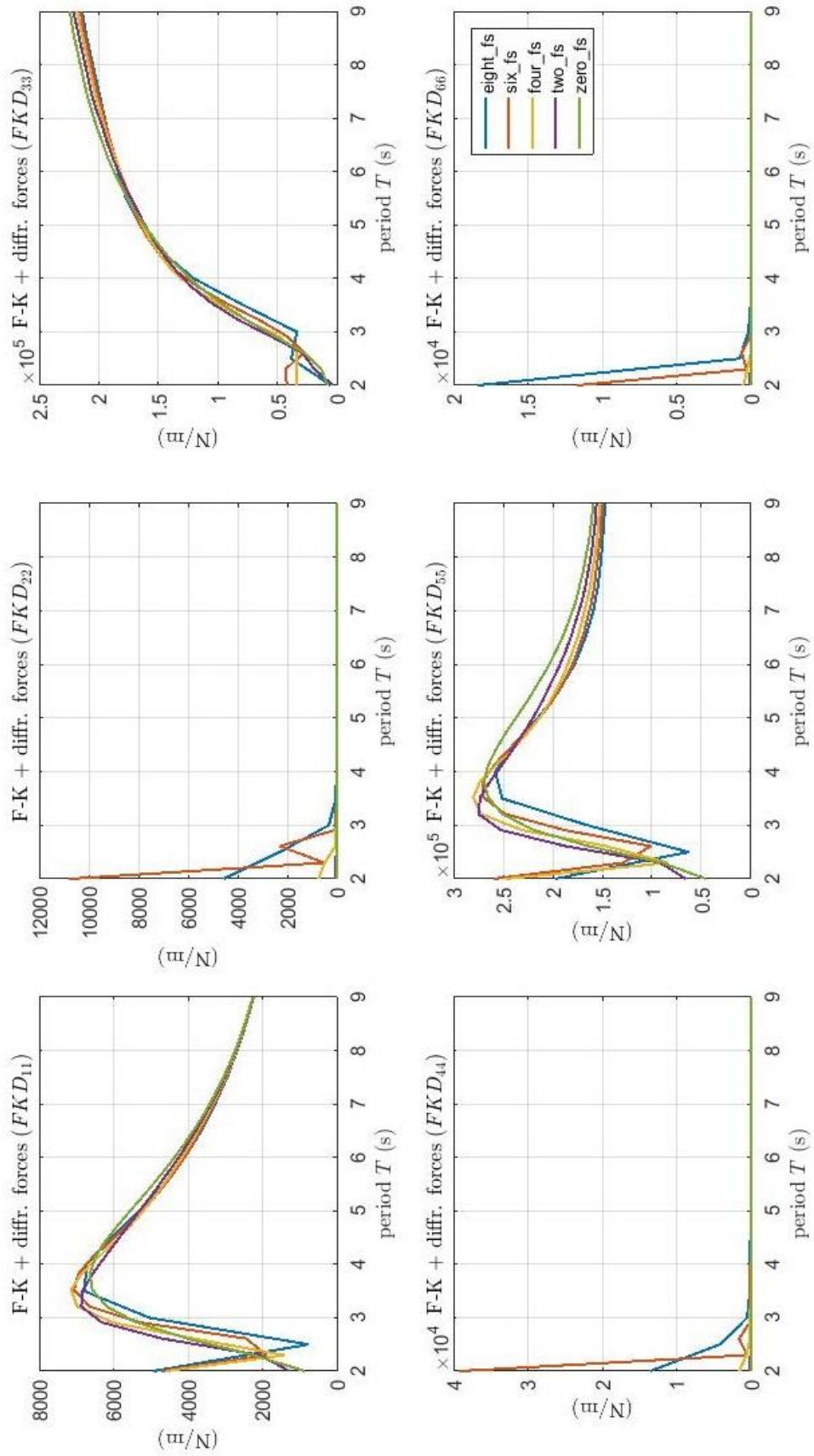


Figure 33: Froude - Krylov and Diffraction forces in pitching degree

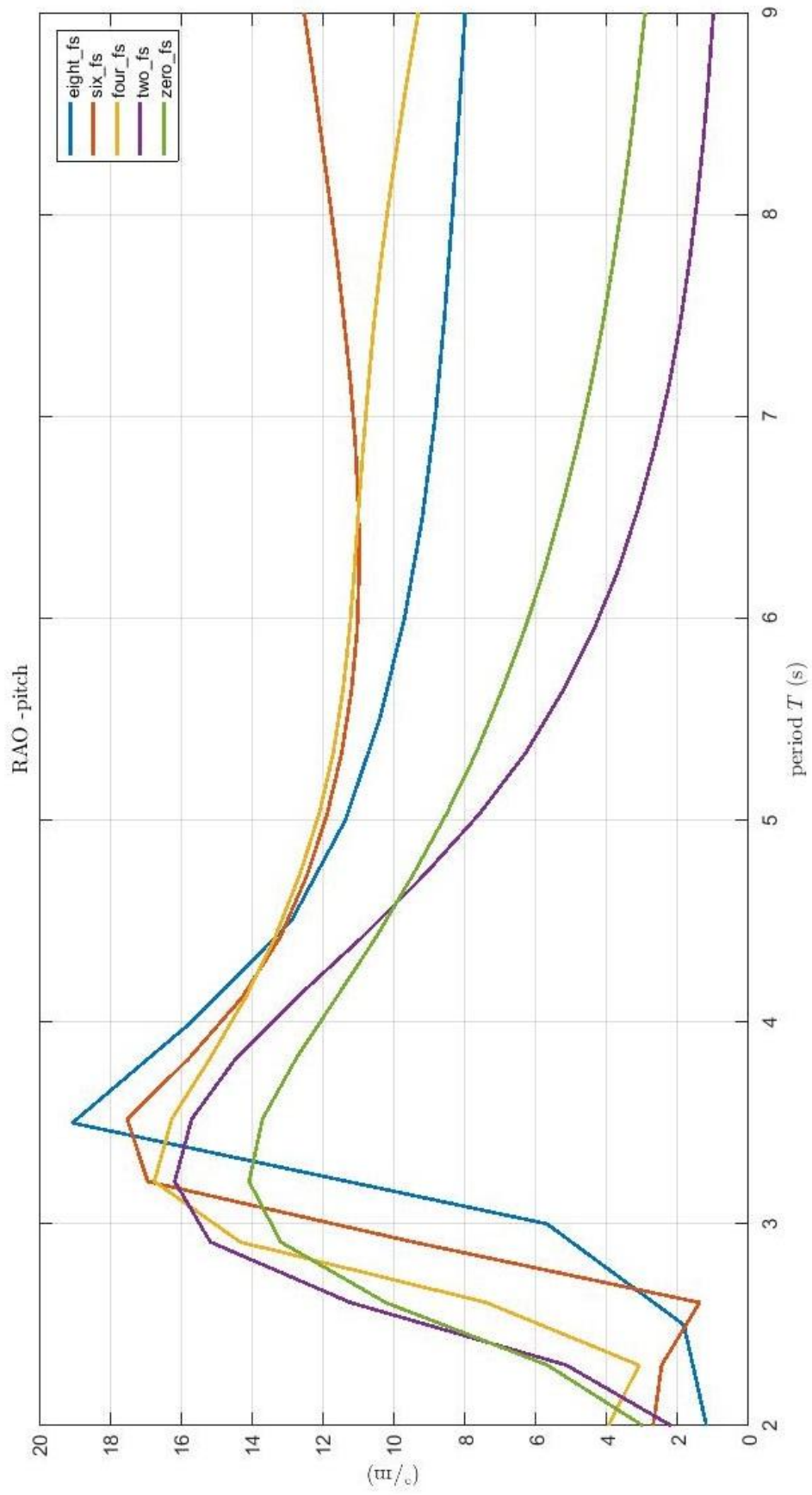


Figure 34: RAO in pitching motion

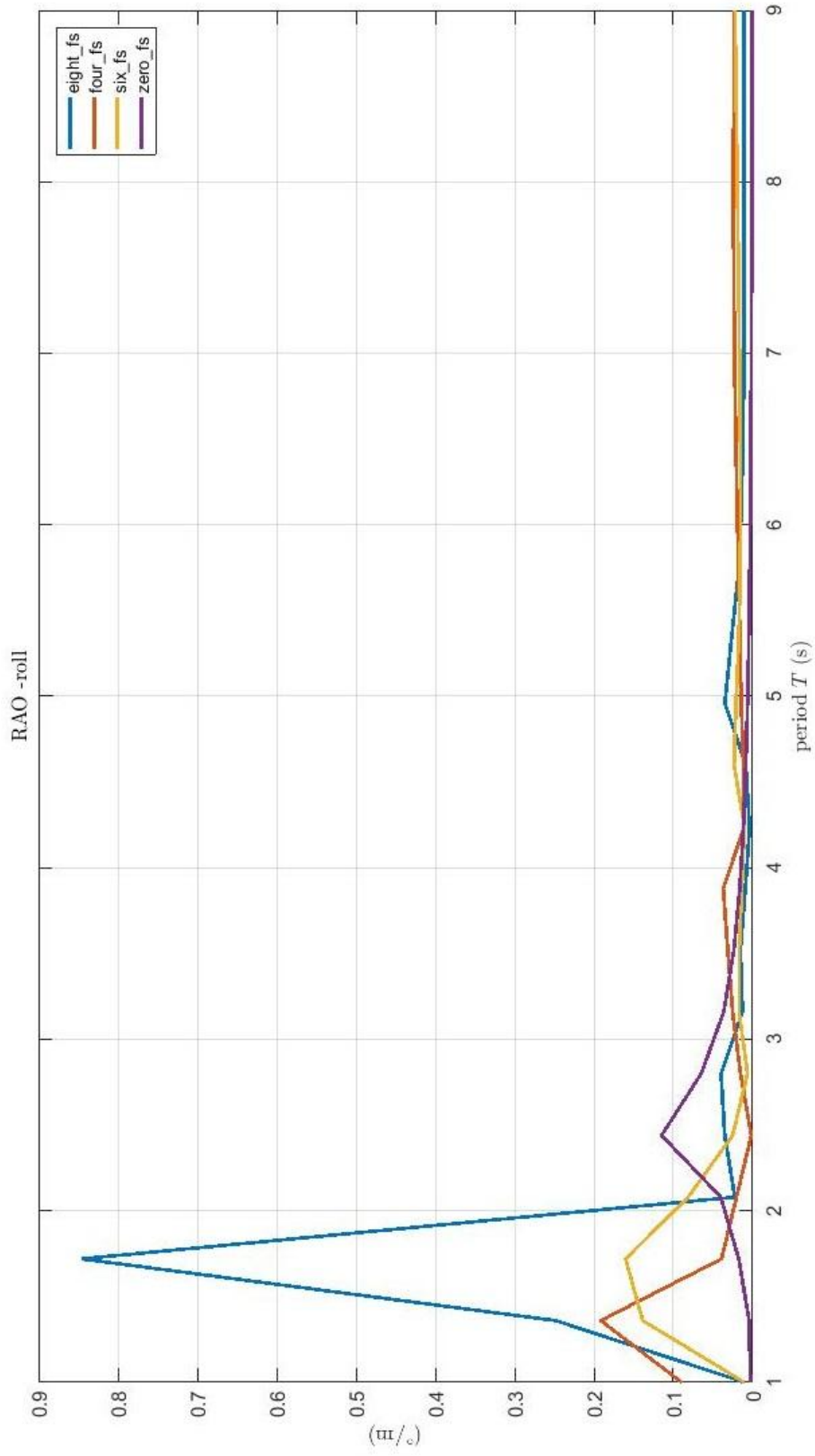


Figure 35: RAO in roll motion

4.3.1 Considerations

The *added mass* can be seen as the added mass of water which is carried by the hull in its motion instead damping corresponds to the energy that is sent in the far field (*radiated energy*). These two contributions make up the *radiation force*. They form, mathematically speaking, two matrices 6x6 where on the diagonals there are the calculated elements by ANSYS AQWA in the graphs ($A_{11}, A_{22}, A_{33}, A_{44}, A_{55}, A_{66}, B_{11}, B_{22}, B_{33}, B_{44}, B_{55}, B_{66}$), for each translations (surge, sway, heave) and rotations (roll, pitch, yaw). Since we are considering an *incident longitudinal wave* to the hull, we will analyze the *pitching degree of freedom* so we will take account only the A_{55} coefficient of the added mass matrix and B_{55} coefficient of damping matrix.

Another important premise that must be made is that these tests are carried out with different forward speed of the hull and since the numerical evaluation of the translating – pulsating Green’s function is very time consuming, the experience suggest us to maintain a value of Froude number $<0,3$. From this observation, applying the inverse formula:

$$v = Fn \sqrt{gL}$$

Where:

- Fn is the Froude number = 0,3
- g is the gravitational acceleration
- L is the length of the hull

Is possible to obtain the maximum velocity (3,6 m/s) beyond which the results could present some errors.

Analyzing the graph of the added mass, A_{55} , we can see that with waves characterized by a relatively small period (until 4.2 s) the effect of the change in the forward speed is indifferent because, as we can see, the value of added mass is almost constant. Instead with waves characterized by a higher period (over 4.2 s) the forward speed of the hull has an increasingly incisive value. This is closely linked to the concept of *hydrodynamic resistance*. We get the maximum added mass value with the maximum forward speed (8m / s) because higher is the hull’s speed, higher would be the hydrodynamic resistance (remembering the equation 4.7.1) and so, consequently, the adhesion condition of the fluid particles on the hull will be more incisive (i.e. the hull will carry with itself more mass).

Then analyzing the radiation damping graph, B_{55} , we can see that as the incident wave and the forward speed of the hull increase, the radiation damping assumes higher and higher values. This means that the relative speed between wet body and water is high, consequently there is a strong dissipation of energy due to the fact that the hull cannot follow perfectly the path of the wave.

Our hull is subject to the action of the waves so there is the presence of additional forces of pressure (in addition to hydrostatic, damping and inertia forces) that play the role of excitation

forces, which are the sum of the Froude - Krylov and diffraction forces. The Froude – Krilov forces hypothesize that at every point of the immersed surface of the hull acts a pressure whose intensity is equal to that exercised by the wave motion, in the same point, if the hull was not there (*hypothesis of the ghost ship*) [23]. The diffraction forces correct the inaccuracy of the Froude - Krylov hypothesis, on the independence from the wave pressure from the presence of the ship (or not), and take into account the effect of the impenetrability of the hull to the fluid particles. In fact, the fluid particles that approach the hull are forced to change speed and direction so that the incident waves are partially reflected and diffracted by the obstacle present on their way. From the graph we can see that the effect of forward speed on the excitation forces is indifferent because all the curves maintain almost the same values and trends. A peak is recorded at about 3.5 s of period, at the same point where the RAO is maximum. This means that the rotations of the hull around the y-axis (pitch) are elevated as a consequence higher will be the generation of diffracted waves that run off from the hull to the far field (increase in diffraction forces). Furthermore, this wave motion generates a greater hydrostatic pressure than that which we would have in still water (increase of the forces of Froude - Krilov).

Then analyzing the graph of the RAO (in pitching motion), figure 27, we can observe that as the forward speed increases, the RAO tends asymptotically (for high wave periods) to higher values. The relative speed between wet vehicle and water increases with increasing forward speed. Then positioning on the hull reference system, the wave period decreases because the hull is moving forward. Consequently, since the wave period becomes smaller, the value of the RAO will be greater (because for smaller wave periods we get closer to the value of the *resonance frequency*) to large values of periods of the incident wave. Generally the RAO may have a peak corresponding to an intermediate wave period due to the low damping factor [2]. On the other hand, the RAO graph in roll motion, in Figure 28, shows a wave peak with a shorter period, precisely at 1.5s. This respects the empirical law that suggest us that the length of the hull must be almost 1/3 of λ . In this case we are considering the transversal length of the vessel that is smaller than the longitudinal length so the hull reaches the resonance frequency to smaller periods of the wave.

4.3.2 Calculation of the wave length and resonance frequency of the system

The RAO graph has a resonance frequency around 3.5s i.e. with wave lengths equal to:

$$\lambda = \frac{gT^2}{2\pi}$$

Where:

- G is the gravitational acceleration;
- T=3,5s is the period of the wave, in resonance conditions;

- $\lambda = 19m$ is the wave length;

Experience teaches us that if the length of the hull is equal to 1/3 of the wavelength then the hull is able to follow perfectly the inclination of the wave, performing correctly the rotation (in this case) of the pitch around the y axis [22]. In our case the length of the hull obtained by $\frac{\lambda}{3} = 6m$ that is smaller than the real length of the hull (15m). So in order to reach the maximum value of the pitch the hull should be long 6m, but in our case the vessel must be more stable because it has to transport people.

Applying the concept of *resonance*, that is when the natural frequency of the system (the hull) is equal to the frequency of the forcing (the wave), we can verify the comparison between the two frequencies and obtain an indicative value of the resonance frequency of the hull.

Considering the equation of motion of the system, in the frequency domain:

$$(M + A(\omega)) \ddot{X}(\omega) + B(\omega) \dot{X}(\omega) + K_H X(\omega) = F_{ex}(\omega) \quad (5.4.1)$$

And rewriting it in a more exhaustive form:

$$\sum_{j=1}^6 \left[(m_{i,j} + a_{i,j}(\omega)) \cdot \ddot{x}_j(\omega, t) + b_{i,j}(\omega) \cdot \dot{x}_j(\omega, t) + k_{i,j} \cdot x_j(\omega, t) \right] = F_{\omega a_i}(\omega) \cdot \cos(\omega t + \phi_i) \quad (5.4.2)$$

Where:

- $a_{i,j}(\omega)$ is the added mass matrix;
- $b_{i,j}(\omega)$ is the damping matrix;
- $k_{i,j}$ is the hydrodynamic stiffness matrix;

Where:

$$k = \rho g A_w \quad (5.4.3)$$

Where A_w is the water plane area, like in the figure below.

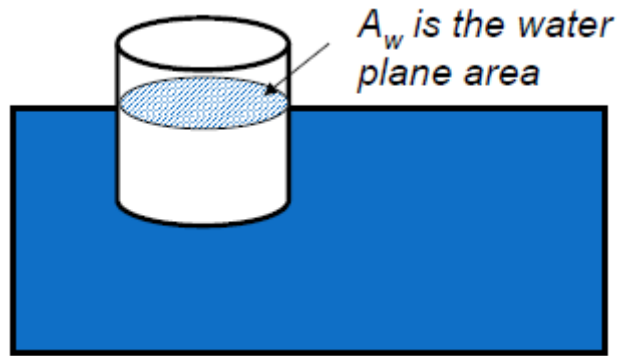


Figure 36: Water plane area [18]

And now, similarly at mass – spring system, we divided by the mass the equation 5.4.2 and we obtain the angular frequency of the system:

$$\omega^2 = \frac{k}{m + a} = \frac{\rho g A_w}{m + a} \quad (5.4.4)$$

For an approximate calculation we have considered the following values:

ρ	1000 kg/m ³
A_w	25,5 m ²
m	4500 kg
a	150000 kg

Where the value of A_w is obtained by solidworks making an extruded cut along the floating plane of our sailboat, like in the figure below.

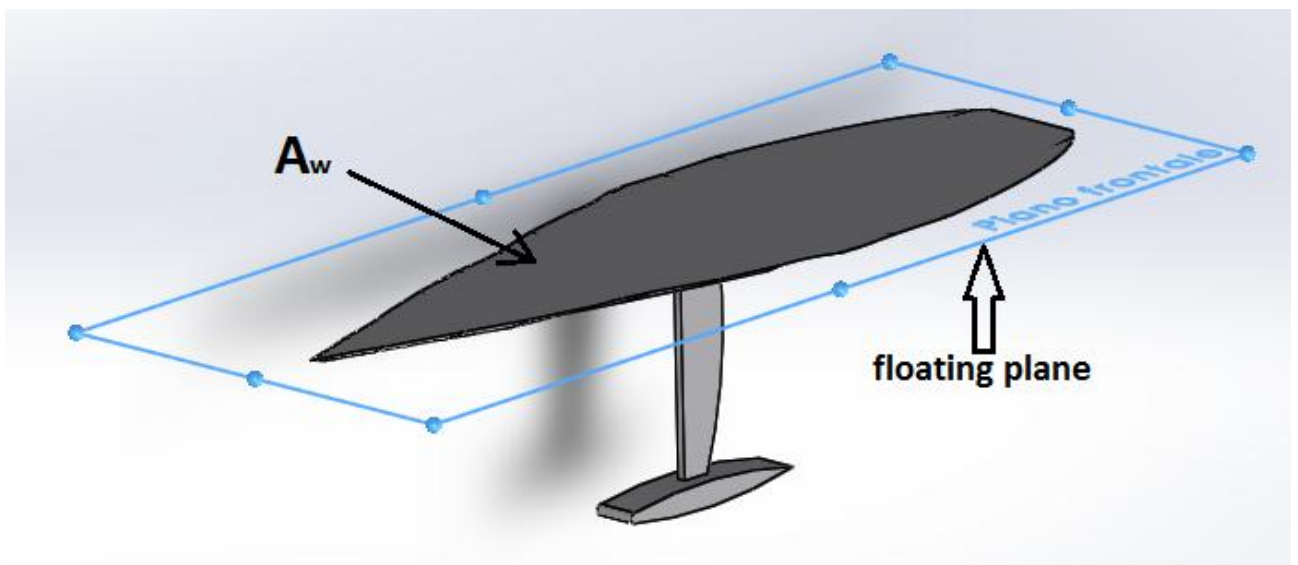


Figure 37: Floating plane of the hull

And the value of the added mass ($a=150000$ kg) is obtained from the graph in figure 22 for a correspondent value of 3,5 s.

The resonance frequency of the hull is $\omega=1,27$ rad/s, i.e.

$$T = \frac{2\pi}{\omega} = 4,7 \text{ s}$$

That it is a value close to the resonance period of the wave (3,5 s). So this means that the resonance condition is *almost* respected because we have to take into account that the added mass value varies greatly depending on the wavelength and forward speed of the hull.

Obviously the natural frequency of the hull in roll motion is lower and it is equal to $\omega = 15,2 \frac{\text{rad}}{\text{s}}$ so its period is nearer to the value of period, where we obtain the condition of resonance, that correspond to 1,3s.

5 Gyroscope system

ISWEC (*Inertial Sea Wave Energy Converter*) is a gyroscopic system for the conversion of wave energy, whose peculiarity lies in the fact that the converter has no mechanical parts immersed in water[24]. The main energy conversion system is therefore completely protected by the hull, allowing it to operate in conditions of reduced maintenance and high reliability. ISWEC is mainly composed of a rotating (flywheel) disk[2].

This disk is placed inside a chamber and is therefore mounted on a platform that allows the rotation of precession. In this device the precession is induced by the combination of the flywheel rotation speed with the pitching one of the hull and is used to start the motion of the generator shaft. In short, therefore, the waves disturb the flywheel rotation, which reacts with the precession, rotates the generator shaft and produces electricity. The system is regulated by a control that acts on the flywheel speed and on the power extracted from the generator and guarantees instant by instant an optimal absorption of energy from the sea[4].

A consideration must be made on the power spent to keep the flywheel in rotation. If the flywheel rotates in the atmosphere, the losses due to aerodynamic friction are relevant, corresponding to an important fraction of the power produced. The chamber, in addition to protecting the flywheel from external agents, also serves to maintain a degree of vacuum that minimizes losses due to aerodynamic friction.

5.1 The ISWEC working principles

The figure below shows the three main components of the gyroscopic system: the flywheel (red), the gyro – structure (blue), the PTO (green). To describe the system dynamics three reference frames have to be introduced:

- The fixed reference axes (FRA) is the inertial one and its axes are x_0, y_0, z_0 .
- The hull – fixed coordinate system (LSA) is composed by x_1, y_1, z_1 .
- The gyroscope structure fixed coordinate system (GSA) is composed by x_2, y_2, z_2 .

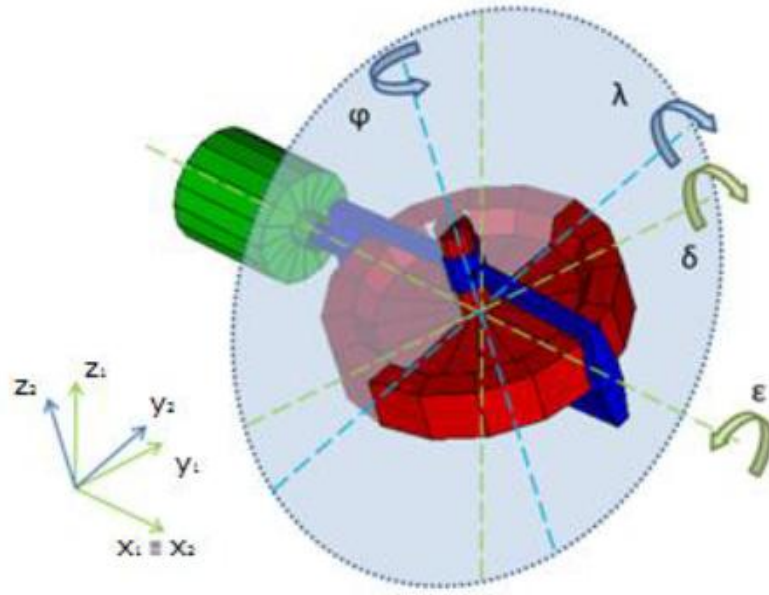


Figure 38: Gyroscope system reference frame.

The combination of the pitch speed $\dot{\delta}$ with the flywheel speed $\dot{\phi}$ about the z_2 axis generates a gyroscope torque T_ε around the $x_2 \equiv x_1$ axis, which can be exploited by the PTO for power conversion. So that the gyroscopic moment is given by the cross product of the pitch speed $\dot{\delta}$ along y_1 by the flywheel angular momentum L along z_2 thus the resulting torque is T_ε along the x_1 axis

$$T_\varepsilon \vec{i}_2 = \dot{\delta} \vec{j}_1 \times L \vec{k}_2 \quad (5.1)$$

5.2 The gyroscope mathematical model (Newtonian Approach)

The angular momentum conservation theorem is[2]:

$$\sum \vec{T}_E = \vec{M}_E = \frac{dL}{dt} \quad (5.2)$$

The absolute angular velocities of the GSA and the flywheel respectively are:

$$\vec{\omega}_2 = \dot{\varepsilon} \vec{i}_2 + \dot{\lambda} \vec{j}_2 + \dot{\psi} \vec{k}_2 \quad (5.3)$$

$$\vec{\omega}_3 = \vec{\omega}_2 + \dot{\phi} \vec{k}_2 = \dot{\varepsilon} \vec{i}_2 + \dot{\lambda} \vec{j}_2 + (\dot{\phi} + \dot{\psi}) \vec{k}_2 \quad (5.4)$$

Principal axes of inertia are GSA axes versors and so the tensor of inertia of the flywheel \hat{I} is:

$$\hat{I}_g = \begin{pmatrix} I_g & 0 & 0 \\ 0 & I_g & 0 \\ 0 & 0 & J \end{pmatrix}$$

Where J is the gyro moment of inertia around its axis, while I_g is its moment of inertia around any axis perpendicular to the first one [2]. The gyroscope angular momentum can be expressed as:

$$\vec{L} = \hat{I}_g \cdot \vec{\omega}_3$$

Since its time derivative involves the versors derivation, it has to be remembered that the time derivative of a versor is equal to:

$$\frac{d\vec{t}_2}{dt} = \vec{\omega}_2 \times \vec{t}_2 = -\dot{\lambda} \vec{k}_2 + \dot{\psi} \vec{j}_2 \quad (5.5)$$

$$\frac{d\vec{j}_2}{dt} = \vec{\omega}_2 \times \vec{j}_2 = \dot{\varepsilon} \vec{k}_2 - \dot{\psi} \vec{t}_2 \quad (5.6)$$

$$\frac{d\vec{k}_2}{dt} = \vec{\omega}_2 \times \vec{j}_2 = -\dot{\varepsilon} \vec{j}_2 + \dot{\lambda} \vec{t}_2 \quad (5.7)$$

The dynamic equation of the gyroscope relates the external forces acting on the gyroscope to its angular momentum variation:

$$\vec{M}_E = I_g \frac{d(\dot{\varepsilon} \vec{t}_2)}{dt} + I_g \frac{d(\dot{\lambda} \vec{j}_2)}{dt} + J \frac{d((\dot{\phi} + \dot{\psi}) \vec{k}_2)}{dt} \quad (5.8)$$

Its three scalar component in GSA are the following:

$$M_{E,x2} = \vec{M}_E \cdot \vec{t}_2 = I_g \ddot{\varepsilon} + (J - I_g) \dot{\lambda} \dot{\psi} + J \dot{\phi} \dot{\lambda} \quad (5.9)$$

$$M_{E,y2} = \vec{M}_E \cdot \vec{j}_2 = I_g \ddot{\lambda} - (J - I_g) \dot{\varepsilon} \dot{\psi} - J \dot{\phi} \dot{\varepsilon} \quad (5.10)$$

$$M_{E,z2} = \vec{M}_E \cdot \vec{k}_2 = J(\ddot{\phi} + \ddot{\psi}) \quad (5.11)$$

5.3 Gyroscope equations in hull reference frame

In order to couple the hull model and the gyroscope model, it is useful to write the gyroscope equations in LSA. The $\dot{\lambda}$ and $\dot{\psi}$ angular velocities are related to the pitch speed $\dot{\delta}$ as:

$$\dot{\lambda} = \dot{\delta} \cos \varepsilon \quad (5.12)$$

$$\dot{\psi} = -\dot{\delta} \sin \varepsilon \quad (5.13)$$

And for the acceleration is:

$$\ddot{\lambda} = \ddot{\delta} \cos \varepsilon - \dot{\delta} \dot{\varepsilon} \sin \varepsilon \quad (5.14)$$

$$\ddot{\psi} = -\ddot{\delta} \sin \varepsilon - \dot{\delta} \dot{\varepsilon} \cos \varepsilon \quad (5.15)$$

Using such relations 5.8, 5.9, 5.10 become:

$$M_{E,x2} = I_g \ddot{\varepsilon} - (J - I_g) \dot{\delta}^2 \sin \varepsilon \cos \varepsilon + J \dot{\varphi} \dot{\delta} \cos \varepsilon \quad (5.16)$$

$$M_{E,y2} = I_g \ddot{\delta} \cos \varepsilon + (J - 2I_g) \dot{\delta} \dot{\varepsilon} \sin \varepsilon - J \dot{\varphi} \dot{\varepsilon} \quad (5.17)$$

$$M_{E,z2} = J \ddot{\varphi} - J \ddot{\delta} \sin \varepsilon - J \dot{\delta} \dot{\varepsilon} \cos \varepsilon \quad (5.18)$$

In LSA the pitch torque can be obtained as the product of \overline{M}_E by \overline{j}_1 being the projection of (5.8) on y_1 . Similarly the yaw torque may be obtained being the projection of (5.8) on z_1 , while the roll torque is directly given by the PTO to the floater, so it is equal to $M_{E,x2}$.

$$M_{E,x1} = \overline{M}_E \cdot \overline{i}_1 = \overline{M}_E \cdot \overline{i}_2 = M_{E,x2} \quad (5.19)$$

$$\begin{aligned} M_{E,y1} &= \overline{M}_E \cdot \overline{j}_1 = \overline{M}_E (\overline{j}_2 \cos \varepsilon - \overline{k}_2 \sin \varepsilon) = M_{E,y2} \cos \varepsilon - M_{E,z2} \sin \varepsilon \\ &= (I_g \cos^2 \varepsilon + J \sin^2 \varepsilon) \ddot{\delta} + 2(J - I_g) \dot{\delta} \dot{\varepsilon} \sin \varepsilon \cos \varepsilon \\ &\quad - J \dot{\varphi} \dot{\varepsilon} \cos \varepsilon - J \ddot{\varphi} \sin \varepsilon \end{aligned} \quad (5.20)$$

$$\begin{aligned} M_{E,z1} &= \overline{M}_E \cdot \overline{k}_1 = \overline{M}_E (\overline{j}_2 \sin \varepsilon + \overline{k}_2 \cos \varepsilon) = M_{E,y2} \sin \varepsilon - M_{E,z2} \cos \varepsilon \\ &= -(J - I_g) \ddot{\delta} \sin \varepsilon \cos \varepsilon + [(J - 2I_g) \sin^2 \varepsilon - J \cos^2 \varepsilon] \dot{\delta} \dot{\varepsilon} \\ &\quad - J \dot{\varphi} \dot{\varepsilon} \sin \varepsilon + J \ddot{\varphi} \cos \varepsilon \end{aligned} \quad (5.21)$$

5.4 Simplifications

Looking at the equations (5.8) and (5.9) it is possible to see that the second term can be neglected being small with respect to the last one. In fact the inertial part in both equations have the same order of magnitude in all terms, while the speed $\dot{\psi}$ is two order of magnitude lower than $\dot{\varphi}$. Note that the speed $\dot{\lambda}$ appears in both the terms of (5.8) and the same is for $\dot{\varepsilon}$ in (5.9), so they don't affect this balance [2].

$$M_{E,x2} \cong I\ddot{\varepsilon} + J\dot{\varphi}\dot{\lambda} \quad (5.22)$$

$$M_{E,y2} \cong I\ddot{\lambda} - J\dot{\varphi}\dot{\varepsilon} \quad (5.23)$$

$$M_{E,z2} = J(\ddot{\varphi} + \ddot{\psi}) = J\ddot{\varphi} - J\dot{\delta}\dot{\varepsilon} \cos \varepsilon \quad (5.24)$$

The same considerations may be done for (3.19), (3.20), (3.21) obtaining:

$$M_{E,x1} \cong I\ddot{\varepsilon} + J\dot{\varphi}\dot{\delta} \cos \varepsilon \quad (5.25)$$

$$M_{E,y1} \cong I\ddot{\delta} - J\dot{\varphi}\dot{\varepsilon} \cos \varepsilon \quad (5.26)$$

$$M_{E,z1} \cong -J\dot{\varphi}\dot{\varepsilon} \sin \varepsilon \quad (5.27)$$

It useful to define new variables to refer to the gyroscopic torques:

$$T_{\lambda} = J\dot{\varphi}\dot{\varepsilon} \quad \text{Around } \vec{j} \quad (5.28)$$

$$T_{\varepsilon} = J\dot{\varphi}\dot{\delta} \cos \varepsilon \quad \text{Around } \vec{i} \quad (5.29)$$

$$T_{\varphi} = J\dot{\varepsilon}\dot{\delta} \sin \varepsilon \quad \text{Around } \vec{k} \quad (5.30)$$

6. Design of a 1:7 scale of a gyroscopic model

Knowing the 1: 1 scale model, I have designed a 1: 7 scale model with Solidworks respecting the following geometrical data:

Quantity	Scale 1:1	Scale 1:7
D_e	2100 mm	300 mm
H	1000 mm	150 mm
D_b	1400 mm	200 mm

Where:

- D_e external diameter of the flywheel;
- H is the height of the flywheel;
- D_b inter – axis between the bearings.

6.1 Dimensions of the system

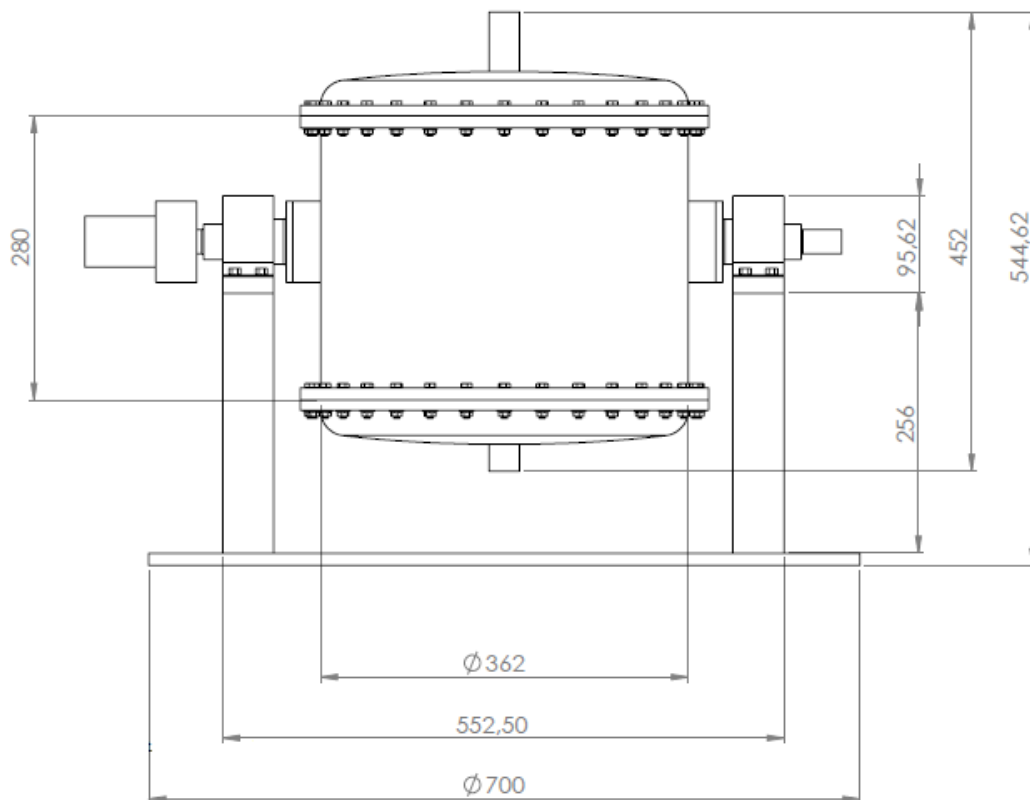


Figure 39: General dimensions of the system

6.2 External structure

In the picture there is the designed gyroscopic system. Its main components are:

- Vacuum chamber in which is located the flywheel;
- PTO (power take – off);
- Supports;

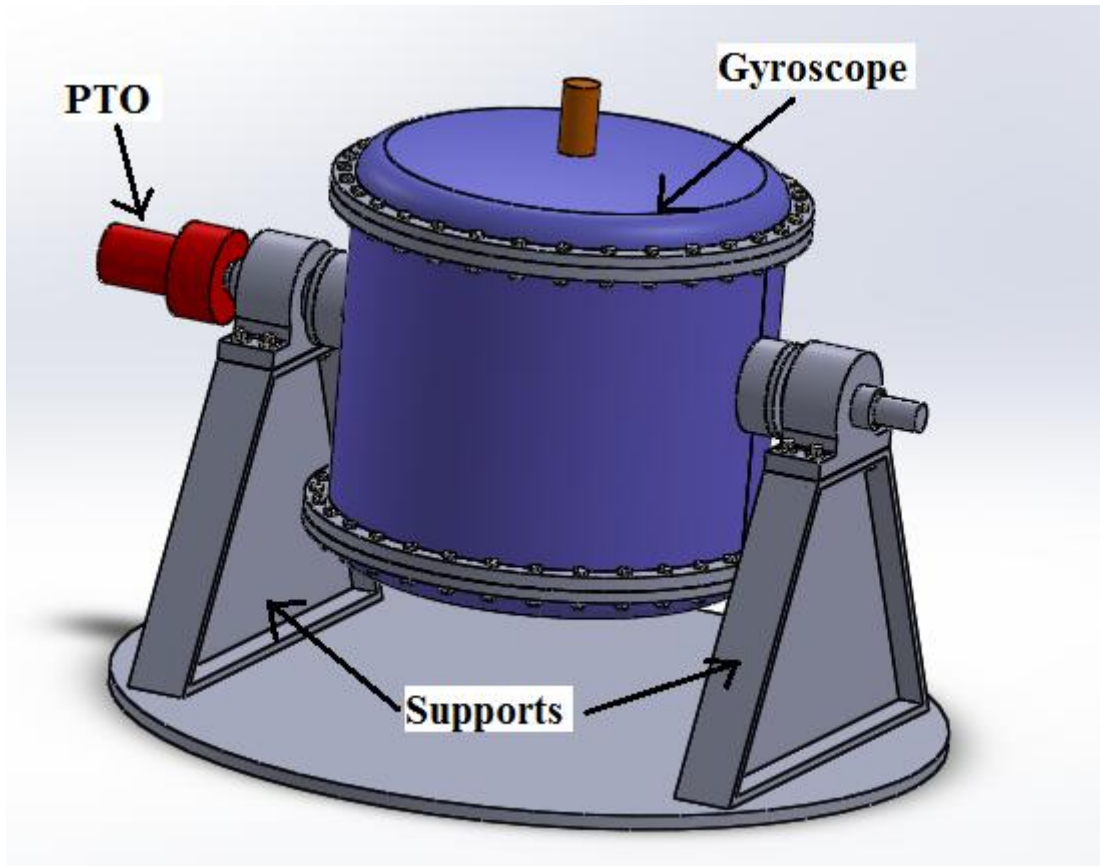


Figure 40: External chamber view

The choice of the vacuum system have a justified reason: the viscous forces acting on the surface of the flywheel depend on the rotation speed and pressure around the flywheel. For the ISWEC system it was estimated that reducing the value from 1 bar to 0,01 bar the aerodynamic drag force is reduced of 80 – 90%. The graph evidences the magnitude of the power losses due to the aerodynamic viscous forces depending on different value of internal chamber pressure.

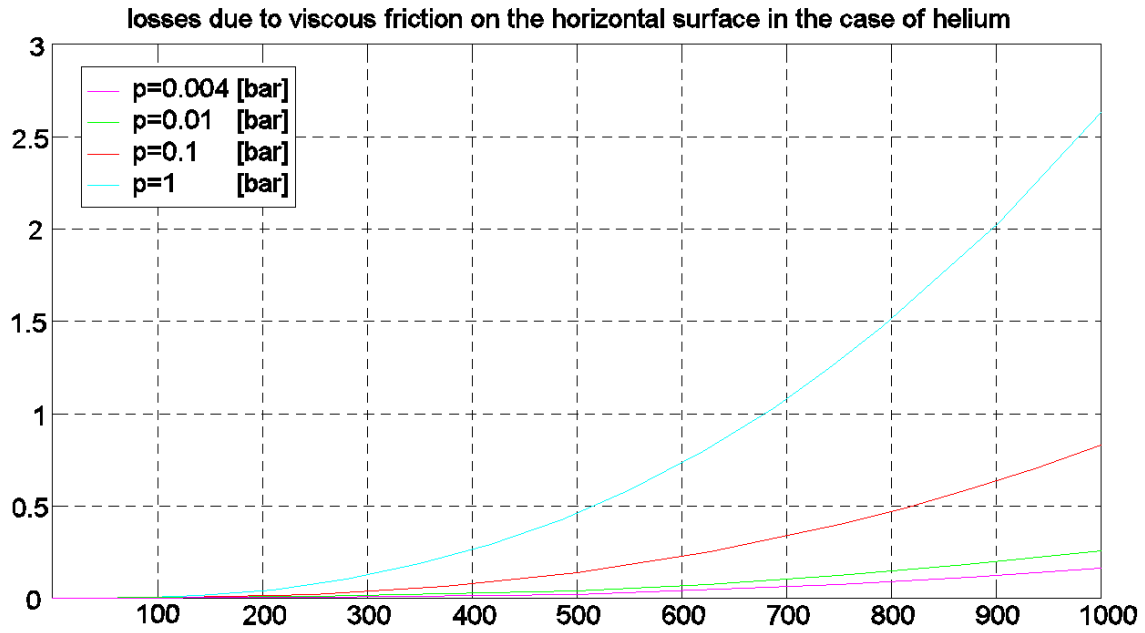


Figure 41: Aerodynamic drag acting on the ISWEC flywheel as a function of the chamber pressure

6.3 Internal structure

The flywheel is enclosed in a sealed case where a low pressure is made. The flywheel is connected to the cylindrical body by means of two *spoked wheels* aimed at the bearings support. Its main components:

- Flywheel;
- Radial bearings;
- Axial bearing.

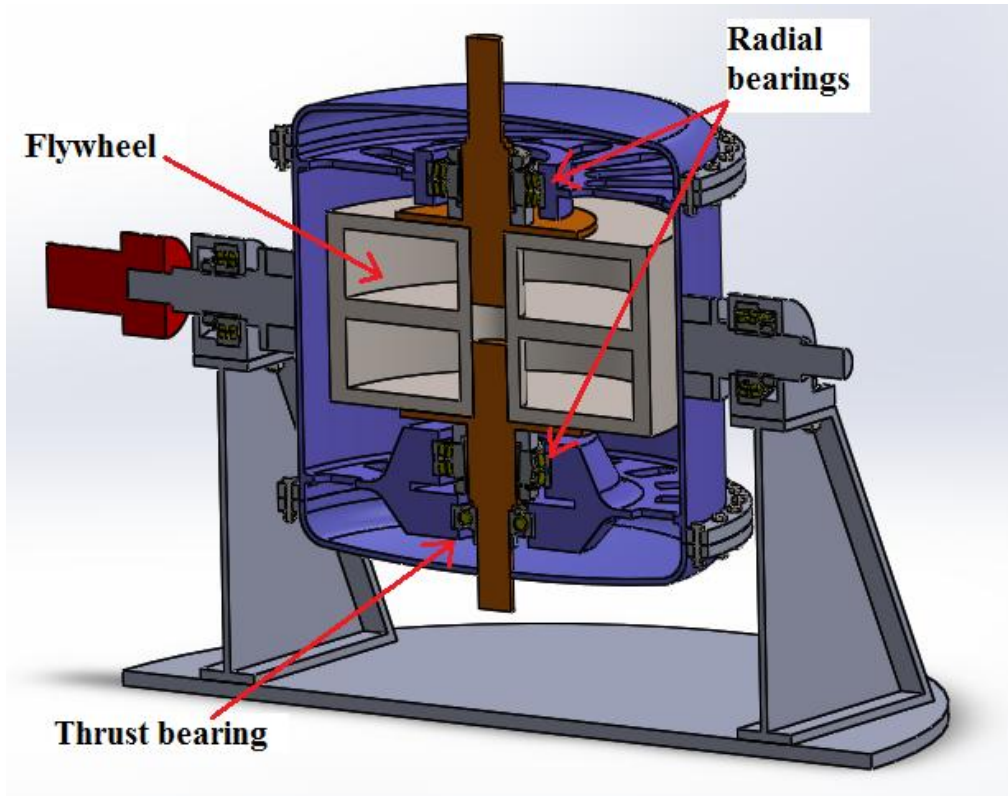


Figure 42: Internal chamber view

The flywheel is connected to the bearings through two half – shafts.

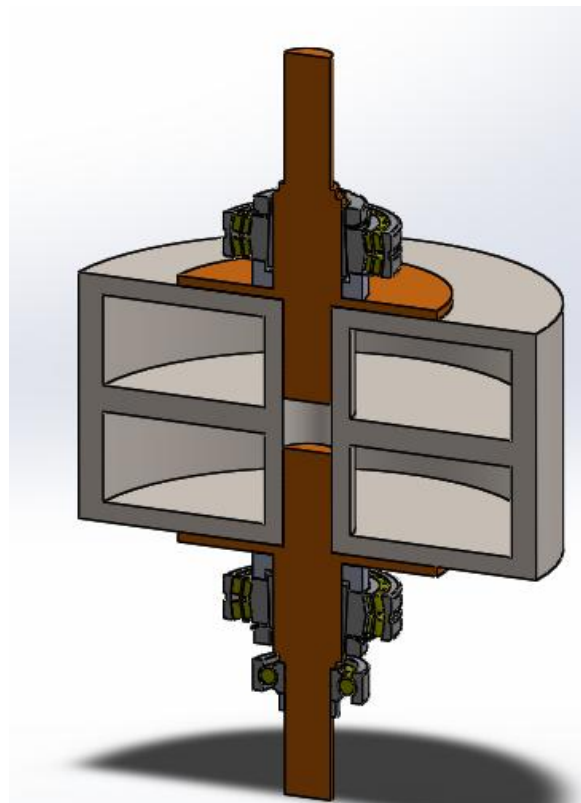


Figure 43: Flywheel with the two half shafts

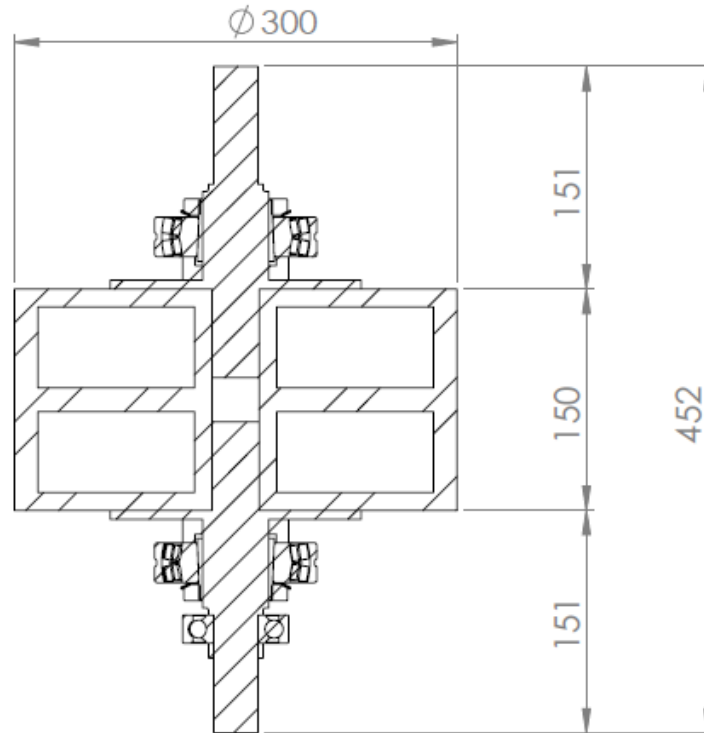


Figure 44: flywheel dimensions with the two half shaft

6.4 Functioning

An electric motor is placed inside or outside the vacuum chamber, which allows to adjust the angular speed of the flywheel with respect to the sea conditions. The angular momentum that is generated by the rotation of the flywheel combined with the pitching motion of the hull, causes a gyroscopic torque (as explained in the equation below) along the axis of the PTO generator, which converts it into electrical energy that can be exploited on the sailing ship.

$$T_g = \dot{\delta} \times L$$

Where:

- $\dot{\delta}$ is the pitch speed;
- L is the flywheel angular momentum.

There is a strong coupling between the hull hydrodynamics and gyroscope mechanics due to torques and energy interactions. The flywheel speed is a control parameter that can be tuned to optimize the coupling between gyroscope system and sea waves and consequently the power generation. Of course the main disadvantage of this device is the flywheel consumption.

So the *power path* that takes place can be summarized as follows:

1. The wave motion transfers kinetic energy to the hull;
2. The hull follows the path of the wave with its pitch motion (therefore kinetic energy of the hull increase);
3. The flywheel has a certain level of kinetic energy because of its rotation caused by the electric motor;
4. The combination of these motions, together with the respective kinetic energies, causes the formation of a torque that exploited by the PTO becomes electrical energy.

Adjustment of the flywheel angular velocity with respect to the sea state is a very important factor that affects the productivity of the system. This is demonstrated by the following graph, which is referred to the ISWEC system, from which emerges that keeping a constant speed of the rotating disk will produce an annual production of electricity lower than that considered with an adaptation of the angular velocity of the flywheel.

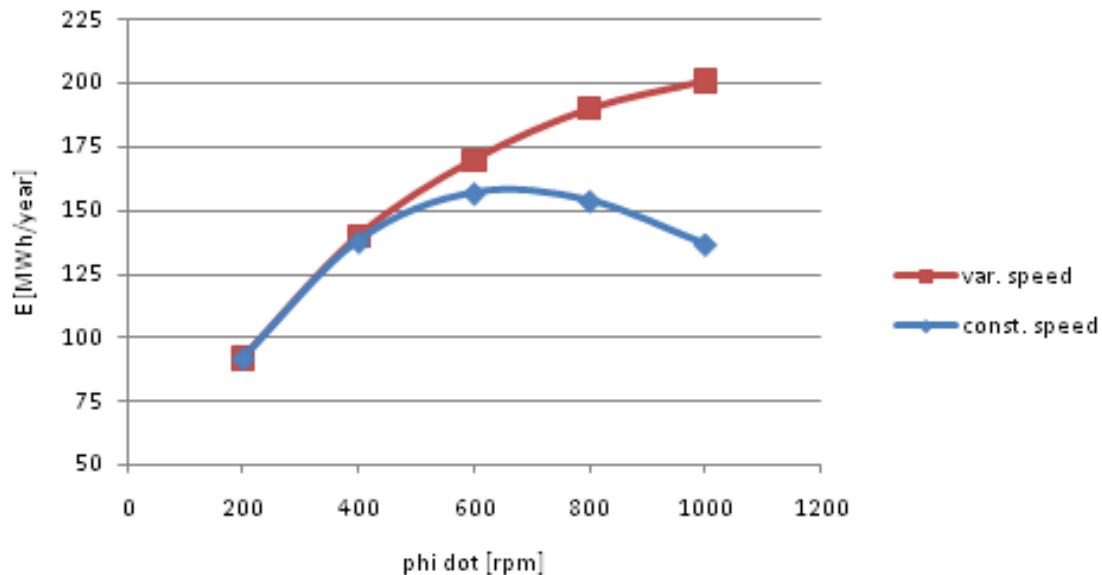


Figure 45: Annual productivity for ISWEC system

6.5 Bearing study

The dimensions and typologies of bearings affect widely the system efficiency. The total losses are due to the combination of:

- Radial loads (caused by gyroscopic torques and flywheel weight);
- Axial loads (caused by weight only);

The following considerations may be done for the bearing size:

1. Higher bearing size is needed to obtain an acceptable rated life. But this led to higher power loss so it may be not convenient.

2. Raising the flywheel shaft length lead to lower bearing load since the gyroscopic torque is unchanged. The bearing size can be reduced thus reducing its power loss too. Nevertheless the moment of inertia I around the PTO axis becomes higher and the torque needed to reserve its motion raises too. This led to higher power dissipation, so the global effect have to be considered.
3. The flywheel speed may be limited in order to reduce the power loss. Moreover the lower angular moment lead to lower forces acting on the bearings further reducing the losses. On the other hand if the maximum angular moment is low the gross energy production is limited too.
4. The maximum load acting on the bearing may be controlled as well. That way the bearing size and thus the losses can be reduced. The energy production is affected by this reduction, so it have to be evaluated how low the limit has to be.
5. Since the axial load appear to be significant for the system efficiency, it should be evaluated to use thrust bearings to support the flywheel weight. If so, the radial bearings can be downsized and their dissipations becomes lower. Clearly a new loss source is introduced so it have to be evaluated the total balance. Moreover the cost and complexity of the system are increased.

To summarize:

Solutions	Advantages	Disadvantages
Higher bearing size	Higher capacity factor	Higher power loss
Higher bearing distance	Lower bearing load and loss	Higher value of I
Lower flywheel speed	Lower power loss	Lower energy production
Bearing load limitation	Lower bearing size and loss	Lower energy production
Thrust bearings	Lower bearing size and loss	High cost and loss sources

6.5 Gyroscope bearing adopted

The figure shows the gyroscopic group in which are identified five bearings, three are inside the chamber (two identical roller bearing and one spherical roller thrust bearing), and two outside it. The latter are subjected to very low angular speed, and therefore do not require any special maintenance except an occasional manual lubrication after a certain number of operation hours. Instead the bearings inside the chamber are more stressed both in bearing load then in temperature. Therefore a lubricating/ cooling action is required.

These bearings belong to the new developed SKF explorer performance class [25]. This class realize improvement in performance by optimizing the internal geometry and surface finish of all contact surfaces, combining the extremely clean and homogeneous steel with a unique heat treatment, improving the cage, roller profile and the geometry of the raceways.

These improvements provide the following benefits [25]:

- Higher dynamic load carrying capacity compared to conventional design bearings;
- Improved wear – resistance;
- Reduced noise and vibration levels;
- Less frictional heat;
- Significantly extended bearing service life.

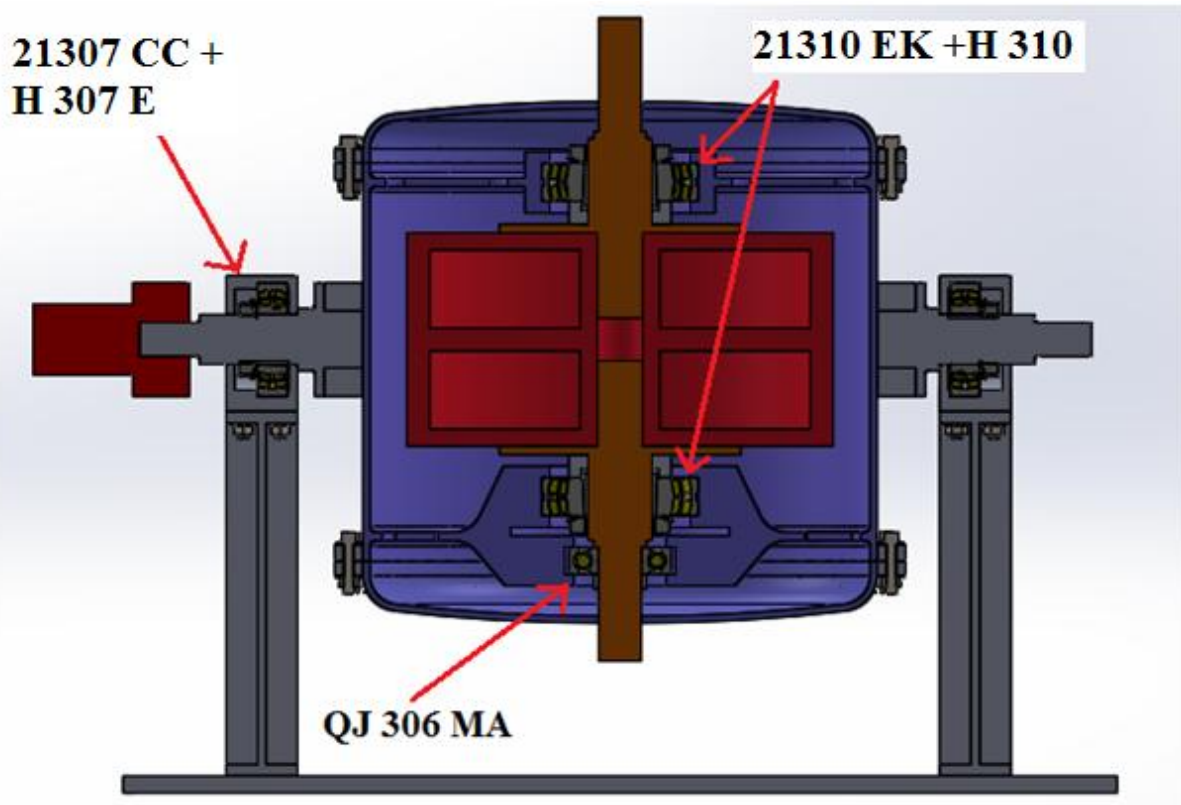


Figure 46: Bearings of the gyroscopic system

The *spherical roller bearings* (figure 46) adopted inside and outside the chamber have two rows of symmetrical rollers, a common sphered outer ring raceway and two inner ring raceways inclined at an angle to the bearing axis. The centre point of the sphere in the outer ring raceway is at the bearing axis[26].



Figure 47: Spherical roller bearing

Their features are:

- *Accommodate misalignment*: spherical roller bearing are self – aligning;

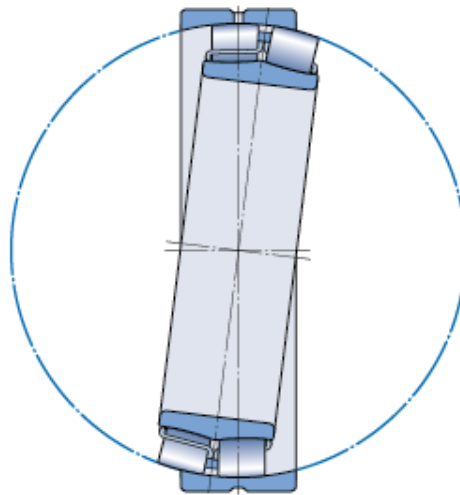


Figure 48: self - alignment property of the bearing

- *High load carrying capacity*: spherical roller bearings are designed to accommodate heavy radial loads, as well as, heavy axial loads in both directions.
- *Long service life*: the rollers are manufactured to such tight dimensional and geometrical tolerances that they are practically identical in a roller set. The symmetrical rollers self – adjust (figure 48), providing optimal load distribution along

the roller length and together with the spherical profile prevent stress peaks at the roller ends (figure 49).

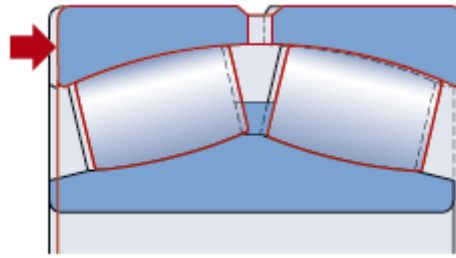


Figure 49: self - adjusting property of the rollers

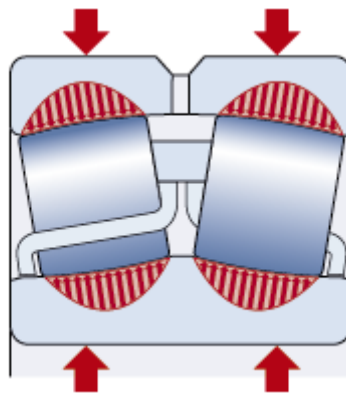


Figure 50: load distribution over the roller length

- *Low friction*: self guiding rollers keep friction and frictional heat at low levels. A floating guide ring guides unloaded rollers so that they enter the load zone in the optimal position.

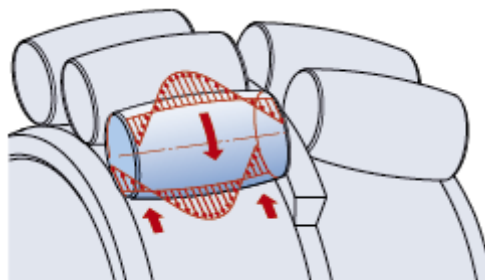


Figure 51: optimal roller guidance

- *Robust*: contain strong window type cages[26].

Instead for the thrust bearing I have chose *four – point contact ball bearings* (figure 51). They are radial single row angular contact ball bearings with raceways that are designed to support axial loads in both directions. For a given axial load, a limited radial load can also be supported. The bearings are separable, i.e. the outer ring with ball and cage assembly can be mounted separately from the two inner ring halves. Both inner ring halves of SKF Explorer

four- point contact ball bearings have a recessed shoulder. This improves oil flow when the bearing is used in combination with an SKF cylindrical roller bearing. In addition, these recesses can be used to facilitate dismounting[25].



Figure 52: four contact point ball bearing

The bearing features are:

- Accommodate axial loads in both directions;
- Less axial space: these bearings take up considerably less axial space than double row bearings;
- High load carrying capacity: a large number of balls are incorporated, giving the bearing its high load carrying capacity.
- Separable design: the split inner ring leads to easier mounting and dismounting of the bearing;
- Improved oil flow;
- Limited inner ring deformation when subjected to high clamping forces[26].

6.5.1 SKF spherical roller bearing 21310 EK

In the figure 53 is presented the technical design of the spherical roller bearing, with representative quotes.

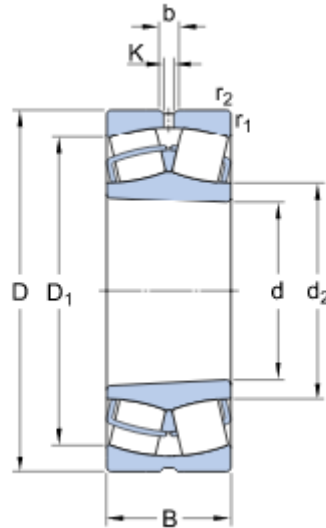


Figure 53: dimensions of 21310 EK bearing [26]

The dimensions are listed below:

Dimension	d	D	B	d ₂	D ₁	b	K	r _{1,2}
[mm]	50	110	27	72,7	96,8	6	3	2

Table 1: Geometrical dimensions of 21310 EK bearing [26]

All the calculation data given by SKF catalogue are:

Calculation data

Basic dynamic load rating	C	159	kN
Basic static load rating	C ₀	166	kN
Fatigue load limit	P _u	18.6	kN
Reference speed	-	5600	r/min
Limiting speed	-	7500	r/min
Calculation factor	E	0.24	-
Calculation factor	Y ₁	2.8	-
Calculation factor	Y ₂	4.2	-
Calculation factor	Y ₀	2.8	-
Mass	-	1.35	Kg

Table 2: Calculation data of 21310 EK bearing [26]

Due to the design of spherical roller bearings, the rings and roller complement may be displaced axially from the normal position during handling. Therefore, SKF recommends mounting spherical roller bearings when the shaft or housing is in the horizontal position.

Also, whenever possible, rotate the inner and the outer ring to align the rollers during mounting. If spherical roller bearings are mounted when the shaft or housing is in the vertical position, the roller complement, together with the inner or outer ring will move downward until there is no more clearance. Then, when the bearing rings expand or contract as a result of an interference fit, a preload is likely to result. To prevent this preload condition from occurring, rotate the inner or outer ring during mounting. If this is not feasible, use a bearing handling tool or other device to keep the bearing components arranged centrally.

6.5.2 SKF four - point contact ball bearing QJ 306 MA

In the figure 54 is presented the technical design of the spherical roller bearing, with representative quotes.

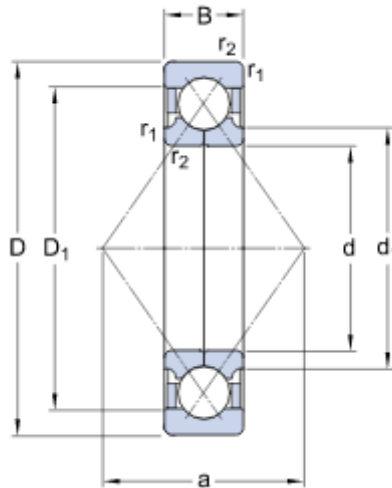


Figure 54: dimensions of QJ 306 MA bearing [26]

The dimensions are listed below:

Dimension	d	D	B	d ₁	D ₁	a	r _{1,2}
[mm]	30	72	19	40.5	58.2	36	1.1

Table 3: Geometrical dimensions of QJ 306 MA bearing[26]

All the calculation data given by SKF catalogue are:

Calculation data			
Basic dynamic load rating	C	53	kN
Basic static load rating	C ₀	41.5	kN
Fatigue load limit	P _u	1.76	kN

Limiting speed	-	17000	r/min
Calculation factor	A	0.00508	-
Calculation factor	E	0.95	-
Calculation factor	X	0.6	-
Calculation factor	Y₁	0.66	-
Calculation factor	Y₂	1.07	-
Calculation factor	Y₀	0.58	-
Mass	-	0.42	Kg

Table 4: Calculation data of QJ 306 MA bearing [26]

6.5.3 SKF spherical roller bearing 21307 CC

In the figure 55 is presented the technical design of the spherical roller bearing, with representative quotes.

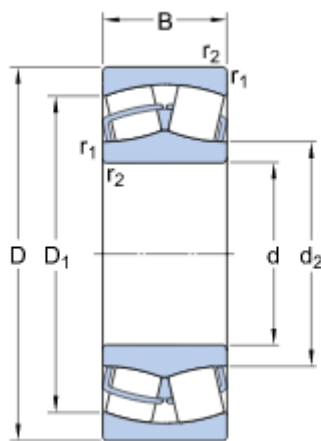


Figure 55: dimensions of 21307 CC bearing [26]

The dimensions are listed below:

Dimension	d	D	B	d₂	D₁	r_{1,2}
[mm]	35	80	21	47.2	65.6	1.5

Table 5: geometrical dimensions of 21307 CC bearing [26]

All the calculation data given by SKF catalogue are:

Calculation data			
Basic dynamic load rating	C	79.2	kN

Basic static load rating	C_0	72	kN
Fatigue load limit	P_u	8.15	kN
Reference speed	-	7300	r/min
Limiting speed	-	9500	r/min
Calculation factor	E	0.28	-
Calculation factor	Y_1	2.4	-
Calculation factor	Y_2	3.6	-
Calculation factor	Y_0	2.5	-
Mass	-	0.55	Kg

Table 6: Calculation data of 21307 CC [26]

Due to the design of spherical roller bearings, the rings and roller complement may be displaced axially from the normal position during handling. Therefore, SKF recommends mounting spherical roller bearings when the shaft or housing is in the horizontal position. Also, whenever possible, rotate the inner and the outer ring to align the rollers during mounting. If spherical roller bearings are mounted when the shaft or housing is in the vertical position, the roller complement, together with the inner or outer ring will move downward until there is no more clearance. Then, when the bearing rings expand or contract as a result of an interference fit, a preload is likely to result. To prevent this preload condition from occurring, rotate the inner or outer ring during mounting. If this is not feasible, use a bearing handling tool or other device to keep the bearing components arranged centrally.

6.5.4 Adapter sleeve H 307 E for 21307 CC bearing

Adapter sleeve are the most commonly used components for locating bearings with a tapered bore onto a cylindrical seat as they can be used on:

- Plain shaft
- Stepped shafts

In our case we used it in stepped shafts together with an L- shaped spacer ring, the bearing can be accurately positioned axially, thereby facilitating bearing mounting and dismounting.

In the figure there are the principal dimensions of the adapted sleeve adopted:

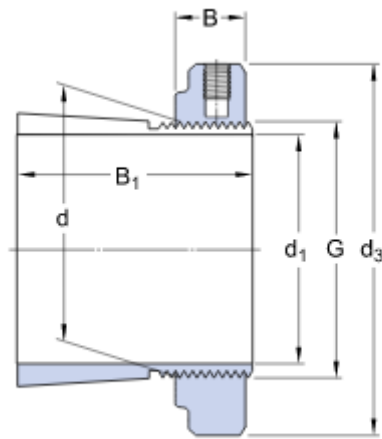


Figure 56: dimensions of H 307 E adapter sleeve [26]

The dimensions are listed below:

Dimensions		
d₁	30	mm
d	35	mm
d₃	52	mm
B₁	35	mm
B	11.5	mm
G	M 35x1.5	

Table 7: geometrical dimensions of H 307 E adapter sleeve [26]

6.5.5 Adapter sleeve H 310 for 21310 EK bearing

In the figure there are the principal dimensions of the adapted sleeve adopted:

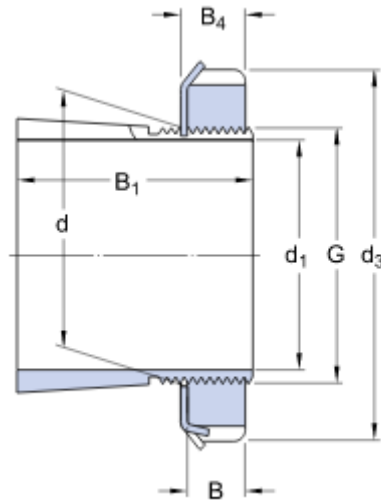


Figure 57: dimensions of H 310 adapter sleeve [26]

The dimensions are listed below:

Dimensions		
d_1	45	mm
d	50	mm
d_3	70	mm
B_1	42	mm
B	11	mm
B_4	12	mm
G	M 50x1.5	

Table 8: Geometrical dimensions of H 310 adapter sleeve [26]

6.5.6 Description of bearing mounting

In the figure 58 there is the bearing that is positioned above the flywheel. Since axial loads are not present on this section, but only radials, it has been completely blocked. The outer ring, which does not rotate, is blocked by the spoked wheel thanks to the shoulders that it presents. The inner ring rotates integrally to the shaft, is blocked axially by an adapter sleeve and an L-shaped spaced ring. It may possibly support any misalignment of the shaft due to the pitching motion of the hull.

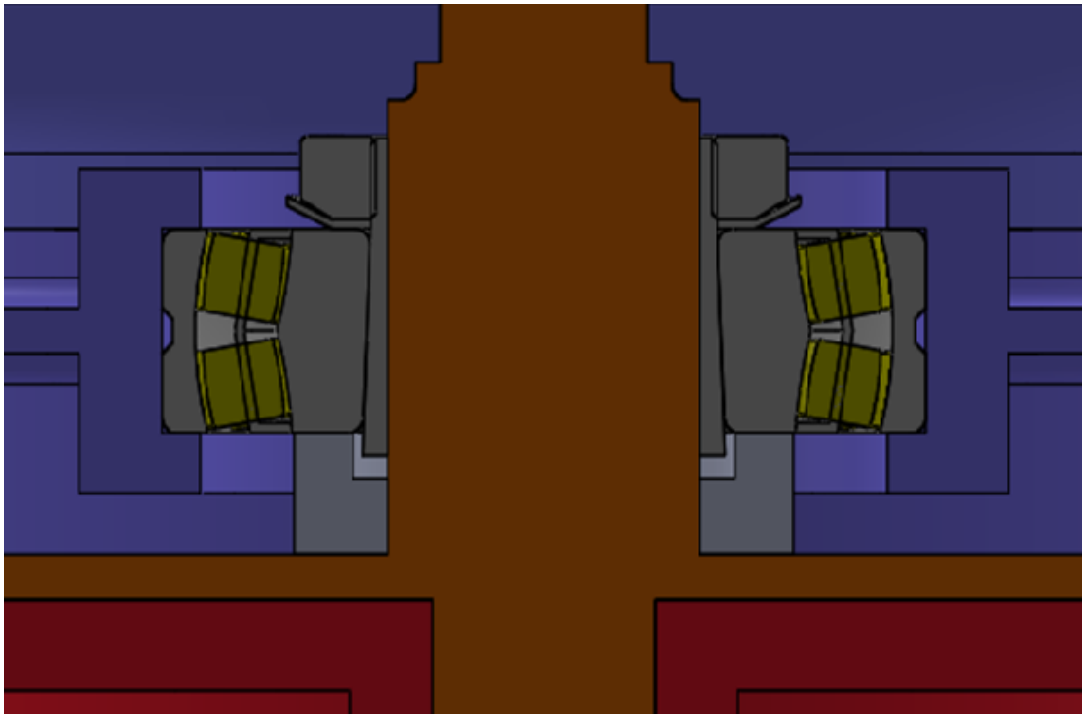


Figure 58: mounting of spherical roller bearing above the flywheel

Instead in the group of bearings placed below the flywheel (figure 59) there is a spherical roller bearing, that is mounted in a similar way of the first one and a four – point contact ball bearing that support axial load. The latter holds less axial loads than a spherical roller thrust bearing but, remembering that the flywheel mass is relatively small, as it is designed in 1: 7 scale, there will be smaller axial loads and moreover occupies a notably smaller axial space. Ball bearing is located axially from a shoulder of the shaft and on the other side from another ring fixed on the shaft.

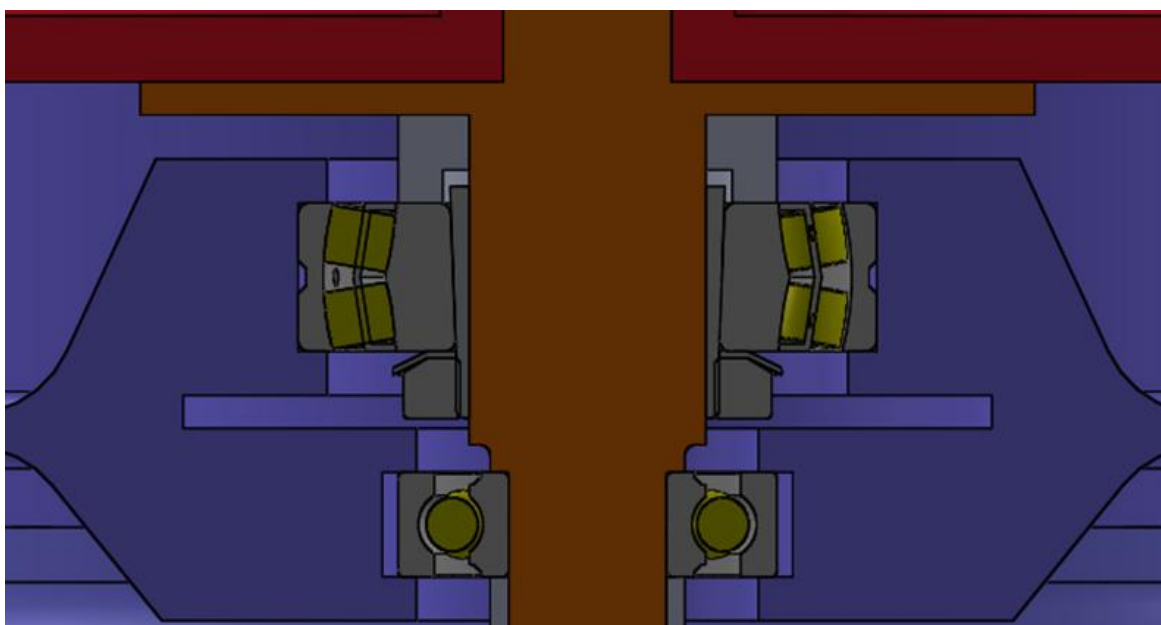


Figure 59: mounting of bearings down the flywheel

The two spherical roller bearings positioned outside the vacuum chamber (figure 60) on the PTO axis, were completely blocked axially: the outer ring from the shoulders of the casing and instead the inner ring from the adapter sleeve. They are not subject to high wear because here very low angular speeds are recorded.

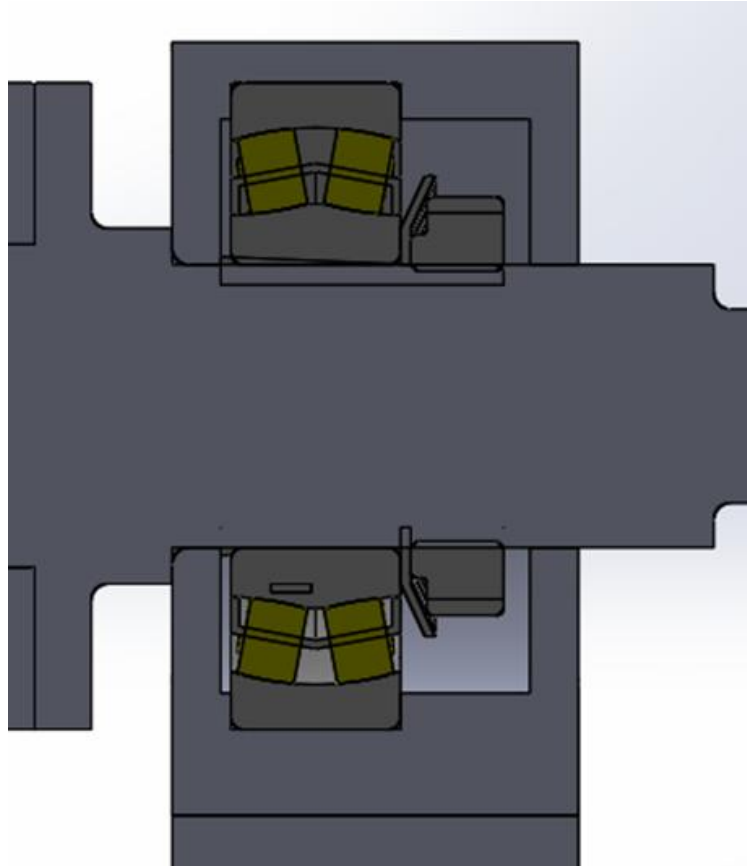


Figure 60: mounting of spherical roller bearing outside the vacuum chamber

6.6 Hexagonal head bolt with nut

The bolt adopted in the system is: ISO 4016 M6 x 30 x 18 – WC.

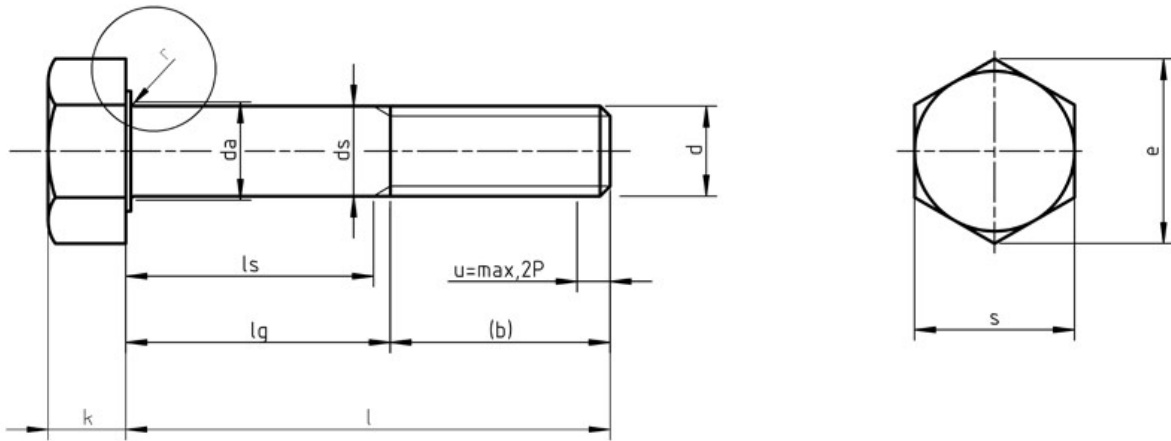


Figure 61: bolt ISO 4016

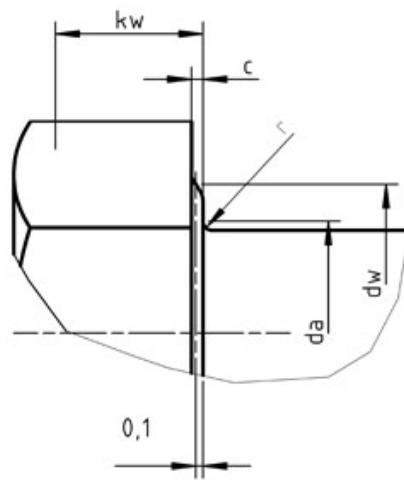


Figure 62: particular of bolt ISO 4016

DIMENSIONS IN [mm]		
Thread pitch	P	1
Length of the thread	b	18
Thickness of mounting collar	c	0.5
-	d_a	7.2
-	d_s	6.48
-	d_w	8.74
Diameter of circumscribed circle	e	10.89
Head height	k	4
-	k_w	2.54
radius	r	0.25
Size hex head turnkey	s	10

Table 9: Geometrical dimensions of bolt ISO 4016

The nut adopted is: ISO 4161 – M6 – N.

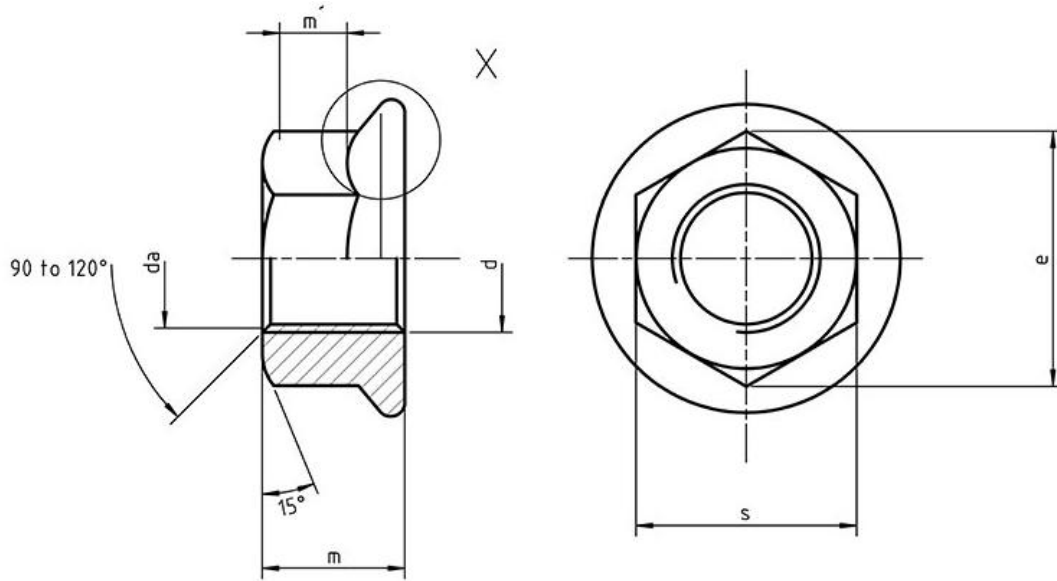


Figure 63: nut ISO 4161

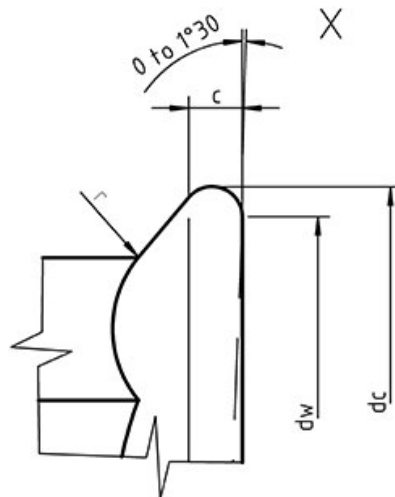


Figure 64: particular of nut ISO 4161

DIMENSIONS IN [mm]		
Thread pitch	P	1
-	c	1.1
-	da	6
Outer diameter of the ring	dc	14.2
Contact surface diameter	dw	12.2
Diameter of the circumscribed circle	e	11.05
-	m	6
-	m'	3.1
Size of the exagon	s	10
radius	r	0.36

Table 10: Geometrical dimensions of nut ISO 4161

7. Power losses on a gyroscopic system

When scaling a system, productivity and the respective power losses vary with the scale factor. In this chapter a mathematical formulation has been reported that allows us to calculate the power losses based on the scale factor that has been used.

7.1 Hypotheses

The hypotheses relate to the scale types, to the order of magnitude of the flywheel speed and to the gyroscope gross power linearized expression. These hypotheses are[25]:

- The hydrodynamic phenomena are scaled following the Froude scaling law;
- The angular momentum ($L = J\dot{\phi}$) is the physical quantity involved into the power conversion chain. Since the angular momentum has been scaled with the Froude scaling law, both the flywheel inertia (J) and flywheel speed ($\dot{\phi}$) are scaled in the same way.
- Scaling the gyroscope geometry and speed with the Froude scaling law, the fluid – dynamics phenomena involved in the aerodynamic interaction between air and flywheel do not respect the Reynolds scale;
- It is possible to couple Froude and Reynolds scales by varying the air properties between the full – scale and scaled models;
- The air contained in the flywheel vacuum chamber is modeled as a perfect gas with a constant temperature and volume;
- The flywheel speed ($\dot{\phi}$) is an order of magnitude higher than the gyroscope speed. This lead to not consider the mechanical power losses of the precession axis bearings. Moreover, since only the gyroscope mechanics are taken into account, the losses due to the PTO are not taken into account[25].

7.2 Flywheel shaft power losses

The mechanical power losses on the flywheel spinning axis can be identified as follow[25]:

$$P_{losses} = P_v + P_{bear} + P_{seal} \quad (7.1)$$

Where:

- P_v are the power losses due to the aerodynamics forces;

- P_{bear} are the power losses carried by the flywheel roller bearings;
- P_{seal} are the power losses provided by seals friction forces.

7.2.1 Fluid – dynamic power losses

The fluid – dynamic losses arise from the interaction between the flywheel surface and air. These power losses depending on both the fluid speed regime (laminar or turbulent) and the spaces between the flywheel and the vacuum chamber. In the vacuum chamber there are two meatus (figure) identified as -s- and -m-. the interaction between the air that fills these meatus and the flywheel surface leads to two different power losses contributes[25]:

$$P_v = P_{v,lateral} + P_{v,disk} \quad (7.2)$$

Where:

- $P_{v,lateral}$ refers to the lateral meatus (m);
- $P_{v,disk}$ refers to the top and bottom meatus (s)

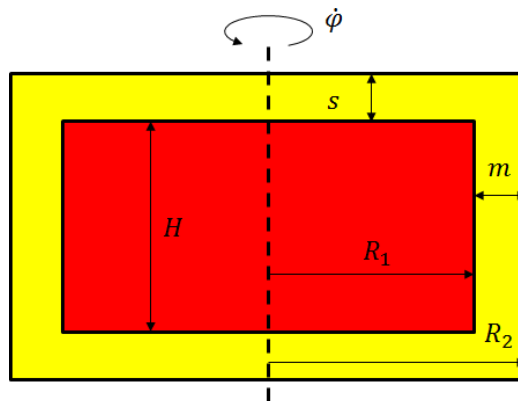


Figure 65: Flywheel and vacuum chamber scheme

Starting from the lateral meatus, the mathematical expression of $P_{v,lateral}$ is:

$$P_{v,lateral} = \frac{1}{2} C_M \cdot \pi \cdot \rho_{air} \cdot \dot{\phi}^3 \cdot R_1^4 \cdot H \quad (7.3)$$

Where:

- C_M is the torque coefficient;
- $\dot{\phi}$ is the flywheel speed;
- R_1 is the external diameter of the flywheel;
- H is the height of the flywheel;

Considering the Reynolds number for this kind of meatus is possible to define the torque coefficient:

$$Re_{\phi m} = \frac{R_1 \dot{\phi} (R_2 - R_1)}{\nu_{air}} = \frac{R_1 \dot{\phi} m}{\nu_{air}} \quad (7.4)$$

Speed regime	Reynold number	Torque coefficient
Low - turbulent	$Re_{\phi m} \leq 10^4$	$C_M = 1.03 \left(\frac{m}{R_1}\right)^{0.3} Re_{\phi m}^{-0.5}$
High - turbulent	$Re_{\phi m} > 10^4$	$C_M = 0.065 \left(\frac{m}{R_1}\right)^{0.3} Re_{\phi m}^{-0.2}$

Table 11: Values of torque coefficient in relation to Reynolds number in lateral meatus

And we obtain the power loss expressions related to the lateral meatus:

$$P_{v,lateral,low-turb} = 0.515\pi \cdot \dot{\phi}^{\frac{5}{2}} \cdot \rho_{air}^{\frac{1}{2}} \cdot \mu_{air}^{\frac{1}{2}} \cdot R_1^{\frac{16}{5}} \cdot m^{-\frac{1}{5}} \cdot H \quad (7.5)$$

$$P_{v,lateral,high-turb} = 0.0325\pi \cdot \dot{\phi}^{\frac{14}{5}} \cdot \rho_{air}^{\frac{4}{5}} \cdot \mu_{air}^{\frac{1}{5}} \cdot R_1^{\frac{7}{2}} \cdot m^{\frac{1}{10}} \cdot H \quad (7.6)$$

For what concern the top and bottom meatus, the power loss carried by the air friction on the top and bottom surfaces of the flywheel can be determined as follow:

$$P_{v,disk} = 2 \cdot \left(\frac{1}{2} \cdot C_M \cdot \rho_{air} \cdot \dot{\phi}^3 \cdot R_1^5\right) \quad (7.7)$$

In a similar way the power losses can be expressed considering the Reynolds number for two speed regimes:

Speed regime	Reynolds number	Torque coefficient
Low turbulent	$10^4 < Re_{disk} < 2 * 10^5$	$C_M = \frac{1.334}{Re_{disk}^{1/2}}$
High turbulent	$Re_{disk} > 2 * 10^5$	$C_M = \frac{0.0311}{Re_{disk}^{1/5}}$

Table 12: Values of torque coefficient in relation to Reynolds number in the top and bottom meatus

$$Re_{disk} = \frac{R_1^2 \dot{\phi}}{\nu_{air}} \quad (7.8)$$

$$P_{v,disk,low-turb} = 1.334 \cdot \dot{\phi}^{\frac{5}{2}} \cdot \rho_{air}^{\frac{1}{2}} \cdot \mu_{aria}^{\frac{1}{2}} \cdot R_1^4 \quad (7.9)$$

$$P_{v,disk,high-turb} = 0.0311 \cdot \dot{\varphi}^{\frac{14}{5}} \cdot \rho_{air}^{\frac{4}{5}} \cdot \mu_{aria}^{\frac{1}{5}} \cdot R_1^{\frac{23}{5}} \quad (7.10)$$

The mathematical expressions of power losses carried by the air inside the vacuum chamber depend on several parameters such as geometrical features (R_1, m, H), flywheel speed and air thermodynamic conditions (ρ_{air}, μ_{air}). Each of these terms have a different influence on P_v : taking into account the most important contributes on power losses, it is possible to design both the flywheel and vacuum chamber in order to avoid high dissipations. More in details, the influence of the flywheel speed depends on the speed regime: passing from a low turbulent speed regime to a high turbulent speed regime results in a higher exponent on the flywheel speed for both $P_{v,lateral}$ and $P_{v,disk}$ [25].

7.2.2 Bearing power losses

The gyroscope flywheel is supported by two spherical roller bearings that allow its spinning motion around the z_2 axis, as showed in figure 63

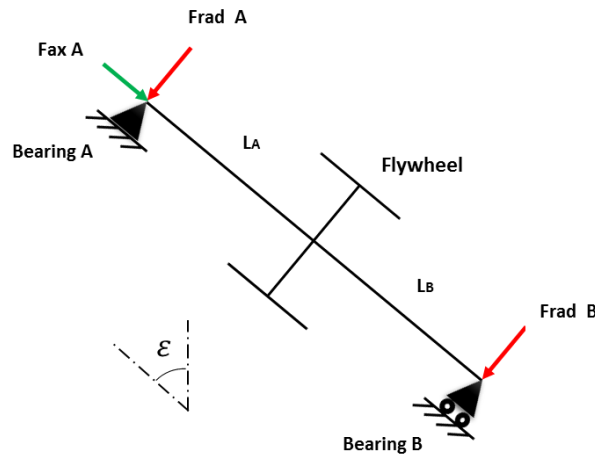


Figure 66: Simplified flywheel shaft scheme

The bearing A can support both axial and radial load, the bearing B only the radial one. Considering the gyroscopic reaction torque on the flywheel shaft and the flywheel mass, is possible to obtain the mathematical equation of the radial and axial forces on bearings[25]:

$$F_{rad A} = F_{rad B} = F_{rad} = \sqrt{\left(\frac{1}{2} m_v g \cdot \sin \varepsilon\right)^2 + \left(J \dot{\varphi} \dot{\varepsilon} \cdot \frac{1}{L}\right)^2} \quad (7.11)$$

$$F_{ax, A} = m_v g \cdot \cos \varepsilon \quad (7.12)$$

Where:

- m_v is the flywheel mass;

- L is the inter axis between bearings ($L_A = L_B = \frac{L}{2}$);
- $\dot{\varepsilon}$ is the precession gyroscope speed.

Since the system has been linearized considering small gyroscope oscillations around its vertical position ($\varepsilon = 0$ deg), it is possible to neglect its first term, obtaining the following equation:

$$F_{rad} = J\dot{\varphi}\dot{\varepsilon} \cdot \frac{1}{L} = \frac{T_\lambda}{L} \quad (7.13)$$

Moreover, the linearization hypothesis can be enforced taking into account that the gyroscopic action on the bearings is greater than the contribution of the flywheel weight[25]. Once calculated the forces acting on bearings, the mathematical expression of the power losses for both axial and radial loads can be determined according to the simplified SKF friction moment formulation:

$$P_{bear,rad} = \frac{1}{2}\mu_{bear} \cdot F_{rad} \cdot d_{bear} \cdot \dot{\varphi} = \frac{1}{2L} \mu_{bear} J \cdot \dot{\varphi} \cdot \dot{\varphi} \cdot \dot{\varepsilon} \cdot d_{bear} \quad (7.14)$$

$$P_{bear,ax} = g \cdot \mu_{bear} m_v \cdot d_{bear} \cdot \dot{\varphi} \quad (7.15)$$

The radial power losses depend both on the flywheel rotational speed and flywheel inertia and thus on the angular momentum ($L = J\dot{\varphi}$). On the other hand, the axial power losses depend only on the flywheel speed and flywheel mass. It has been demonstrated that the higher contribute of the power losses provided by bearing is given by the radial forces, so the gyroscopic reaction on the flywheel shaft T_λ , should be limited acting on the flywheel inertia or on its speed[25].

7.2.3 Seal power losses

The last source of power losses is due to the seals: in order to maintain the vacuum inside the flywheel chamber and to prevent oil leakages, two seals are used. The mathematical relation of the seals power loss is :

$$P_{seal} = F_r \cdot \pi \cdot \frac{d_{seal}^2}{2} \cdot \dot{\varphi} \quad (7.16)$$

Where:

- F_r is the friction force per unit of length on the surface contact between the seal and the flywheel shaft;
- d_{seal} is the seal diameter.

Taking into account the F_r , it depends on the pressure difference between the air inside and outside the chamber and on the seal material. The graph below shows the friction force of the seals of the ISWEC full – scale. Interpolating the red curve selecting a proper number of points allows to obtain the mathematical expression of the friction force:

$$F_r = 67 \frac{N}{m} + 201.3 \frac{N}{m \cdot MPa^{0.6}} \cdot \Delta p^{0.6} \quad (7.17)$$

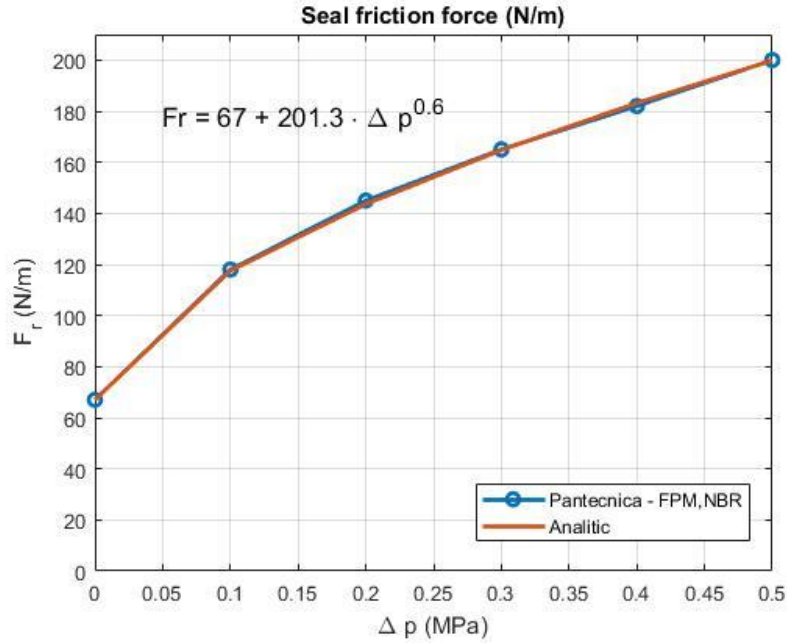


Figure 67: Friction force on seal surface in function of pressure difference on it

Substituting the equation (7.17) in (7.16) the mathematical expression of the seal power losses becomes[25]:

$$P_{seal} = \frac{\pi}{2} (67 + 201.3 \Delta p^{0.6}) \cdot d_{seal}^2 \cdot \dot{\phi} \quad (7.18)$$

7.3 Power losses scaling law

The wave phenomena can be related to the Froude number as the forces induced by the gravity are comparable with the inertial one. Since the angular momentum is the physical quantity that affects the energy transfer from the wave to the poer take – off (PTO), so the angular momentum is scaled according to the Froude scale: this implies that both flywheel inertia (J) and flywheel speed ($\dot{\phi}$) will follow the same scale method. Scaling the whole system according to the Froude scale leads to not consider the Reynolds number, so the fluid – dynamics in the meatus are not scaled properly correctly.

The Reynolds number concern about the ratio between the inertial forces and viscous forces: since the flywheel spins one order of magnitude faster than the hull and the gyroscope, the viscous phenomena have to be scaled according to the Reynolds number, in order to consider correctly all the phenomena involved in the power losses calculation. Thus there are two

different method that can be used in order to obtain the mathematical expression for the power losses scaling as a function of the scale factor: Froude scale and Froude – Reynolds scale[25].

For *geometric* characteristics:

Characteristic	Dimension	Scale factor (Froude)	Scale factor (Reynolds)
Length	[L]	λ	λ
Area	[L ²]	λ^2	λ^2
Volume	[L ³]	λ^3	λ^3
Rotation	[L ⁰]	-	-

Table 13: Scale factors for geometric characteristics

For *kinematic* characteristics:

Characteristic	Dimension	Scale factor (Froude)	Scale factor (Reynolds)
Time	[T]	$\lambda^{\frac{1}{2}}$	λ^2
Velocity	[LT ⁻¹]	$\lambda^{\frac{1}{2}}$	λ^{-1}
Acceleration	[LT ⁻²]	-	λ^{-3}
Volume flow	[L ³ T ⁻¹]	$\lambda^{\frac{5}{2}}$	λ

Table 14: Scale factors for kinematic characteristics

For *dynamic* characteristics:

Characteristic	Dimension	Scale factor (Froude)	Scale factor (Reynolds)
Mass	[M]	λ^3	λ^3
Force	[MLT ⁻²]	λ^3	-
Pressure	[ML ⁻¹ T ⁻²]	λ	λ^2
Power	[ML ² T ⁻³]	$\lambda^{\frac{7}{2}}$	λ^{-1}

Table 15: Scale factors for dynamic characteristics

The table shows the scale factors for different physical quantities with respect to both the Froude and Reynolds numbers. The scale factor (λ) is the ratio between the model dimension and the full – scale dimension:

$$\lambda = \frac{D_M}{D_F} < 1 \quad (7.19)$$

7.3.1 Froude scaling law

Referring to the relations defined in the previous chapter and substituting the scale factors reported in the tables above, the power losses scale factors have been obtained. These relations carries crucial information; firstly, the influence of each system parameter involved into the calculation of the power losses can be determined, allowing a better design process of the system, limiting power losses. Moreover almost all the exponents of the power losses scale factors are smaller than the scale factor of the extracted power ($\lambda^{7/2}$). This allows to conclude that the power losses grow with a smaller rate that the extracted power, as the scale factor increase.

The relations in tables below have been obtained considering the density and kinematic viscosity of the air constant according to the Froude scaling law. Thus, the pressure of the air inside the vacuum chamber is the same for each scale factor. The friction coefficient μ_{bear} has been considered constant for each scale factor[25].

Scale factors for *fluid – dynamics power losses* are:

Power loss name	Relation	Scale factor (Froude)
$P_{v,lateral,low-turb}$	$0.515\pi \cdot \dot{\phi}^2 \cdot \rho_{air}^{\frac{1}{2}} \cdot \mu_{air}^{\frac{1}{2}} \cdot R_1^{\frac{16}{5}} \cdot m^{-\frac{1}{5}} \cdot H$	$\lambda^{\frac{11}{4}}$
$P_{v,lateral,high-turb}$	$0.0325\pi \cdot \dot{\phi}^{\frac{14}{5}} \cdot \rho_{air}^{\frac{4}{5}} \cdot \mu_{air}^{\frac{1}{5}} \cdot R_1^{\frac{7}{2}} \cdot m^{\frac{1}{10}} \cdot H$	$\lambda^{\frac{16}{5}}$
$P_{v,disk,low-turb}$	$1.334 \cdot \dot{\phi}^2 \cdot \rho_{air}^{\frac{1}{2}} \cdot \mu_{air}^{\frac{1}{2}} \cdot R_1^4$	$\lambda^{\frac{11}{4}}$
$P_{v,disk,high-turb}$	$0.0311 \cdot \dot{\phi}^{\frac{14}{5}} \cdot \rho_{air}^{\frac{4}{5}} \cdot \mu_{air}^{\frac{1}{5}} \cdot R_1^{\frac{23}{5}}$	$\lambda^{\frac{16}{5}}$

Table 16: Scale factors for fluid - dynamic power losses

Scale factors for *bearing power losses*:

Power loss name	Relation	Scale factor (Froude)
$P_{bear,rad}$	$\frac{1}{2L} \mu_{bear} J \cdot \dot{\phi}^2 \cdot \varepsilon \cdot d_{bear}$	$\lambda^{\frac{7}{2}}$
$P_{bear,ax}$	$g \cdot \mu_{bear} m_v \cdot d_{bear} \cdot \dot{\phi}$	$\lambda^{\frac{7}{2}}$

Table 17: Scale factors for bearing power losses

Scale factors for *seal power losses*:

Power loss name	Relation	Scale factor (Froude)
P_{seal}	$\frac{\pi}{2} (67 + 201.3 \Delta p^{0.6}) \cdot d_{seal}^2 \cdot \dot{\phi}$	$\lambda^{\frac{3}{2}}$

Table 18: Scale factors for seal power losses

7.3.2 Trends of scaled power losses

Considering the equations obtained in the previous chapter, a numerical example aims to quantify the power losses with respect to the extracted power of the device and to evaluate the effect of the scale factor on the system efficiency.

The kinematic parameter has been defined, considering the experimental hull and gyroscope speed in correspondence of a wave having energetic period equal to 5s and a significant height equal to 1,14m, as well as the flywheel spinning velocity (full – scale device experimental data acquired on 7 October 2015)[25]:

Kinematic parameters		
Hull speed	$\dot{\delta}_0$	1.2 rpm
Gyroscope speed	$\dot{\varepsilon}_0$	6 rpm
Flywheel speed	$\dot{\varphi}$	400 rpm

Table 19: Kinematic parameters of the system

The geometric parameters and the features of the full scale device are:

Geometric parameters		
External diameter of the flywheel	R_1	1.075 m
Height of the flywheel	H	1 m
Flywheel inertia	J	8174 kg m ²
Inter – axis distance	L	1.4 m
Bearings diameter	d_{bear}	0.18 m
Seal diameter	d_{seal}	0.38 m
Friction coefficient of bearing	μ_{bear}	0.0018

Table 20: Geometric parameters of the system

Regarding to the fluid properties, the air viscosity and pressure are set according to the working condition of the device:

μ_{air}	$1.8369 \cdot 10^{-5} N/ms$
$p_{flywheel\ chamber}$	1000 Pa

Table 21: Fluid properties

From the graph we can see that the power losses decrease with a reducing scale of the model. The important losses on the flywheel shaft are carried by the seal, followed by the radial bearing losses and fluid – dynamics losses and then by the axial bearing losses[25].

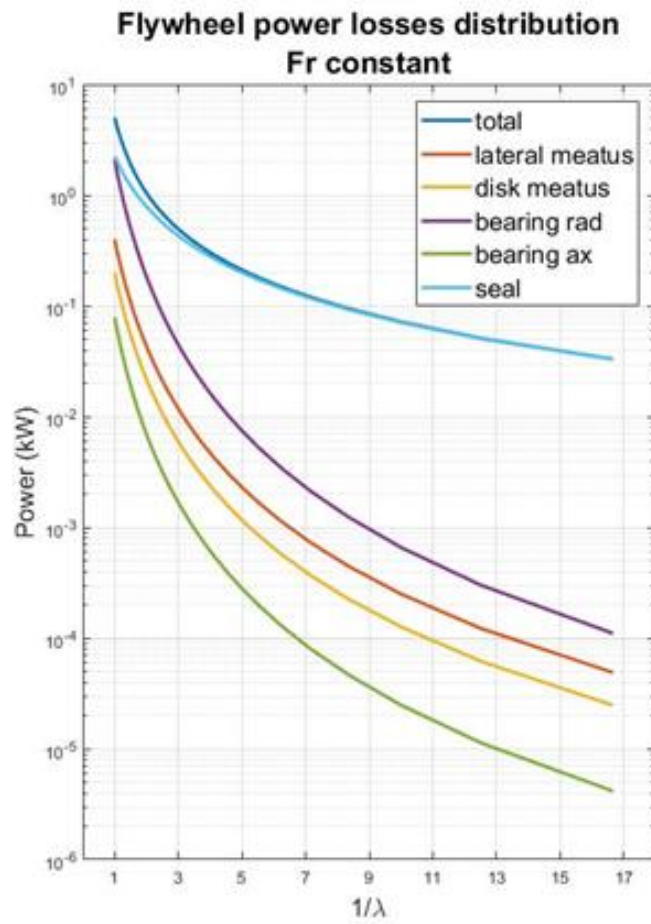


Figure 68: Flywheel power losses on ISWEC[25]

8. Conclusions

The hull of a sailing ship is completely different from that of a simple boat. Its main feature is the presence of a *keel* that is placed below the hull (which can be weighted with *ballast*) that serves to decrease the *leeway* (transversal movement of the boat by the wind) of the ship and to allow stability during navigation.

The *hydrostatic study* of the hull has led to the creation of a graph (figure 30) from which we can evaluate that after a certain inclination of the hull ($\alpha = 65^\circ$), the moment, applied by the hydrostatic thrust that acts on the wet surface of the hull, is no longer *righting* but becomes *heeling*. Instead, through the *hydrodynamic study* of the boat it was possible to evaluate the maximum pitching degree with different forward speed in the case of an incident wave in the longitudinal direction to the hull. The values obtained, for the various forward speed, all record a peak in the period of the wave of 3.5s reaching a maximum value of RAO (figure 34) equal to 19° , with a forward speed equal to 8 m / s. Instead, looking at the RAO - roll graph (figure 35), we can see that the inclinations due to the rolling movement are very low if the hull is hit by a longitudinal wave, so this type of wave does not affect the rolling motion at all. So we get the resonance frequency of the system for an incident wave of period equal to 3.5s and probably we will get the maximum productivity of the system with this wave period value. This is due to the fact that through the value of pitch angle is possible to calculate the momentum that is created around the precession axis of the gyroscope, which will then be transformed by the PTO into electric energy, so higher is the pitch angle, higher would be the pitching speed, greater would be the productivity of the system (according to equation 5.1). The same applies to the angular momentum (L) created by the rotation of the flywheel around its axis: with higher values of L , more electrical energy could be harvest in the system. This is the main reason why the design of the 1: 7 scale prototype started respecting geometric constraints (external diameter of the flywheel, flywheel height, inter-axis between the bearings), because precisely these contribute to an increase in angular momentum, hence in the productivity of the system.

The study, conducted in chapter 7, shows that, from an analytical point of view the speed and the external radius of the flywheel play an important role in the flywheel power losses magnitude. More in details, the flywheel speed appears in all the relations of the power losses representing the most important contributions to the dissipated power. So one of the main steps in design process of a gyroscopic system is the choice of the angular momentum ($L = J\dot{\phi}$) that is the physical quantity involved into the power extraction: make a correct balance between the flywheel inertia (J) and the flywheel speed ($\dot{\phi}$) will allow to limit the power losses.

The gyroscopic model, designed in this thesis in 1:7 scale, will then be constructed in order to assess the system behavior and execute a feasibility analysis. The verifications that will be carried out on the model will give us results in which, despite considering completely different boundary conditions compared to those planned for the design of ISWEC, the mechanical efficiency will be lower than 1:1 scale model and the power losses will have a trend very similar to that calculated for ISWEC in the graph in figure 68, according to Froude scale.

References

- [1] European commission, “Harnessing the power of the sea,” 2012.
- [2] M. Raffero, “Design of a Wave Energy Converter-A case of application: ISWEC,” 2014.
- [3] Ehsan Enferad and Daryoush Nazarpour, “Ocean’s Renewable Power and Review of Technologies: Case Study Waves, New Developments in Renewable Energy.”
- [4] Bracco G., “ISWEC: a Gyroscopic Wave Energy Converter,” 2010.
- [5] BOEM (bureau of Ocean Energy Management), “Ocean Wave Energy | BOEM,” 2007. [Online]. Available: <https://www.boem.gov/Ocean-Wave-Energy/>. [Accessed: 03-Mar-2018].
- [6] “What is Wave Energy and How Wave Energy is Converted into Electricity? - Conserve Energy Future.” [Online]. Available: <https://www.conserve-energy-future.com/waveenergy.php>. [Accessed: 03-Mar-2018].
- [7] J. D. Isaacs and W. R. Schmitt, “Ocean Energy: Forms and Prospects,” *Science*, vol. 207. American Association for the Advancement of Science, pp. 265–273.
- [8] G. Mofk, S. Barstow, A. Kabuth, and M. T. Pontes, “Assessing the Global Wave Energy Potential,” in *29th International Conference on Ocean, Offshore and Arctic Engineering: Volume 3*, 2010, pp. 447–454.
- [9] M. Harvey, D. Gauthier, and J. Munro, “Temporal changes in the composition and abundance of the macro-benthic invertebrate communities at dredged material disposal sites in the anse à Beaufils, baie des Chaleurs, eastern Canada,” *Mar. Pollut. Bull.*, vol. 36, no. 1, pp. 41–55, Jan. 1998.
- [10] J. Hayward and P. Osman, “The potential of wave energy,” 2011.
- [11] P. Jacobson, “Mapping and Assessment of the United States Ocean Wave Energy Resource DISCLAIMER OF WARRANTIES AND LIMITATION OF LIABILITIES,” 2011.
- [12] WATERLAS, “Wind and Wave Atlas of the Mediterranean Sea Wind and Wave Atlas of the Mediterranean Sea,” 2004.
- [13] M. T. Pontes, R. Aguiar, and H. Oliveira Pires, “A Nearshore Wave Energy Atlas for Portugal,” *J. Offshore Mech. Arct. Eng.*, vol. 127, no. 3, p. 249, Aug. 2005.
- [14] S. F. Barstow *et al.*, “WORLDWAVES: High Quality Coastal and Offshore Wave Data Within Minutes for Any Global Site,” in *Volume 3: Materials Technology; Ocean Engineering; Polar and Arctic Sciences and Technology; Workshops*, 2003, pp. 633–642.
- [15] S.H. Salter, “Wave power,” 1974.
- [16] “EMEC: European Marine Energy Centre.” [Online]. Available: <http://www.emec.org.uk/>. [Accessed: 03-Mar-2018].

- [17] D. M. (David M. Ingram, G. Smith, C. Bittencourt-Ferreira, and H. Smith, *Protocols for the equitable assessment of marine energy converters*. Institute for Energy Systems, School of Engineering, University of Edinburgh, 2011.
- [18] B. Devolder, P. Rauwoens, and P. Troch, “Numerical modeling of wave energy converters,” *15th FEA Res. Symp. Abstr.*, no. August, 2014.
- [19] ANSYS Inc., “Aqwa Theory Manual,” *Ansys*, vol. 15317, no. January, p. 174, 2013.
- [20] Francesco De Bonis, “Studio di Tenuta della Nave al Mare con Metodo BEM,” Università degli studi di Napoli Federico II, 2015.
- [21] D. Skandali, “Identification of response amplitude operators for ships based on full scale measurements,” *Tech. Univ. Delft*, no. September, 2015.
- [22] A. Carmagnola, “Metodi di stabilizzazione dello scafo mediante giroscopio con recupero di energia,” pp. 1–103, 2012.
- [23] R. Nabergoj, “Fondamenti di Tenuta della Nave al Mare,” 2007.
- [24] G. Bracco, E. Giorcelli, and G. Mattiazzo, “ISWEC: A gyroscopic mechanism for wave power exploitation,” *Mech. Mach. Theory*, vol. 46, no. 10, pp. 1411–1424, Oct. 2011.
- [25] N. Pozzi, V. Calamusa, and M. Bonfanti, “Power losses on iswec,” *Paper*, 2017.
- [26] SKF Group and S. K. F. Group, “Rolling bearings,” *Skf Bear.*, pp. 97–114, 2012.

Ringraziamenti

Questo percorso è stato lungo e tortuoso pieno di rimorsi, paure e incertezze che mi hanno reso più forte e determinato ad affrontare ardue sfide, a definire e risolvere i problemi e a capire meglio me stesso. Tutto questo, però, non solo grazie al Politecnico ma soprattutto grazie a voi che mi avete sempre sostenuto ed aiutato a superare ogni tipo di difficoltà durante questi anni.

Un infinito grazie va a mamma e papà che hanno dovuto affrontare spese economiche non indifferenti per sostenere i miei studi e i miei numerosi capricci che ingenti, anche loro, sono accorsi inesorabilmente in questi anni.

Mamma, non scorderò mai i tuoi incoraggiamenti, il tuo sostegno morale che puntuali arrivavano dopo ogni esame; mi hai sempre spronato e valorizzato quando mi abbattevo, eri sempre pronta a dare tutto per me. Mi dici sempre “voglio che tu sia felice”, ecco, oggi, è uno di quei giorni in cui lo sono.

Papà grazie anche a te per le mille accortezze, premure e telefonate che puntuali ogni giorno arrivavano per fare un résumé degli impegni affrontati ma soprattutto grazie alle mille ricariche fatte prima della scadenza del mese.

Anche tu, cara Margherita, sempre pronta a sostenermi e a tirarmi su il morale; grazie per i mille pranzi e cene che mi hai regalato e per le bellissime parole che ogni giorno spendi nei miei confronti e ricordati che non sono io “il fratello super – intelligente che fa mille cose” ma tu pure sei bravissima e meravigliosa.

Grazie a tutte le zie e gli zii per la premura nei miei confronti, per i messaggi scambiati e il supporto mostrato in tutti questi anni.

Noemi, cara amica, abbiamo iniziato questo percorso insieme ma siccome tu sei troppo favolosa non lo abbiamo concluso uniti, però è come se lo avessimo fatto. Anche da Piacenza sei stata sempre pronta a consigliarmi, a darmi forza, a dedicarmi ore al telefono per affrontare l'esistenzialismo della mia esistenza che gentilmente hai voluto sempre condividere senza mai scocciarti.

Nicoletta, grazie anche a te per aver sopportato le mie ansie e dolori, per i mille consigli e per le numerose chiacchierate e risate che mi hai dato.

Infine grazie a Gian, Manu, Marco, Greta, Tony che mi avete sempre saputo distogliere, con intelligenza, dai miei impegni e ai tantissimi momenti e serate trascorse tutti insieme dove riconosco che incontrarvi, in questi anni, è stato bellissimo.